UNIVERSITY
OF SUSSEX

MODELLING AND CONTROL OF WASTE HEAT RECOVERY SYSTEMS FOR HEAVY-DUTY APPLICATIONS

by

HAMID ENAYATOLLAHI

A DISSERTATION SUBMITTED TO UNIVERSITY OF SUSSEX FOR THE DEGREE OF DOCTOR OF PHILOSOPHY

SCHOOL OF ENGINEERING AND INFORMATICS

2021

ABSTRACT

Internal combustion engines (ICEs) are likely to be used in heavy-duty applications for many years and it is important to continue improving their efficiency. Undesirable emissions in internal combustion engines are of major concern due to their negative effect on the human health and global warming. One approach is to recover waste heat from the exhaust of heavy-duty diesel engines (HDDEs) using waste heat recovery (WHR) technologies. WHR based on organic Rankine cycle (ORC) is a promising technology, which offers potential to reduce the fuel consumption of HDDEs by converting the wasted thermal energy to alternative useful electrical or mechanical energy.

In the ORC, the evaporator is considered the most critical component of the system. Careful modelling of the evaporator unit is both crucial to assess the dynamic performance of the ORC system and challenging due to the high nonlinearity of its governing equations. This study uses an Adaptive Network-based Fuzzy Inference System (ANFIS) modelling technique to provide efficient control-oriented evaporator models for prediction of heat source and refrigerant temperatures at the evaporator outlet. The ANFIS model benefits from feed-forward output calculation and backpropagation capability of neural network, while keeping the interpretability of fuzzy systems. The effect of training the models using hybrid gradient-descent least-square estimate (GD-LSE) and particle swarm optimisation (PSO) techniques is investigated and the performance of both techniques are compared in terms of RMSE and correlation coefficients. The simulation results indicate strong learning ability and high generalisation performance for both techniques beyond capability of numerical models. However, a better accuracy is achieved for the models trained using the PSO algorithm.

Experimentally-measured data is collected from a 1-kWe ORC prototype developed in Clean Energy Processes (CEP) laboratory at Imperial College London and the proposed ANFIS techniques is applied in order to investigate the application of the neuro-fuzzy technique for modelling the evaporator unit. Comparison of the experimental data and the neuro-fuzzy models predictions reveals an acceptable accuracy in predicting the evaporator outlet temperature and pressure.

A novel control approach is also proposed to ensure the safe operation of ORC waste heat recovery system and stabilize its work output when subjected to transient heat sources in a range of waste heat from heavy-duty diesel engines. The control strategy comprises a neuro-fuzzy controller based on the inverse dynamics of the ORC system to control the superheating at the evaporator outlet by adjusting the pump speed and a PI controller to maintain the expander work output by regulating the mass flow rate at the expander inlet. The performance of the control strategy is investigated with respect to set-point tracking and its robustness is tested in the presence of noise. The simulation results indicate an enhancement in the controller performance by combination of feedforward and feedback controllers based on neuro-fuzzy techniques. The proposed control scheme not only can obtain satisfactory transient response under various loading conditions, but also can achieve desirable disturbance rejection performance.

DECLARATION

This research has been carried out in the Department of Engineering and Design, School of Engineering and Informatics, at the University of Sussex. I hereby declare that this thesis has not been submitted, either in the same of different form to this or any other University for a degree.

Hamid Enayatollahi

ACKNOWLEDGEMENT

I would like to express my gratitude to all those who have made invaluable contributions, both directly and indirectly to my research.

My greatest gratitude first and foremost goes to my supervisor Dr Bao Kha Nguyen for providing constant guidance and support, timely advice and frequent encouragement throughout the entire course of this research without which this research would not have been possible and thesis could never have reached its present form.

My special thanks also go to Prof Peter Fussey for his beneficial guidance, valuable advice and motivation along this journey. Your profound experience and words of wisdom will forever be treasured.

I would also like to thank my colleagues, Alireza Sarmadian and Amirhossein Naseredini who provided much support and many constructive suggestions during the writing of this thesis. My sincere appreciation also goes to Prof Christos Markides and Dr Paul Sapin for allowing me to access the ORC testing facility in the Clean Energy Processes (CEP) Laboratory at Imperial College London.

Finally, I would like to acknowledge with gratitude, the support, love and endless faith of my family – my parents, Mohamad and Sedigheh; my brother, Amin and my wife Ghazaleh. They all kept me going, and this thesis would not have been possible without them.

TABLE OF CONTENTS

ABSTRACT ..... **i**

DECLARATION ..... **ii**

ACKNOWLEDGEMENT ..... **iii**

TABLE OF CONTENTS ..... **iv**

NOMENCLATURE ..... **ix**

VARIABLES ..... **xi**

SUBSCRIPTS ..... **xii**

LIST OF FIGURES ..... **xiii**

LIST OF TABLES ..... **xix**

LIST OF PUBLICATIONS ..... **xx**

Chapter 1: Introduction **1**

1.1 Background and motivation 1

1.2 Objectives 3

1.3 Thesis outline 4

Chapter 2: Waste Heat Recovery Systems **7**

2.1 Waste heat sources 7

2.1.1 Industrial waste heat 7

2.1.2 Waste heat in internal combustion engines 9

2.2 Methods of waste heat recovery 10

2.2.1 Thermoelectric generators 10

2.2.2 Stirling engine 12

2.2.3 Phase change material engines 14

2.2.4 Carnot cycle 16

2.2.5 Rankine cycle 17

2.2.6 Kalina cycle 21

2.2.7 Organic Rankine cycle 22

2.3 Summary 24

Chapter 3: Organic Rankine cycle 26

3.1 Previous research on ICE-WHR 26

3.2 ORC architecture 27

3.3 Working fluid selection 30

3.4 Components of the ORC 33

3.4.1 Pump 33

3.4.2 Evaporator 34

3.4.3 Expander 36

3.4.4 Condenser 40

3.5 Control of the ORC 41

3.6 Summary 44

Chapter 4: Modelling the components of ORC 47

4.1 Pump model 47

4.2 Expander model 48

4.3 Condenser model 48

4.4 Valve model 49

4.5 Liquid receiver model 50

4.6 Evaporator model 51

4.6.1 Finite Volume model 54

4.6.2 Moving Boundary model 59

4.7 Summary 60

Chapter 5: Neuro-fuzzy modelling of evaporator 62

5.1 Artificial intelligence modelling 62

5.2 Artificial neural network modelling 62

5.2.1 Implementation of ANN evaporator model 64

5.3 Fuzzy theory and fuzzy modelling 72

5.3.1 Fuzzy sets and membership function 73

5.3.2 Linguistic variables and fuzzy rules 74

5.3.3 Fuzzy inference system 77

5.3.4 Fuzzy based evaporator model 80

5.4 Adaptive neuro-fuzzy inference system modelling 85

5.4.1 ANFIS architecture 86

5.4.2 Training algorithms of the network 88

5.5 ANFIS evaporator model implementation 94

5.5.1 Training ANFIS evaporator model using hybrid GD-LSE algorithm 96

5.5.2 Training ANFIS evaporator model using PSO algorithm 101

5.6 Comparison of training ANFIS model using GD-LSE and PSO 107

5.7 Case Study: 1kWe-Organic Rankine Cycle prototype 112

5.7.1 Data collection and evaporator model implementation 116

5.7.2 Learning Algorithm 118

5.7.3 Simulation results 119

5.8 Investigation of the ORC cycle using the neuro-fuzzy evaporator 125

5.9 Summary 130

Chapter 6: Control of ORC 132

6.1 PID control 133

6.2 Neuro-fuzzy system as direct inverse controller 136

6.2.1 Development of inverse dynamic model 137

6.2.2 Implementation of inverse neuro-fuzzy controller 141

6.3 Control performance of combination of PID and inverse neuro-fuzzy controller ... 144

6.3.1 Set-point tracking performance of the control system 144

6.3.2 Robustness of the proposed control system 147

6.4 Expander work output control 149

6.5 Summary 154

Chapter 7: Summary, conclusions and future work 156

7.1 Summary 156

7.2 Conclusions 161

7.3 Further work 162

References 165

NOMENCLATURE

ABC	artificial bee colony
ANFIS	adaptive network-based fuzzy inference system
ANN	artificial neural networks
AWPSO	adaptive weighted particle swarm optimization
CAMD	computer aided molecular design
CEP	clean energy processes
CHP	combined heat and power
COG	centre of gravity
DLORC	double loop ORC
DRORC	double stage regenerative ORC
EKF	extended Kalman filter
FCM	fuzzy c-means
FFRLS	forgetting factor recursive least squares
FSI	fuel stratified injection
FV	finite volume
GA	genetic algorithm
GD	gradient descent
GDI	gasoline direct injection
GP	grid partitioning
GWP	global warming potential
HDDE	heavy-duty diesel engine
ICE	internal combustion engine

IWA	inertial weight approach
kW	kilowatt
LSE	least square estimate
MB	moving boundary
MLP	multi-layer perceptron
MOM	mean of maxima
MSE	mean square error
ODP	ozone depletion potential
ORC	organic Rankine cycle
PCM	phase change material
PSO	particle swarm optimization
RMSE	root mean square error
RORC	reheat ORC
SCM	subtractive clustering method
SRC	steam Rankine cycle
SRORC	single stage regenerative ORC
TDI	turbo direct injection
TEG	thermo electric generator
TES	thermal energy storage
TP	two-phase region
TP-V	two-phase and vapour region
WHR	waste heat recovery

VARIABLES

$\dot{m}$	mass flow rate
α	Percentage of valve opening
μ	membership function
η	learning rate
σ	fuzzy set width
ρ	density
ρ	random variable
$\in$	pipe roughness
Ψ	refrigerant level
τ	time constant
φ	activation function
A	area
A, B	linguistic variables
c	fuzzy set centre
C	acceleration constant
D	diameter
H	enthalpy
L	length of evaporator
N	number of control volumes
P	pressure
p, q, r	consequent parameters

Q	evaporator heat input
T	temperature
U	system energy
V	volume
W	inertial weight
W	work

SUBSCRIPTS

con	condenser
ev	evaporator
exp	expander
h	heat source
h	hydraulic
in	inlet
itr	iteration number
lr	liquid receiver
out	outlet
p	pump
p	pipe
r	Refrigerant
V	valve

LIST OF FIGURES

Fig. 2.1. Temperature of exhaust gases for the city and high drive cycles [11] 10

Fig. 2.2. Mass flow rate of exhaust gases for the city and high drive cycles [11] 10

Fig. 2.3. Operation principle of TEGs 12

Fig. 2.4. Alpha-type Stirling engine 14

Fig. 2.5. P-V diagram of a typical Stirling Engine 14

Fig. 2.6. Working principle of PCM engines 15

Fig. 2.7. T-S diagram of Carnot cycle 16

Fig. 2.8. T-S diagram of Rankine cycle a) without superheating b) with superheating 18

Fig. 2.9. Conceptual schematic of ORC system 23

Fig. 3.1. Schematic of single stage regenerative ORC 27

Fig. 3.2. Schematic of double-stage regenerative ORC 28

Fig. 3.3. Schematic of reheat ORC 28

Fig. 3.4. Schematic of ORC with recuperator 29

Fig. 3.5. Schematic of dual loop ORC 29

Fig. 3.6. Some types of heat exchangers a) Finned tube heat exchanger [84] b) shell and tube [85] c) Brazed Plate heat exchanger [86] 36

Fig. 3.7. Twin screw expander [99] 39

Fig. 4.1. Discretisation of evaporator to N control volumes 55

Fig. 5.1. Nonlinear model of a neuron [142] 63

Fig. 5.2. Input-output data gathered from FV model of evaporator (a) Mass flow rate and temperature of generic heat source (b) Mass flow rate of refrigerant (c) Refrigerant and heat source temperatures at the evaporator outlet 65

Fig. 5.3. MLP neural network architecture and refrigerant outlet temperature model input output variables 66

Fig. 5.4. Mean square error during the network training 67

Fig. 5.5. Performance of the network in predicting the evaporator outlet temperature (training data) 68

Fig. 5.6. Performance of the network in predicting the evaporator outlet temperature (test data) 68

Fig. 5.7. MLP neural network architecture and heat source outlet temperature model input output variables 69

Fig. 5.8. Mean square error during the network training 69

Fig. 5.9. Performance of the network in predicting the heat source outlet temperature (training data) 70

Fig. 5.10. Performance of the network in predicting the heat source outlet temperature (test data) 71

Fig. 5.11. Crisp set of a high temperature 74

Fig. 5.12. Fuzzy set of high temperature 74

Fig. 5.13. Fuzzy sets of freezing, cool, warm and hot 75

Fig. 5.14. Fuzzy inference system 77

Fig. 5.15. Defuzzification methods a) center of gravity b) mean of maxima 78

Fig. 5.16. First-order TSK fuzzy inference system [149] 79

Fig. 5.17. Normalized membership functions of input variables [150] 82

Fig. 5.18. Normalized membership functions of outlet variables [150] 82

Fig. 5.19. Comparison of refrigerant outlet temperature between Fuzzy model and FV model [150] 83

Fig. 5.20. Comparison of heat source outlet temperature between Fuzzy model and FV model [150] 83

Fig. 5.21. ANFIS architecture 86

Fig. 5.22. Input-output data gathered from FV model of evaporator (a) Mass flow rate and temperature of generic heat source (b) Mass flow rate of refrigerant (c) Refrigerant and heat source temperatures at the evaporator outlet 95

Fig. 5.23. Trained membership functions of GD-LSE ANFIS model for predicting the heat source output temperature (a) temperature of heat source (b) mass flow rate of heat source (c) mass flow rate of refrigerant 97

Fig. 5.24. Trained membership functions of GD-LSE ANFIS model for predicting the refrigerant output temperature (a) temperature of heat source (b) mass flow rate of heat source (c) mass flow rate of refrigerant 98

Fig. 5.25. Fuzzy surfaces representing the Effect of changing the input parameters on the heat source output temperature in the GD-LSE ANFIS model 99

Fig. 5.26. Fuzzy surfaces representing the Effect of changing the input parameters on the refrigerant output temperature in the GD-LSE ANFIS model 100

Fig. 5.27. Trained membership functions of PSO ANFIS model for predicting the heat source output temperature (a) temperature of heat source (b) mass flow rate of heat source (c) mass flow rate of refrigerant 103

Fig. 5.28. Trained membership functions of PSO ANFIS model for predicting the refrigerant output temperature (a) temperature of heat source (b) mass flow rate of heat source (c) mass flow rate of refrigerant 104

Fig. 5.29. Fuzzy surfaces representing the Effect of changing the input parameters on the heat source output temperature in the PSO ANFIS model 105

Fig. 5.30. Fuzzy surfaces representing the Effect of changing the input parameters on the refrigerant output temperature in the PSO ANFIS model..... 106

Fig. 5.31. Comparison of heat source output temperature prediction between GD-LSE ANFIS model and PSO ANFIS model for (a) training data (b) test data 108

Fig. 5.32. Comparison of regression plots for heat source output temperature prediction between GD-LSE ANFIS model and PSO ANFIS model for (a) training data (b) test data 109

Fig. 5.33. Comparison of refrigerant output temperature prediction between GD-LSE ANFIS model and PSO ANFIS model for (a) training data (b) test data 110

Fig. 5.34. Comparison of regression plots for refrigerant output temperature prediction between GD-LSE ANFIS model and PSO ANFIS model for (a) training data (b) test data 112

Fig. 5.35. schematic of the ORC system (taken from [168])..... 114

Fig. 5.36. Experimental test rig (taken from [168])..... 116

Fig. 5.37. Comparison of GD-LSE ANFIS and PSO ANFIS models for prediction of T_{rout} using the training and test data..... 120

Fig. 5.38. Comparison of regression plots between GD-LSE ANFIS and PSO ANFIS models for prediction of T_{rout} using the training and test data 121

Fig. 5.39. Comparison of GD-LSE ANFIS and PSO ANFIS models for prediction of P_{rout} using the training and test data..... 123

Fig. 5.40. Comparison of regression plots between GD-LSE ANFIS and PSO ANFIS models for prediction of P_{rout} using the training and test data 124

Fig. 5.41. Overall model of the ORC..... 125

Fig. 5.42. The open-loop Simulink diagram of the ORC 126

Fig. 5.43. Random heat source temperature and mass flow rate 128

Fig. 5.44. Working fluid temperature at the evaporator outlet 129

Fig. 5.45. The pressure at the expander inlet after considering the piping pressure losses 129

Fig. 5.46. The expander work output..... 130

Fig. 6.1. Selection of working fluid temperature at the evaporator outlet from the Pressure-Enthalpy diagram of R134a 132

Fig. 6.2. Block diagram of a PID controller 133

Fig. 6.3. Setpoint tracking of PID controller at different operating points..... 135

Fig. 6.4. Inverse neuro-fuzzy controller design procedure 139

Fig. 6.5. Structure of inverse ANFIS controller in the learning phase 140

Fig. 6.6. Comparison of actual and predicted pump speeds for training and test data sets 141

Fig. 6.7. Structure of the ORC with inverse ANFIS controller 142

Fig. 6.8. Simulink diagram of the ORC with inverse ANFIS controller 143

Fig. 6.9. Structure of the ORC with combination of inverse ANFIS and PID controllers 143

Fig. 6.10. Simulink diagram of the ORC with combination of inverse ANFIS and PID controllers..... 144

Fig. 6.11. Heat source mass flow rate and temperature variations 145

Fig. 6.12. Comparison of set-point tracking of control strategies with transient heat source 146

Fig. 6.13. Comparison of response of pump for various control schemes under transient heat source..... 147

Fig. 6.14. Heat source mass-flow rate and temperature variations in the presence of white noise 148

Fig. 6.15. Comparison of set-point tracking of control strategies with transient heat source in the presence of noise 149

Fig. 6.16. Comparison of response of pump for various control schemes with transient heat source in presence of noise 149

Fig. 6.17. Structure for simultaneous control of superheating and expander work output 151

Fig. 6.18. Simulink diagram for simultaneous control of superheating and expander work output 152

Fig. 6.19. Set-point tracking of expander work output 153

Fig. 6.20. Percentage of valve opening using the PI controller 154

LIST OF TABLES

Table 2.1 – Waste heat potential and Carnot potential for several industrial processes [7].. 8

Table 3.1 – Properties of selected working fluids 32

Table 5.1 – Network performance for prediction of refrigerant outlet temperature 67

Table 5.2 – Network performance for prediction of refrigerant outlet temperature 70

Table 5.3 – Fuzzy rules of fuzzy evaporator model [150] 84

Table 5.4 – Summary of studies which utilised metaheuristic algorithms for ANFIS training. 89

Table 5.5 – Hybrid GD-LSE learning algorithm 90

Table 5.6 – GD-LSE ANFIS training parameters 96

Table 5.7 – Parameters of PSO ANFIS algorithm 102

Table 5.8 – Statistical error analysis of the proposed models 111

Table 5.9 – Component specification of the ORC test rig 115

Table 5.10 – Summary of the R coefficient obtained for the evaporator outlet temperature sub-model 118

Table 5.11 – Summary of the R coefficient obtained for the evaporator outlet temperature sub-model 121

Table 5.12 – Summary of the R coefficient obtained for the evaporator outlet pressure sub-model 125

Table 6.1 – Tuned PID gains 134

Table 6.2 – Operating points of the ORC for testing the PID controller 135

Table 6.3 – Inverse ANFIS controller training parameters 140

LIST OF PUBLICATIONS

Journal Papers:

H. Enayatollahi, P. Fussey, and B. Kha Nguyen, "Modelling evaporator in organic Rankine cycle using hybrid GD-LSE ANFIS and PSO ANFIS techniques," *Thermal Science and Engineering Progress*, vol. 19, p. 100570, 2020/10/01/ 2020.

H. Enayatollahi, P. Fussey, and B. K. Nguyen, "Control of Organic Rankine Cycle, a neuro-fuzzy approach," *Control Engineering Practice*, vol. 109, p. 104728, 2021/04/01/ 2021.

Hamid Enayatollahi, Paul Sapin, Peter Fussey, Christos N. Markides, Bao Kha Nguyen, "A Control-Oriented ANFIS Model of Evaporator in a 1-kWe Organic Rankine Cycle Prototype." *Electronics* 10.13 (2021): 1535.

H. A. Moghaddam, A. Sarmadian, M. Shafaee, and H. Enayatollahi, "Flow pattern maps, pressure drop and performance assessment of horizontal tubes with coiled wire inserts during condensation of R-600a," *International Journal of Heat and Mass Transfer*, vol. 148, p. 119062, 2020/02/01/ 2020.

Conference Paper:

H. Enayatollahi, P. Fussey, and B. K. Nguyen, "A Neuro-Fuzzy Model of Evaporator in Organic Rankine Cycle.", *HTFF'19 - 6th International Conference on Heat Transfer and Fluid Flow*, Lisbon, Portugal, 2019.

Chapter 1: Introduction

1.1 Background and motivation

The world is in growing demand for energy. The U.S. Energy Information Administration (EIA) in its international energy outlook 2017 predicted that between 2015 and 2040 the energy consumption would experience 28% increase. Most of this energy will be achieved through burning fossil fuels. This raises the concern about surge in greenhouse gas emissions and global warming that result in demand for efficient use of energy resources. The United Nations (UN) addressed these global concerns regarding greenhouse gas emissions and climate change by establishing Kyoto Protocol. Transportation, industry, electricity, and heat production are responsible for almost 60% of production of greenhouse gasses [1]. Efforts on reducing the amount of greenhouse gas production in these sectors are focused on improving the energy efficiency by reducing the energy consumption of equipment and enhancing the processes to consume less energy. An alternative approach is to harvest the wasted thermal energy by deploying waste heat recovery technologies in order to improve the overall efficiency of systems. Waste heat from these sources is usually lost to the atmosphere in form of streams of hot exhaust gases and liquids as well as heat conduction and convection. This wasted heat can be reutilised either by enhancing previously available waste heat recovery technologies to improve their feasibility, or by discovering new methods of utilising waste heat, especially from uncommon sources, where the recovery technology is still immature and needs to be targeted for further research.

Almost 95% of transportation power is achieved through burning fuel in Internal Combustion Engines (ICEs). In today's technology of ICEs, with maximum efficiency of 42%, a

significant amount of energy is lost to the atmosphere in form of heat, through hot exhaust gases (22-46%) and coolant system (18-42%) [1, 2]. Moreover, ICEs are likely to be used in heavy-duty applications for many years and it is important to enhance their efficiency to reduce their environmental impact that caused by their low conversion efficiency. To this end, technologies such as gasoline direct injection (GDI) [3], turbo direct injection (TDI) [4] and fuel stratified injection (FSI) [5] are developed and implemented in recent years to increase the efficiency of ICEs. Despite the advantages of such technologies, a substantial amount of energy is still lost to the atmosphere in form of waste heat. Therefore, to improve the efficiency of ICEs, recently engine-bottoming technologies such as waste heat recovery (WHR) are investigated and emphasized by researchers. WHR technologies can contribute to improving the efficiency of ICEs and mitigate their undesirable environmental impact by harvesting some of the wasted heat and converting it to some form of beneficial electrical or mechanical energy within the vehicle [3-5].

One approach to improve the efficiency of ICEs and reduce their environmental impact is to deploy organic Rankine cycle (ORC) in order to convert the exhaust and coolant waste heat to useful mechanical and electrical energy. To meet the safety demand of automotive industry a real-time and accurate control system is required for the ORC system. This need has focused attentions on developing agile control-oriented models of the ORC components. In the ORC heat exchanging components are considered the most critical components of the system due to their slow response and high nonlinearity of their governing equations. Previous numerical models of the heat exchanging units are useful at the design stage of the ORC for component selection and cycle optimisation but these models are computationally

expensive and cannot be used for real-time application. Therefore, alternative modelling approaches should be considered for modelling these components.

1.2 Objectives

This aim of this study is to develop a control-oriented model of organic Rankine cycle suitable for recovery of waste heat from the exhaust of ICEs. An appropriate control method is also developed to address the heat source transitions during the various driving cycles of ICEs in heavy-duty applications.

The following research questions are identified to address the aims of this study:

- Is it possible to recover the wasted heat of ICEs in order to reduce their fuel consumption?
- What waste heat recovery method is most feasible for ICEs?
- How to model the components of the waste heat recovery system?
- How to control the waste heat recovery system to meet the automotive industry regulations and ensure the safety of the system?

To answer these research questions, the specific research objectives of this study are as follows:

- To investigate the most efficient waste heat recovery technologies currently available for harvesting wasted heat of ICEs.
- To develop a control-oriented organic Rankine cycle model for achieving the real-time control objectives in heavy-duty applications.

- To develop a control scheme for the organic Rankine cycle model that constantly adapt to the heat source variations due to the different driving conditions in order to ensure the safety of components.
- To develop a control scheme for the mass flow rate of working fluid at the expander inlet to prevent any potential damage to the expander and stabilise the cycle efficiency.

1.3 Thesis outline

This thesis is structured as follows:

In chapter 2, a detailed study on potential waste heat recovery systems for applications in automotive industries is presented, and organic Rankine cycle due to its superior efficiency, simplicity and availability of components and adequate temperature profile matching with the heat source is chosen as the technology for further investigation.

Chapter 3 describes various architectures of the ORC system, selection of the components for low-grade waste heat recovery in the range of internal combustion engines and working fluid selection for the cycle. Moreover, the requirements for integration of control systems with the ORC for mobile applications is also discussed in this chapter.

Chapter 4 presents the model for the main components of the ORC system including pump, evaporator, expander, condenser, valve and liquid receiver. Particular emphasis is given to the study of a dynamic model of evaporator, due to its characteristics such as high nonlinearity and thermal inertia, high pressure and slow response. Final volume and moving boundary methods for modelling the evaporator in the ORC are discussed and their limitations in automotive applications are also pointed out.

In chapter 5, given the superior predictive potential of artificial intelligence techniques, they are used to model the evaporator behaviour to overcome the limitations arising in modelling the evaporator using conventional methods. A MLP neural network is trained to model the highly nonlinear behaviour of the evaporator. Despite acceptable performance and generalisation of this model, due to the black-box nature, its mathematical relations are unknown to the designer and have no physical meaning. Therefore, by merging the benefits of Takagi_Sugeno fuzzy system and feedforward neural networks a novel hybrid neuro-fuzzy model of evaporator is proposed for modelling the evaporator behaviour. The effect of training the neuro-fuzzy network using conventional gradient descent least square algorithm and particle swarm optimisation technique is also discussed. Furthermore, in this chapter, a case study using the proposed neuro-fuzzy technique of modelling the evaporator in a 1kW-e ORC system is investigated. Finally, the proposed neuro-fuzzy evaporator model is integrated in the ORC system and the open loop response of the ORC system is presented.

Chapter 6 describes the development of an inverse neuro-fuzzy controller and its implementation in different closed loop configurations to control the superheating at the evaporator outlet. Configuration of the control loop for simultaneous control of superheating at the evaporator outlet and control of expander output is also described. Moreover, the results of set-point tracking and controller robustness in presence of high frequency noise for different control loop configurations are also investigated. These simulation tests are designed to evaluate the effectiveness of the proposed control strategy. The objective of this study is to confirm the potential of utilizing the proposed inverse neuro-fuzzy controller for ORC under transient heat source of heavy-duty diesel engines.

Finally, in chapter 7, the conclusions of study and recommendations for future work are provided.

Chapter 2: Waste Heat Recovery Systems

2.1 Waste heat sources

According to the EU energy roadmap 2050, the greenhouse gas emissions should be reduced by 90-95% by 2050 [6]. Accordingly, this goal requires modification of the current policies regarding energy sector. The electricity production should be emission-free and about two thirds of energy should be achieved from renewable sources. This goal demands intensive investment in the energy sector in order to transform the current energy systems or enhance their efficiency by reducing the energy wastage. The later objective requires identifying the sources of waste heat emitted to the atmosphere. The most common sources of waste heat are industrial applications and transportation sector.

2.1.1 Industrial waste heat

Almost 26% of European energy is consumed in industrial processes [7]. The waste heat rejected from industrial processes such as aluminium and copper reverberatory furnaces, glass melting furnace, steel heating furnace, etc, is referred to as industrial waste heat. This waste heat is released to the atmosphere by a thermal carrier. The thermal carrier can be gaseous streams such as exhaust gases, liquid streams such as cooling water or even solids (e.g., products such as hot glass or steel). The quality of waste heat from these sources can be further categorised based on the temperature of thermal carrier to high, medium and low grade as follows [8]:

- High grade waste heat has temperature higher than 923.15 K
- Medium grade waste heat has temperature ranges between 505.15 K and 923.15 K
- Low grade waste heat has temperature lower than 505.15 K

The appropriate WHR technology for various industries is determined based on their waste heat grade. Peris et al. [9] presented a summary of waste heat temperature in various industrial processes. In another study, Panayiotou et al. [7] outlined the waste heat grade in major European industries and assessed their opportunity and potential of WHR as follows:

Table 2.1 – Waste heat potential and Carnot potential for several industrial processes [7]

The industry type	Waste heat potential	Carnot's potential
Iron and Steel	11.40%	6.40%
Chemical and Petrochemical	11.00%	5.13%
Non-ferrous metal industry	9.59%	4.93%
Non-metallic minerals (e.g., glass and pottery)	11.40%	6.40%
Food and Tobacco	8.64%	1.89%
Paper, Pulp and Print	10.56%	4.59%
Wood and Wood products	6%	2.00%
Textile and Leather	11.04%	2.72%
Other industry	10.38%	4.84%

In terms of thermodynamic analysis, the exergy content of the rejected waste heat to the atmosphere can be determined using the Carnot efficiency (η_C). Carnot efficiency is defined as the maximum efficiency that a heat engine can achieve when it is operating between two heat reservoirs as follows:

$$\eta_C = \eta_{max} = 1 - \frac{T_H}{T_C} \tag{1.1}$$

where T_H and T_C are the heat source and heat sink temperatures, respectively. Although from practical point of view the Carnot efficiency has little value (due to the role of dissipative processes and irreversibility), but it can be used as a benchmark to compare the other

thermodynamic cycles. Furthermore, the Carnot efficiency better reveals the potential of the waste heat from the heat source for technical work or recovery [7]. Based on the Carnot's potential in industrial processes, WHR technologies can offer significant reduction in greenhouse gas emission and considerable reduction in energy consumption.

2.1.2 Waste heat in internal combustion engines

Over the past century internal combustion engines (ICEs) have been the main power source of transportation. Automobiles, heavy-duty trucks, locomotives and ships are all using ICEs for generating power from fossil fuels. The United States Environmental Protection Agency (EPA) reported that transportation sector is responsible for the greatest share of greenhouse gas emissions with 28.2% of total emissions in 2018 [1]. Despite all the technologies implemented in the ICEs still about 60-70% of fuel energy is wasted to the atmosphere. Furthermore, stringent legislation on ICE emissions motivates manufacturers to improve the efficiency of the engines to reduce the emission levels. Most of the waste heat from ICEs is lost to the atmosphere through the engine exhaust and coolant. Exhaust gas recirculation (EGR) and charge air cooler (CAC) are another source of waste heat which have relatively lower energy content [2]. From the exergy point of view, the exhaust waste heat is considered medium-grade and coolant waste heat is regarded as low-grade [10]. Although both of primary sources of waste heat in ICEs have similar energy content, the higher grade of engine exhaust makes it more thermodynamically attractive for WHR purposes. Moreover, the engine coolant temperature fluctuates moderately, but the temperature and mass flow rate of engine exhaust gases are highly dynamic. The temperature and mass flow rate of exhaust gases of a typical ICE for city and highway drive cycles are shown in **Figs. 2.1** and **2.2**

respectively. This unsteady nature of exhaust gases in ICEs makes the recovery of waste heat from this source a challenging task.

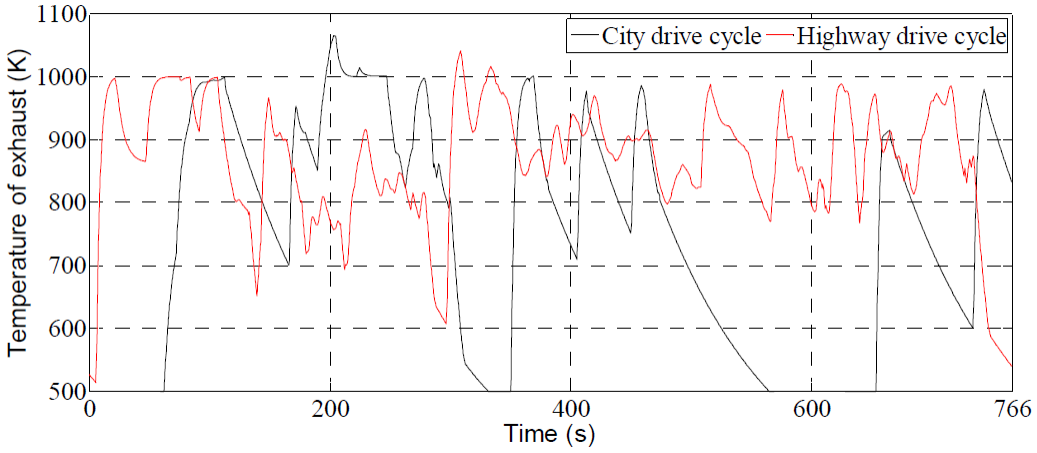

Fig. 2.1. *Temperature of exhaust gases for the city and high drive cycles [11]*

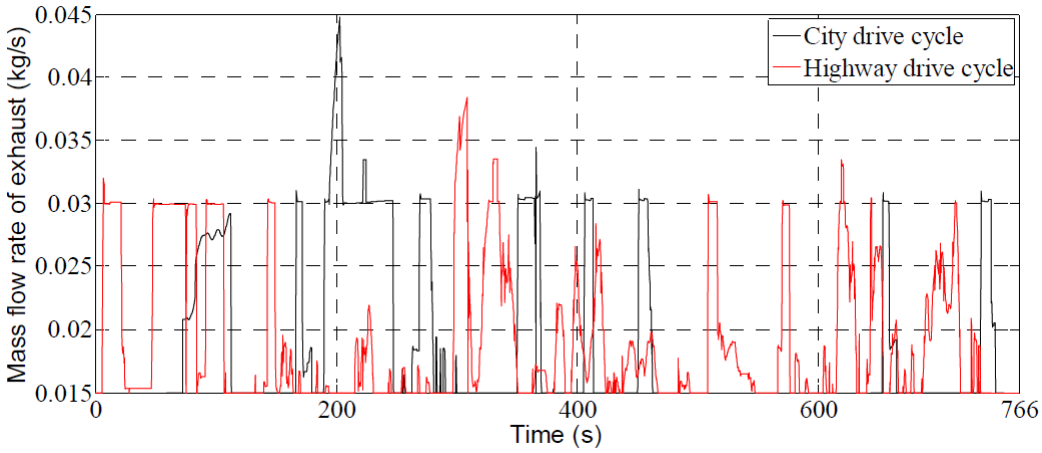

Fig. 2.2. *Mass flow rate of exhaust gases for the city and high drive cycles [11]*

2.2 Methods of waste heat recovery

2.2.1 Thermoelectric generators

Thermoelectric generators (TEGs) are solid state devices that allow direct conversion of heat flux into electrical energy. TEGs are working based on a phenomenon called Seebeck effect which was discovered in 1821 by Thomas Johann Seebeck. TEGs are consisting of a set of

different thermoelectric materials such as semiconductors and when these materials are subjected to a temperature gradient, electric voltage is created between them. The operating principle of TEGs is shown in **Fig. 2.3**. Direct conversion of energy, long lifespan, elimination of mechanical moving parts and working fluids (thus low maintenance costs) and noiseless operation are some of the advantages of the TEGs. This technology is considered as a highly reliable WHR method with efficiency of up to 5% [12]. Despite these advantages, for many years, the high cost of semiconductors limited the demand for TEGs to space application where the high price tag is justified by high reliability [13]. The materials require to have high electrical conductivity and low thermal conductivity in order to be considered as proper candidates for thermoelectric generation. The automotive industry is one the most attracting sectors for deploying TEGs. In the automotive industry, the objective is to integrate TEGs into ICEs with minimum pressure losses (in range of a few tens of millibars) and high efficiency. Moreover, the operating point of the engine should not be affected and the maximum temperature difference across the TEGs must not exceed the materials maximum operating temperature. Therefore, control systems for bypassing the excessive hot gases must be added to the system to protect the overload of engine cooling system under full-load condition, restrict the pressure drop under full-load condition and prevent temperature shock in thermoelectric modules [14]. The research for finding cost-effective, environmentally friendly and recyclable materials which qualify as thermoelectric materials for WHR is still ongoing. Several vehicle manufacturing companies such as BMW [15, 16], Ford [17], Renault [18], Honda [19] have investigated integrating TEGs for internal combustion engines. However, high manufacturing price and relatively low efficiency are the obstacles in development of TEGs for mass production in common applications such as ICE waste heat recovery.

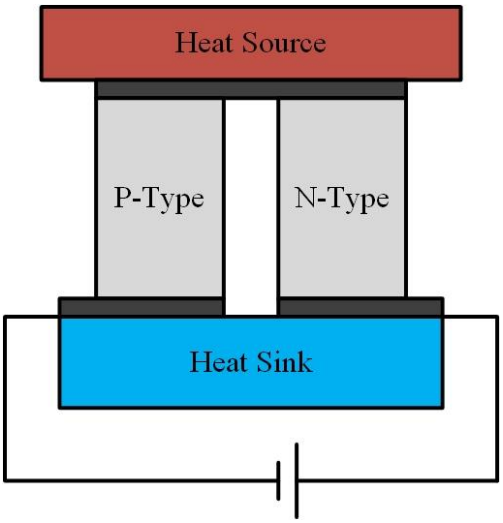

Fig. 2.3. *Operation principle of TEGs*

2.2.2 Stirling engine

Stirling engine is a closed-cycle regenerative heat engine, which is operated by cyclic compression and expansion of a working fluid in a cylinder between two heat reservoirs in order to convert heat energy to mechanical work. The Stirling engines are categorised as external combustion engines and are first introduced by Robert Stirling in 1816. As shown in **Fig. 2.4**, the working principle of Stirling engine is based on the expansion and contraction property of gases when heated and cooled, respectively. A fixed amount of working fluid (usually gaseous substances) is sealed between two cylinders that are held at different temperatures. Since the volume of the working fluid is fixed, temperature variation changes its pressure, resulting in expansion on hot cylinder and contraction in cold cylinder. The Stirling engines based on the configuration of their components are divided to four types of alpha, beta, gamma and double-acting. Several studies investigated application of Stirling engines for ICE waste heat recovery. The P-V diagram of a typical Stirling Engine is presented in **Fig. 2.5**.

Alfarawi et al. [20], investigated the integration of a small-scale beta type Stirling engine with the exhaust system in order to drive the alternator. Adopting a CFD approach, authors claimed that a power output of 1.5 to 2 kW is achieved at an ideal thermal efficiency of 40% from a heat source and a heat sink at 850K and 450K, respectively. Güven et al. [21], studied optimization and application of three types of Stirling engine for WHR from exhaust of a heavy-duty truck. They concluded that, Beta-type Stirling engine due to its higher dimensionless work output and moderate pressure ratio is the most appropriate configuration for WHR from exhaust gases in ICEs. Despite increasing the exhaust back-pressure and imposing additional weight to the truck, the designed Stirling engine improved the engines power output by 1.3%, reduced fuel consumption by 1% and generated around 3 kW. Kubo [22] studied various configurations of Stirling engine as a bottoming cycle for heavy-duty diesel engines and concluded that using Stirling engines for WHR in diesel engine is not economically attractive as they fail to match the performance of other applicable cycles such as organic Rankine cycle. In another study, Bianchi et al. [23] performed a thermodynamic analysis on three bottoming cycles for generating electrical energy from low to medium temperature heat sources and concluded that despite the promising performance of Stirling engine for high temperature sources (in order of 800 °C), it's been outperformed by organic Rankine cycle in terms of thermodynamic performance for exploiting low to medium heat sources ranging from 200 to 500 °C.

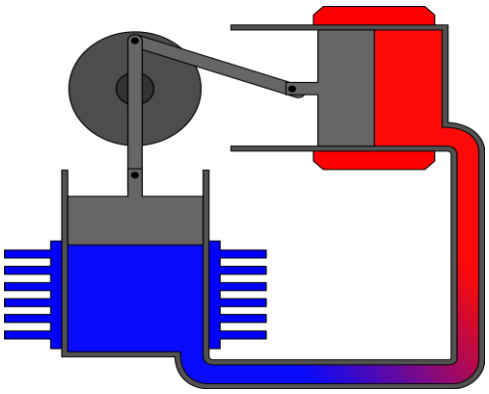

Fig. 2.4. *Alpha-type Stirling engine*

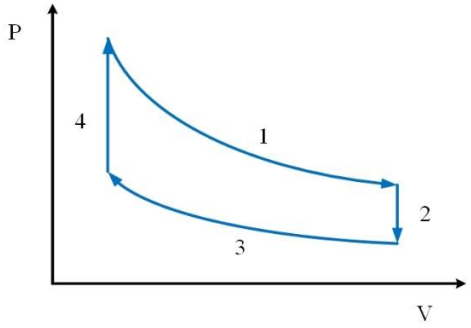

Fig. 2.5. *P-V diagram of a typical Stirling Engine*

2.2.3 Phase change material engines

Phase change materials (PCMs) are substances that encounter phase transition when heated or cooled. Due to their high capacity for storing thermal energy, they are also known as latent heat storage materials. The research on PCMs has received considerable attention for their application as a thermal energy storage (TES) material. For instance, their ability to store a large amount of energy is studied to regulate the temperature of lightweight buildings with low thermal mass in order to reduce their energy consumption [24, 25]. Other applications of PCMs include latent heat TES systems for heat pumps, thermal control of spacecrafts and solar engineering [26]. Zalba et al. [27] reviewed materials, applications and heat transfer

analysis of TES devices with PCM technology. Paraffin due to its high latent heat, chemical stability, low cost, non-toxicity and non-corrosive characteristics is one of the most promising PCMs for various applications [28].

PCM engines can be deployed for recovery of waste heat from low quality applications. They are taking advantage of the volume expansion of PCMs when changing from solid to liquid phase to generate electricity. The working principle of PCM engines is represented in **Fig. 2.6**. PCM engines consist of a hydraulic system, an electric system, a heat sink and a heat source (usually in the liquid form [29]). The PCM (e.g., paraffine mixture) is cyclically expanded and contracted by exposing it to the heat source and heat sink. The volume change in the PCM caused by the expansion and contraction is captured using the hydraulic system. The linear movement of the hydraulic system is used to produce electricity by deploying a generator. PCM engines are suitable for recovery of low-grade waste heat in the range of 25 to 95 °C and 2.5% conversion efficiency is reported when the temperature difference between the heat source and heat sink is 24 °C [29].

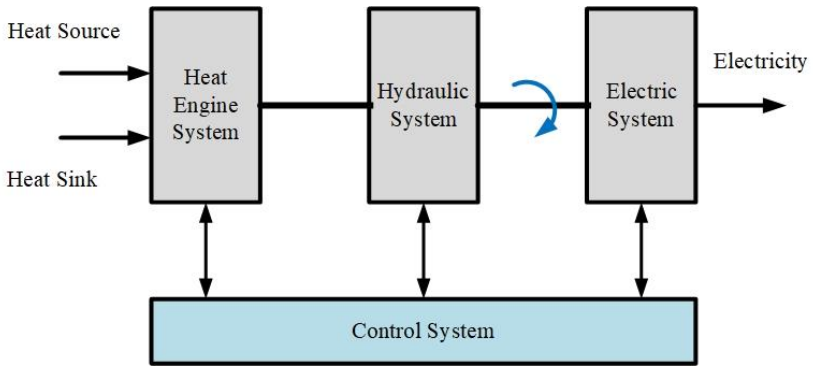

Fig. 2.6. *Working principle of PCM engines*

2.2.4 Carnot cycle

Carnot cycle is a thermodynamic cycle proposed by French physicist Nicolas Léonard Sadi Carnot in 1824. It is considered as an ideal cycle which defines the maximum achievable amount of efficiency by any thermodynamic engine or refrigeration system that converts heat into work or vice versa. A heat engine that undergoes Carnot cycle is referred to as Carnot heat engine. Although Carnot efficiency is impossible to be achieved in practice, it can put an upper limit on the maximum obtainable efficiency by other practical heat engines. In a Carnot cycle with T_H and T_C as the heat and cold reservoirs, respectively, a working media is circulated in a closed loop and experiences several state changes. However, since the Carnot cycle is a perfect theoretical reversible cycle, no entropy is generated during the cycle. The T-S diagram of the Carnot cycle is represented in **Fig. 2.7**.

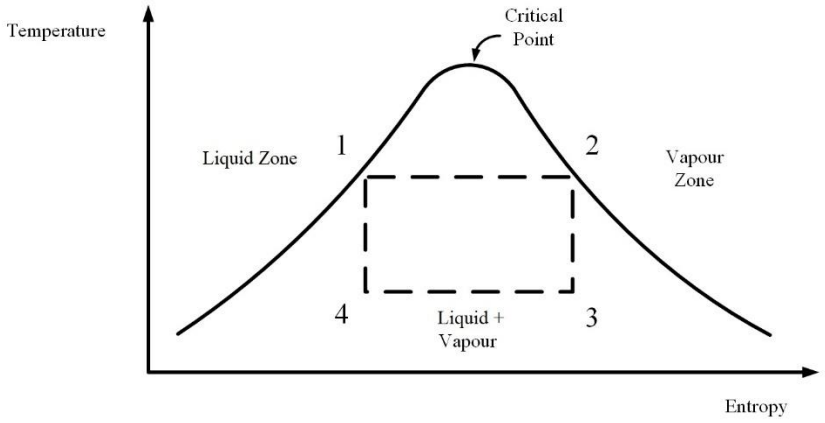

Fig. 2.7. *T-S diagram of Carnot cycle*

When the Carnot acts as a heat engine, it comprises following thermodynamic processes:

- Isothermal expansion (1-2): at the constant temperature T_H, heat is transferred from the hot reservoir to the working fluid.

- Isentropic expansion (2-3): in an adiabatic process the pressure of working fluid decreases and it expands resulting in reduction of temperature to T_C. In this process, the internal energy of working fluid is converted to the work on the surrounding.
- Isothermal compression (3-4): at the constant temperature T_C, heat is transferred from the working fluid to the low temperature reservoir.
- Isentropic compression (4-1): in this process in an adiabatic reversible process the work is done by surrounding on the working fluid. The pressure of the working fluid increases and its temperature returns back to T_H.

In Carnot cycle the entire cycle takes place in the two-phase liquid-vapor dome. Therefore, some drawbacks can be noted for its application in WHR from practical point of view. The fact that the isentropic compression happens in the two-phase mixture zone implies the need for a pump that is able to handle two-phase mixture which is currently impractical. Moreover, since the working fluid is not superheated, during the isentropic expansion two-phase mixture enters the expander, which increases the chance of corrosion and reduces the lifespan of equipment. Furthermore, since isothermal heat transfer is very difficult to achieve in real applications, Carnot cycle could not exist in reality.

2.2.5 Rankine cycle

Rankine cycle is an idealised thermodynamic cycle developed by Scottish engineer William J.M. Rankine in 1859 which converts heat to mechanical shaft work in order to generate electrical energy. It is the dominant method of electricity generation deployed in large thermal power plants across the world. Modern power plants by utilising the water as the working fluid in the Rankine cycle achieved efficiency of around 50% [30]. The thermal energy for deriving the cycle is mostly obtained from burning fossil fuels or nuclear fission.

The Rankine cycle uses the phase change between vapor and liquid in order to maximise the specific volume difference during the expansion and compression. The T-S diagram of the Rankine cycle is shown in **Fig. 2.8**.

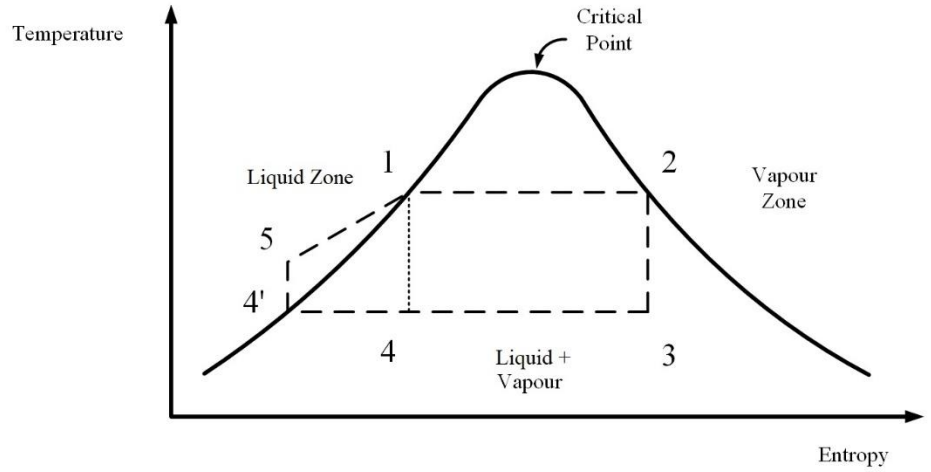

a)

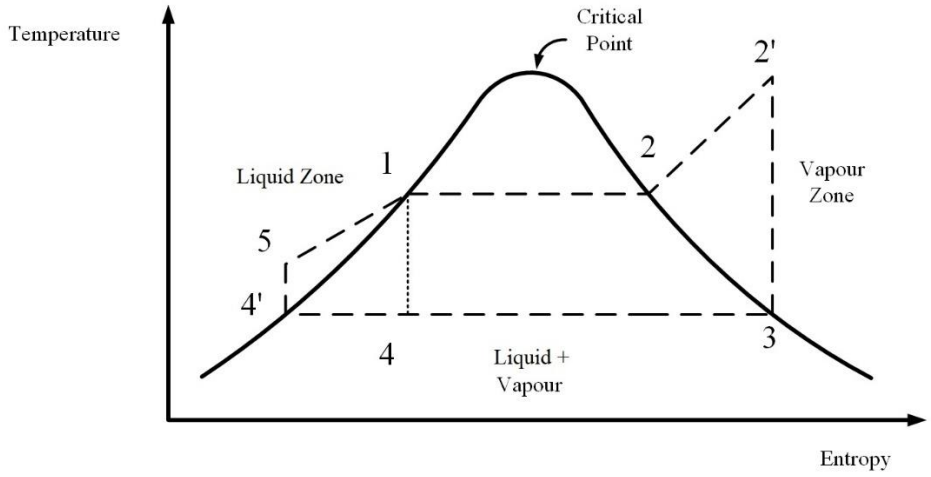

b)

Fig. 2.8. *T-S diagram of Rankine cycle a) without superheating b) with superheating*

The ideal Rankine cycle consists of the following thermodynamic processes:

- Isentropic compression (4′-5): the pressure of water increases in an adiabatic pumping process.
- Isobaric heat addition (5-2): the pressurized water enters the boiler, where it is heated in constant-pressure to obtain saturated vapor.
- Isentropic expansion (2-3): the pressurized saturated vapor expands in an adiabatic expansion process to generate power. This process results in decreasing the temperature and pressure of water.
- Isobaric heat rejection (3-4′): the wet vapor enters the condenser where it is cooled down in a constant-pressure process to achieve saturated liquid.

As illustrated in the T-S diagram of **Fig. 2.8**, in the Rankine cycles, the working fluid is pumped at the saturated liquid state 4′. Pumping the water at the saturated state reduces the risk of formation of cavity which can damage the pump and decreases the pumping work.

In an ideal Rankine cycle the pressure drops caused by the fluid friction is not considered and compression and expansion processes are assumed isentropic. However, in an actual cycle there is some irreversibility associated with the heat loss to the surrounding and pressure drops due to the friction. Hence, the work output of actual cycle is less than the ideal cycle. Although the efficiency of Rankine cycle is less than that of ideal Carnot cycle, it eliminates the practical drawbacks of the Carnot cycle. Therefore, it can be considered as the ideal cycle that can be approximated in practice.

In a Rankine cycle, the irreversibility can be reduced if the cycle is operated as close as possible to the hot and cold reservoirs. Therefore, one approach to prevent formation of liquid

droplets in the turbine and reduce the irreversibility is to superheat the vapor before the expansion process. During the heat addition the boiler temperature is limited by saturation pressure of the working fluid. At the saturation pressure increasing the temperature beyond the boiling point of substance results in superheating the vapor. As illustrated in **Fig. 2.8**, the process of heat addition to the pressurized water is further extended to point 2′, where it is superheated in constant-pressure to obtain superheated vapor.

Another approach to improve the efficiency of Rankine cycle is to increase its net produced work by increasing the pressure in the high-pressure region of the cycle (boiler) during the heat addition and reducing the pressure in the low-pressure region (condenser) during the heat rejection. In an actual power plant, the lifespan and efficiency of turbine is reduced if condensation happen during the expansion. When the pressure in the high-pressure region of Rankine cycle increases, the moisture content in the low-pressure region of the turbine also increases. In WHR applications from the high-grade heat sources elimination of the liquid droplets and increasing the vapor quality at the expander can be obtained by using the Reheat Cycle [31]. The Reheat Cycle can help to achieve the advantage of high-pressure in the cycle, yet avoid the excessive moisture in the low-pressure stage of the turbine. In this cycle the vapor is expanded to some intermediate pressures in a high-pressure turbine, then the vapor is reheated in the boiler again before enters the second low-pressure turbine. Although this method is beneficial for preventing the formation of liquid droplets it adds complexity to the expansion device in the cycle. Another variation of Rankine cycle is known as Regenerative Cycle. In Regenerative Cycle some of partially expanded working fluid is used to preheat the liquid entering the boiler, thus, increasing the efficiency of the cycle by increasing the mean temperature during the heat addition process [32].

In low to medium-grade WHR such as recovery of wasted heat in internal combustion engines the temperature is not enough to superheat the water at all conditions. This is due to the large operating range of the internal combustion engines. In other words, the heat source in the mobile application is not working under steady-state condition and mass flow rate and temperature of exhaust gases fluctuates during different driving conditions. Therefore, to adopt the cycle for the low to medium waste heat sources, alternative working fluids with lower boiling points should be considered.

2.2.6 Kalina cycle

Kalina cycle introduced by Dr. Alexander Kalina in 1984. It is an alternative to steam Rankine cycle which utilises a mixture of water and ammonia as a working fluid to change the thermodynamic properties of pure water. The main difference between Kalina cycle and conventional steam Rankine cycle is the change in temperature profile during evaporation and condensation that makes it more flexible with respect to fluctuation of the heat source. In this cycle water prevents the effect of nitridation in temperatures below 400 °C that can damage the equipment and in temperatures above 400 °C the amount of ammonia is far less than the threshold for causing any damage. The boiling and condensation temperature of working fluid mixture in Kalina cycle can be adjusted by manipulating the percentage of ammonia in mixture, thus as compared to steam Rankine cycle better efficiency in part-load situation can be achieved. Flammability of mixture is one of the disadvantages of the Kalina cycle and therefore, an intermediary fluid loop should be integrated to avoid contact of exhaust flows with the working fluid [33]. Another competitor of the Kalina cycle is the organic Rankine cycle which benefits from an organic working fluid in the cycle. Nemati et al. [34] carried out a comparison between the Kalina cycle and the organic Rankine cycle for

different operating conditions and reported that due to the lower pressure in the organic Rankine cycle, the material and sealing costs of the system is much lower than that of the Kalina cycle. Furthermore, the authors pointed out that in the Kalina cycle the output of turbine is a two-phase flow compared to superheated vapour in the organic Rankine cycle. They concluded that in all operating conditions the energy and exergy efficiencies of the organic Rankine cycle are more than that of the Kalina cycle.

2.2.7 Organic Rankine cycle

Organic Rankine cycle (ORC) has long been considered as a promising waste heat recovery technology that can be adopted for low to medium grade heat sources such as mobile applications [33, 35, 36]. The ORC is similar to the Rankine cycle but instead of water, an organic fluid with lower boiling temperature and higher molecular weight is used in the cycle. As shown in **Fig 2.9**, the basic ORC is comprised of several components including evaporator, expander, condenser and pump. Some other components such as accumulator and regenerator can be added to the configuration to increase the efficiency of cycle or improve the working condition of basic components. The principle of ORC is to evaporate an organic fluid in a closed cycle and use the superheated vapour pressure as the electromotive force to produce mechanical energy in the expander. After expansion, the vapour is cooled down in the condenser to saturated liquid temperature and then pumped back to the evaporator.

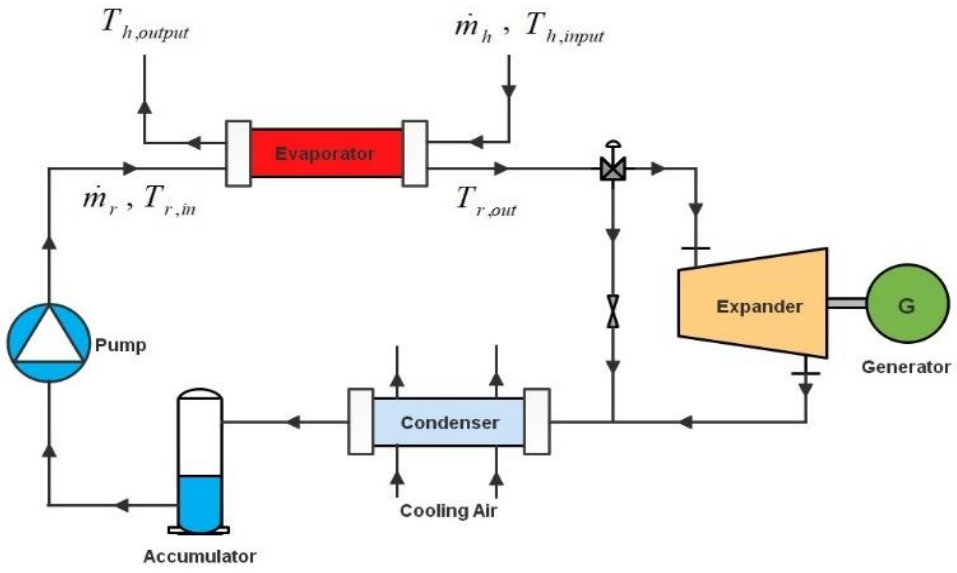

Fig. 2.9. *Conceptual schematic of ORC system*

The ORC has several advantages over the traditional steam Rankine cycle for low to medium WHR. Firstly, owing to the lower boiling point of the working fluid the evaporation process requires less heat and it can happen in lower pressures. Secondly, the risk of turbine blade erosion is substantially reduced. This is because the expansion process happens at the vapor region. However, superheating should be kept as low as possible in the evaporator since risk of decomposition of organic fluid at higher temperatures exists [37]. Thirdly, due to the smaller temperature gradient and pressure drop between the evaporation and condensation processes in the ORC, there is no need for a multi-stage turbine and a single stage turbine can be deployed [33]. Lastly, the higher molecular weight of organic fluid compared to the water, reduces the required pumping work in the cycle and thus, improves the overall efficiency of the cycle [38]. These advantages enable the ORC to be exploited for recovery of energy from low to medium grade heat sources. Biomass power plants, geothermal power plants and solar power plants are some examples of the ORC application [33].

The ORC is characterised by its relatively high efficiency and low cost. Modularity, versatility, maturity of components (similar to refrigeration system) and ability to recover waste heat from small to moderate temperature differences are characteristics of the ORC technology that made it a preferable choice for recovering energy from ICEs. Therefore, since organic Rankine cycle has the highest feasibility potential for recovering energy from highly dynamic waste heat sources, this cycle is chosen in this study for further investigation with focus on modelling and control of the cycle.

2.3 Summary

In this chapter several waste heat recovery technologies are introduced and their advantages and drawbacks for adopting them for mobile applications are pointed out. The findings of this chapter can be summarised as follows:

- Reducing the greenhouse gas emissions requires the transformation of the current energy system or enhancement of their efficiency. Internal combustion engines used in mobile applications have the greatest share of greenhouse gas emissions and are likely to be used for many years. Therefore, it is important to enhance their efficiencies.
- The two main sources of waste heat in internal combustion engines are the medium-grade exhaust gases and low-grade coolant. Other sources of the waste heat are exhaust gas recirculation and charge air cooler which have lower energy content. Although both of the primary sources of waste heat have similar energy content, the higher grade of engine exhaust makes it more thermodynamically attractive for WHR purposes.

- Some of the current waste heat recovery technologies are either too expensive due to deploying rare and expensive materials or have low efficiencies and are not feasible for adopting in automotive applications.
- The Rankine cycle is a practical alternative of ideal Carnot cycle. It is currently being used for waste heat recovery in industrial applications with high-grade waste heat. However, due to the large operating range of ICEs, the waste heat from ICEs could not superheat the water in Rankine cycle at all driving conditions. Therefore, this could result in a reduction in efficiencies and formation of liquid droplets which can cause component damage.
- Organic Rankine cycle is an alternative to the Rankine cycle which can be adopted for waste heat recovery from low to medium range heat sources. It utilises an organic fluid with lower boiling temperature and higher molecular weight which can be superheated across all the operating range of ICEs.
- Implementing ORC as the waste heat recovery method for the ICE has several advantages as compared to the other methods, including superior efficiency, reduced pumping work, modularity, versatility, maturity of components (similar to refrigeration system) and ability to recover waste heat from small to moderate temperature differences. Therefore, in this study, ORC is considered for further investigation.

Chapter 3: Organic Rankine cycle

3.1 Previous research on ICE-WHR

Investigations on the ORC as a waste heat recovery method for ICEs started during the energy crisis of 70's. Thermoelectron Corporation and Mach Trucks started research on developing ORC for internal combustion engines waste heat recovery in 1970s [39-41], and thereafter, companies such as Cummins [42], BMW [43-45] and AVL [46, 47] started research on implementing ORC in their projects. Cummins reported that by implementing ORC on a diesel engine efficiency increased from 47.5% to 51%. The research was part of the US Department of Energy (DOE) "SuperTruck" program with approximate cost of $284 million [42].

An extensive literature review revealed that several studies reviewed the development of ORC as a waste heat recovery method for ICEs since 2011 [10, 48-53]. These studies mostly compared the ORC with other applicable technologies, such as Rankine cycle, Kalina cycle, TEGs and turbochargers. The superior conversion efficiency of ORC along with features such as availability of components, high thermal efficiency, low pressure and flexibility in handling low to medium grade heat sources draw the attention of researchers to the ORC and made it one of the research-intensive subjects in the waste heat recovery applications. The reviews on ORC also suggest that selection of the cycle architecture or working fluid depends on the characteristics of the heat source and a thermodynamic analysis should be carried out at the design stage of the cycle. Furthermore, for successful integration of the ORC as a bottoming cycle for the ICEs, the safety of system must be ensured. Therefore, a control system needs to be designed for the ORC system that not only ensure the system safety but also regulate its work output.

3.2 ORC architecture

There are several ORC architectures applicable to WHR systems recovering waste heat from various heat sources. Single-stage regenerative ORC (SRORC), double-stage regenerative ORC (DRORC), reheat ORC (RORC), ORC with recuperator and double loop ORC (DLORC) are the variant architectures of the ORC [53]. In SRORC, to increase the thermal efficiency of cycle, a two-stage turbine is used and a portion of expanded vapour in the turbine is redirected to the feed water heater [54]. DRORC architecture is similar to the SRORC, but utilises two feed water heaters (in series) to enhance the cycle efficiency and reduce the load on evaporator [55]. The extracted vapour is taken out from the turbine and fed to both water heaters. The schematics for SRORC and DRORC architectures are represented in **Figs. 3.1** and **3.2**, respectively.

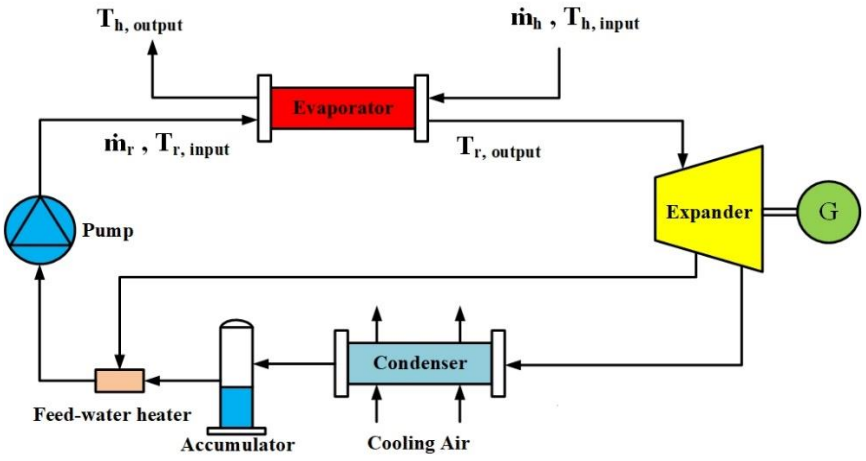

Fig. 3.1. *Schematic of single stage regenerative ORC*

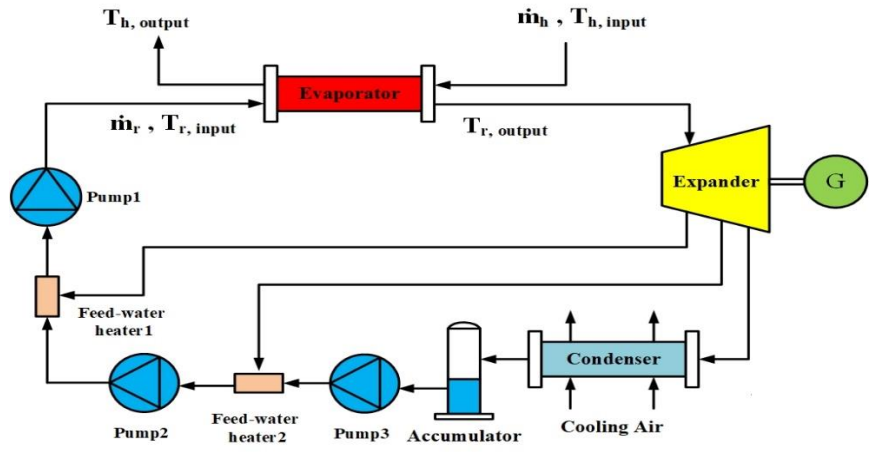

Fig. 3.2. *Schematic of double-stage regenerative ORC*

The schematic of reheat ORC architecture is shown in **Fig. 3.3**. As shown in **Fig. 3.3,** Reheat ORC takes advantage of two turbines; the vapour is fed to the first turbine and then is returned back to the evaporator before feeding the second turbine. This process reduces the moisture content of the vapour at the final stage of expansion process [53]. In the ORC with recuperator architecture, a recuperator is deployed between the high-pressure and low-pressure sides of the ORC. The expanded vapour enters the recuperator to increase the temperature of pressurised working fluid after the pump [56, 57]. The schematics of ORC with recuperator architectures is represented in **Fig 3.4**.

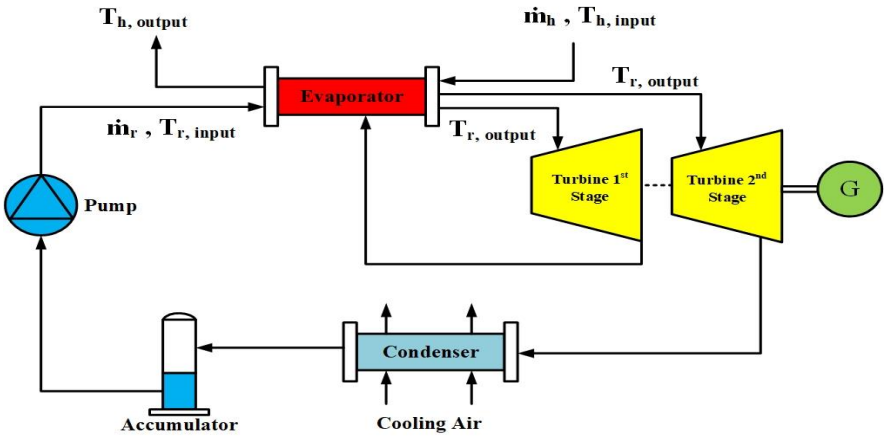

Fig. 3.3. *Schematic of reheat ORC*

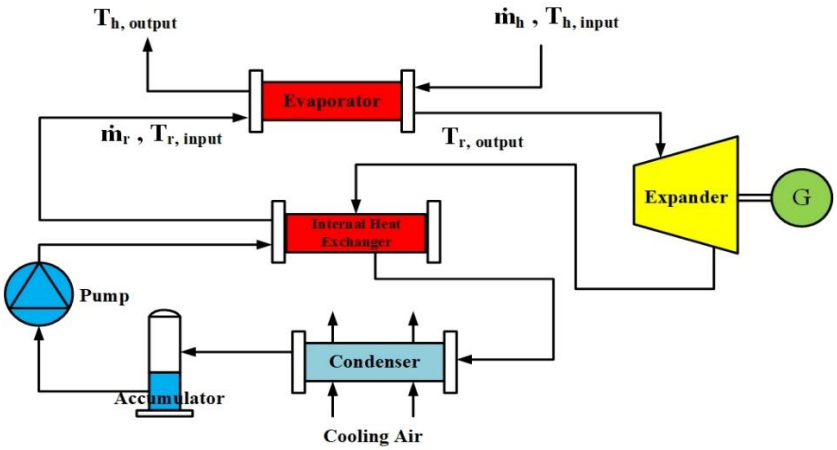

Fig. 3.4. *Schematic of ORC with recuperator*

Fig. 3.5 represents the schematic for DLORC architecture. DLORC takes advantage of a high-temperature loop and a low-temperature loop. The High-temperature loop is used to recover the wasted energy from the main source and the low-temperature loop is used to recover the energy of jacket cooling water as well as the energy dissipated from condenser of high-temperature loop [58, 59].

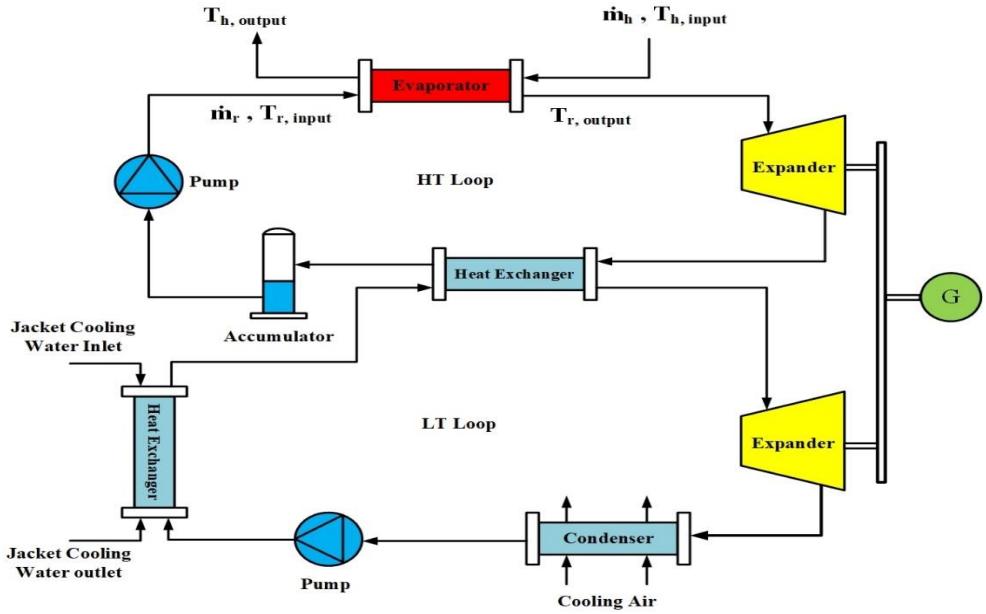

Fig. 3.5. *Schematic of dual loop ORC*

In applications of WHR from internal combustion engines, SRORC, DRORC and RORC are not generally suitable architectures, because of the complexity of the expander. However, ORC with recuperator architecture can be deployed to preheat the working fluid entering evaporator. This cycle will be beneficial as it reduces the amount of heat required for vaporizing the working fluid in the evaporator. Furthermore, a heat transfer loop (using a separate thermal oil loop) can be deployed in the cycle to reduce the transients of exhaust gases. In this architecture, the heat from exhaust gases is transferred to the thermal oil in a separate loop, and then, the heated thermal oil is fed to the ORC's evaporator. The thermal oil acts as a buffer which reduces the temperature fluctuation of the heat source.

3.3 Working fluid selection

Selection of the optimal working fluid for the ORC system is of prominent impotence as it has a critical impact on the performance of the system [60]. As mentioned in section 2.1.2, ICEs are categorized as low to medium grade waste heat sources. In applications of WHR in ICEs since the temperature and mass flow rate of the heat source is not enough to superheat the water in the Rankine cycle at all conditions, utilizing the organic working fluids due to their lower boiling temperature and higher molecular weight is preferable [38]. In part-load condition where the temperature and mass flow rate of heat source fluctuates, ORC can tolerate up to 10% fluctuation in maximum power output [61], therefore, ORC has a wider working range compared to the steam Rankine cycle under unsteady heat source. Most of early studies on the ORC deployed refrigerants such as R11 or R13 as the working fluid in the cycle which have high ozone depletion potential (ODP). However, environmental concerns restrict the use of substances with high ODP or global warming potential (GWP). Therefore, since the performance of ORC is strongly affected by the selected working fluid,

a preliminary study of various working fluids needs to be carried out based on the thermodynamic performance, industry legislation, availability and cost of the substance, ODP and GWP. The substances need to have certain properties to be considered as a potential working fluid for the ORC application. The desired properties include adequate temperature profile match with the heat source, low boiling point, high auto-ignition temperature, chemical stability, high flash point, low ODP and GWP, etc.

Several studies investigated the selection of most suitable working fluid for the ORC and concluded that the utilizing working fluids with higher critical temperature improves the system thermodynamic efficiency [62-66]. However, the density of vapour decreases at higher critical temperatures and this results in higher system costs; therefore, in addition to the thermodynamic performance of the system, the practical design of the ORC should be considered and the working fluid selection should be integrated in the ORC design process [67].

Shu et al. [68], established a multi-approach evaluation system and used four organic substances (R123, R245fa, R134a and R32) to comprehensively evaluate the performance of ORC in WHR. The outcome of their research suggests that the performance of ORC increases in supercritical mode. Moreover, the economic performance of ORC with R134a and R32 improves when it is operated under supercritical pressures; however, the authors concluded that R123 and R245fa are the most appropriate substances for ICE-WHR. Wang et al. [66], analysed the performance of potential working fluids for ICE-ORC using a thermodynamic model of cycle developed in MATLAB linked to REFPROP. The authors concluded that despite better thermodynamic performance of R11, R141b, R113 and R123, the most environmental-friendly substances for ICE-WHR applications are R254fa and R245ca.

Glover et al. [69], compared the performance of 18 working fluids with critical pressure below 70 bar for automotive WHR by deploying a thermodynamic ORC model considering the boundary conditions. The authors concluded that there is a direct correlation between the critical temperature of substance and the expansion or density ratio, and substances with higher critical temperature will generally perform better as they result in higher expansion ratio. Furthermore, they pointed out that the coolant temperature is not enough to allow supercritical expansion and for meeting the minimum temperature for expansion the exhaust heat is required.

From study of literature on the selection of working fluid for ORC systems it is apparent that, despite the broad range of available substances, there is not a single optimal working fluid for all applications of the ORC and only a few of the available substances are deployed in commercial ORC applications [67]. Therefore, in this study R134a and R245fa due to their suitable critical temperature, appropriate temperature profile matching with the heat source, low cost, relatively high auto-ignition temperature, zero ODP and wide availability are chosen for investigation of ORC waste heat recovery system in simulation and practice. The properties of these substances are listed in **Table 3.1**.

Table 3.1 *– Properties of selected working fluids*

Working fluid	**Critical temperature (K)**	**Critical pressure (MPa)**	**Boiling temperature (K)**	**C_p $(kJ.kg^{-1}.K^{-1})$**	**Critical density $(kg.m^{-3})$**	**Molar mass $(kg.kmol^{-1})$**	**Auto-ignition temperature (K)**	**ODP**	**GWP**
R134a	374.2	4.059	247.08	1.280	511.90	102.03	1043.15	0	1200
R245fa	427.2	3.64	288.05	1.318	519.43	134.05	685	0	950

3.4 Components of the ORC

The ORC cycle is comprised of four main components: pump, evaporator, expander and condenser. The cycle may also take advantage of some other auxiliary components such as valve, accumulator, etc, for control purposes, preventing damage to main components or improving the cycle efficiency. Selection of the components of the ORC mostly depends on the application and the heat source characteristics. In automotive applications, however, the size and weight of the components should be taken into account at the design stage since excessive weight or size has a negative impact on the fuel consumption of the vehicle [70] and increases the frictional forces acting on the vehicle [71]. A review of the main components of the ORC is presented in the following sections.

3.4.1 Pump

The ORC architecture is divided to two zones based on the pressure level of the organic fluid. The organic fluid needs to be pressurized before entering the evaporator and its pressure decreases after the expansion process. Therefore, two zones with high-pressure and low-pressure can be distinguished within the cycle. In order to meet the pressure requirements of the high-pressure zone a pump is deployed within the cycle. Selection of the pump depends on the pressure and flow rate demands of the cycle. Additionally, due to the stringent regulations of automotive industry, in mobile applications compatibility with working fluid and being leak proof are extra features that are required. Centrifugal [72, 73] and volumetric pumps [74-76] are the most common types of the pumps used in the ORC for various applications. Due to the fluctuating nature of the heat source in ICEs the flow rate of pump is usually used to control the superheating at the evaporator outlet. Therefore, the pump needs

to be able to deliver the organic fluid in low flow rates while keeping the pressure at the required level.

The pump can be severely damaged during the operation of the cycle through a phenomenon called cavitation. Cavitation is formation of small vapour-filled cavities in the pump inlet at low pressures and usually happens when the working fluid gets close to its saturation state. Because of the lower latent heat of organic fluids, cavitation results in more serious negative consequences on the pump in the ORC as compared to the water in Rankine cycle [77]. Furthermore, cavitation reduces the efficiency of the ORC by reducing the volumetric flow and increasing the vibrations that results in the higher input energy loss of the pump [78]. Therefore, some extra measures should be taken at the design stage to prevent cavitation in the pump. The most common method is deploying a liquid receiver between the condenser and pump to ensure that no vapour-filled cavities are forming in the pump.

3.4.2 Evaporator

Evaporator is considered as the most critical component of the ORC in a waste heat recovery system. When dealing with low-capacity heat source in kW range such as internal combustion engines, the governing dynamics of system is dominated by behaviour of the heat exchanging components. Additionally, due to the high thermal inertial of the evaporator, as compared to the other components of the ORC system, it dominates the dynamic response of the system. While the condenser (as a heat exchanging component) also affects the heat transfer greatly, the impact of evaporator is of much greater importance. This is because the evaporator is located in the high-pressure region of the cycle and heat transfer from the exhaust or other available resources of heat takes place in this component. Therefore, selection of the evaporator not only impacts the heat transfer efficiency, but also has a

remarkable effect on the ORC economy [79]. Nonetheless, operating conditions of the cycle, heat transfer mechanism (single-phase or two-phase), characteristics of working fluid, and heat transfer requirements of the ORC are the crucial criteria in the evaporator selection process [80].

Shell and tube [81, 82] and plate heat exchangers [38, 75] are the most common types of heat exchangers in the ORC for WHR applications from low-grade heat sources. Walraven et al. [83] compared the performance of shell and tube and plate heat exchangers in the ORC applications and concluded that the ORCs utilizing plate type heat exchangers are performing better than the ORCs with shell and tube heat exchangers. In mobile applications of the ORC, limitations of size and weight of the components should be considered at the design stage. Therefore, compact and lightweight heat exchangers due to their influence on the economy of the system are preferred. Plate heat exchangers are highly compact and acquiring the benefit of a large heat transfer area, hence, they are able to recover maximum amount of heat from the heat source [72]. Furthermore, minimum pressure drop, minimum risk of internal leakage and straightforward maintenance are the features that make plate heat exchanger a proper choice for ORC in mobile applications [80]. Some types of evaporators used in ORC applications are shown in **Fig. 3.6**.

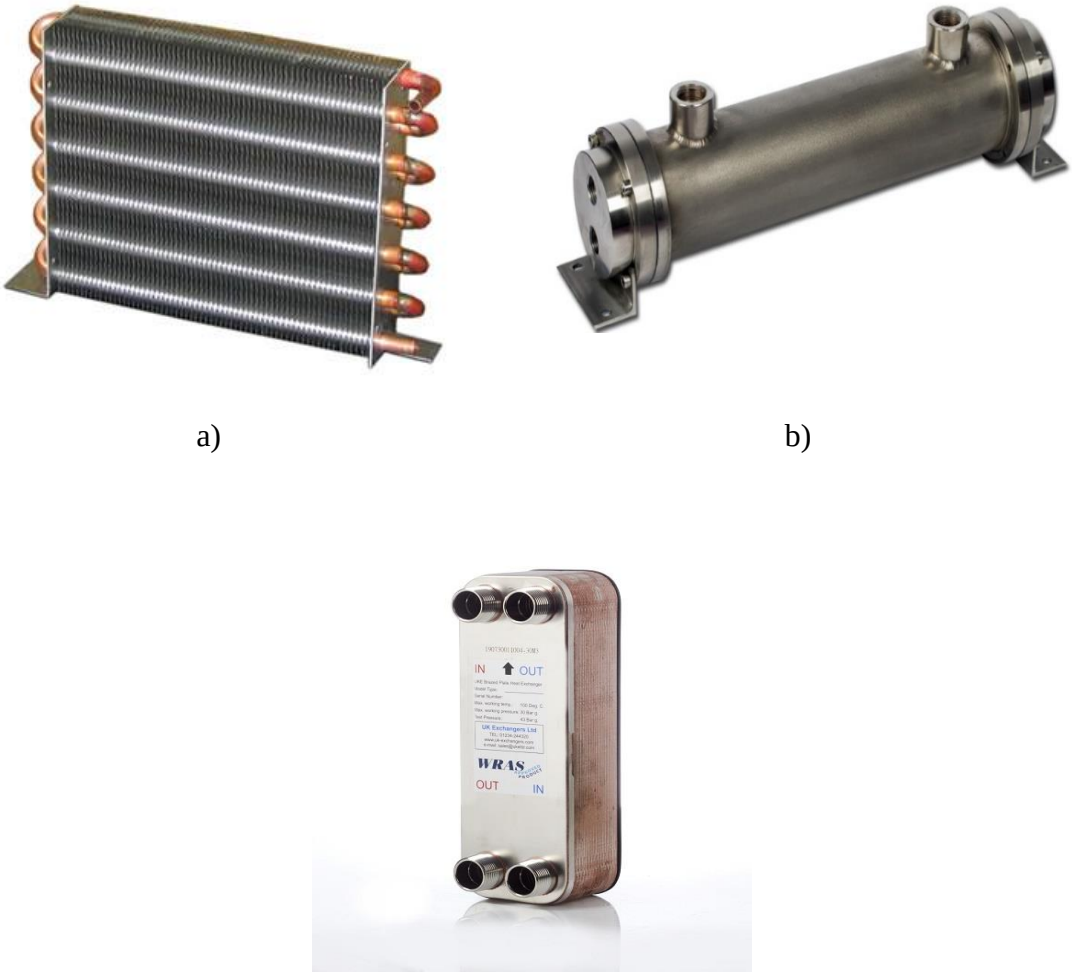

a) b)

c)

Fig. 3.6. *Some types of heat exchangers a) Finned tube heat exchanger [84] b) shell and tube [85] c) Brazed Plate heat exchanger [86]*

3.4.3 Expander

Expander is a device which converts the heat energy into useful rotational mechanical energy. There are several types of expanders available in the market for small-scale ORCs that can be categorized to two main types of velocity (i.e., turbomachine expanders) and volumetric (e.g., screw, scroll and reciprocating piston) expanders [87]. Since expanders are relatively expensive devices, selection of the expander type plays a vital role in the overall performance and cost of the ORC for small scale ORC applications. Selection of an appropriate expander

for the cycle strongly depends on the criteria such as type and characteristics of the working fluid, system size and weight, power range, required pressure ratio, lubrication requirements, complexity, reliability, availability, noise and safety. [71, 87, 88].

Velocity type expanders can be categorized as the radial and axial flow turbines. While the axial flow turbines are preferred for the applications with high mass flow rates and low pressure ratios, radial flow turbines are more appropriate for the applications involving low mass flow rates and high pressure ratios [71]. Velocity type expanders, are usually deployed for WHR applications such as CHP with the expected regenerative power capacity in the range of 50 kW [87]. Moreover, due to the high cost and high rotational speed of these type of expanders (i.e., turbine) they are not viable options for the plants with power outputs less than 50 kW [71], and hence, they are not commercially available with a few exceptions for experimental purposes. Fiaschi et al. [89], studied the preliminary design of turbo-expanders for ORC and investigated the behavior of different working fluids. The results revealed that among the selected working fluids, the ORC with R134a as the working fluid achieved the highest efficiency of 0.85. Bao et al. [88], reviewed the working fluid and expander selection for ORC and mentioned the potential of one-stage radial inflow turbines for ORCs with higher pressure and lower pressure ratio, however, they pointed out the leakage of organic fluid to the atmosphere and overspeed issues of turbine at the peak load are among the problems of turbine expanders.

An alternative type of expanders that could be used in small-scale ORC applications is the volumetric type expander which is also known as positive displacement expanders. As the name implies, volumetric expanders are featuring a fixed volumetric ratio. Compared to the velocity type expanders, volumetric type expanders such as screw, scroll and reciprocating

piston expanders, generally acquire the benefit of operating under lower flow rates, higher pressure ratios and much lower rotational speeds, and therefore, are a preferred choice for low grade heat recovery in the range of 1-50 kW [71]. Nonetheless, considering the similarities between the ORC and refrigeration systems, most of the volumetric expanders studied in the literature are modified and reversed type of compressors used in the refrigeration systems.

Screw expanders are volumetric type expanders which comprise a helical rotor with an approximate 50 μm clearance. There are two types of screw expanders: synchronized and unsynchronized. Screw expanders are characterized with their wide power output range of 1.5 kW to 1 MW [90-94] and the isentropic efficiency ranging between 20% to 70% [95-97]. Despite ability to handle two-phase region, because of higher manufacturing cost and high risk of working fluid leakage, this type of expander is not usually recommended for ORC applications with the rated output power less than 10 kW [87, 88, 98]. Furthermore, due to their relatively high rotational speed they may need a speed reduction gearbox which increases the cost of plant [87]. Also, lubrication of unsynchronized expanders escalates the complexity of the system by adding an external lubrication loop to the expander while reducing the risk of working fluid leakage [71].

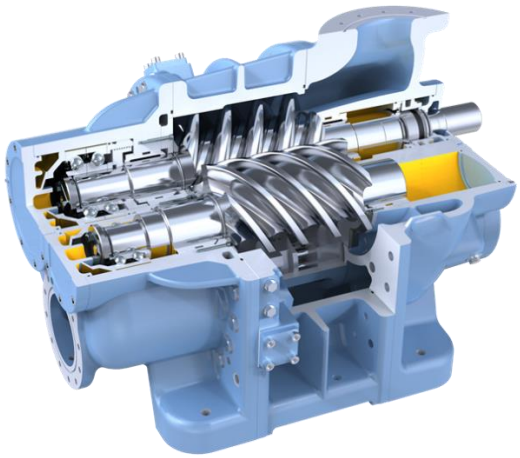

Fig. 3.7. *Twin screw expander [99]*

Piston expanders are another type of volumetric expanders with applications in small scale CHP systems, WHR in ICEs and refrigeration cycles. The efficiency of piston expanders is usually lower than 50% [100-102]. The reported operating temperature range and pressure of piston expander is ranging from 380 to 560 ℃ and 9 MPa, respectively [102-104]. The lower speed of piston expanders (600-2000 rpm) as compared to the screw expanders, eliminates the need for a gearbox and expander can be directly coupled with the generator [105]. However, lubrication requirements, possibility of leakage losses and high manufacturing complexity makes it a less attractive option among other types of volumetric expanders, and restricts its commercial production for small-scale ORC systems.

Scroll expanders are the most widely used volumetric expanders for small-scale ORC applications with maximum reported expander output of 12 kW [106]. Scroll expanders comprise of two spirals and have a fixed built-in volume ratio. They are characterized by their simple structure, low cost, wide availability and reduced number of moving parts. The isentropic efficiency of scroll expanders is reported between 38% to 86% in the literature [107, 108]. Due to the similarities of ORC with refrigeration cycles scroll compressors can

be restructured and deployed as scroll expanders [71]. Scroll expanders can be categorized to two groups of compliant and cinematically constrained scroll expanders. Compliant scroll expanders require lubrication during operation. In contrast, cinematically constrained scroll expanders, due to their linking mechanism between the two spirals can operate without lubrication. Moreover, since in the design of cinematically constrained scroll expanders the inlet and exhaust valves are eliminated, they can operate with lower noise and better durability [109]. However, to prevent internal leakage sealing is required.

3.4.4 Condenser

The condenser is a heat exchanger which is responsible for removing the excessive heat from the working fluid through an isobaric heat transfer process and condense it to the liquid form. The working fluid exits the expander in form of vapour or mixture of the liquid and vapour. In order to ensure that the pump is supplied with liquid, the excessive energy of the working fluid needs to be removed by the condenser. This energy is transferred to a cooling medium such as water or air. In the ORC applications two types of condensers based on their cooling medium can be distinguished: water-cooled condensers and air-cooled condensers. The former type is mostly used for the ORC applications which have access to consistent supply of water. Plate type heat exchangers are commonly used as water-cooled condensers [74-76]. The later type is usually used where there are limitations in terms of water supply. Finned tube heat exchangers are the most frequently deployed air-cooled condensers in the literature [110-112]. The condenser selection criteria depend on factors such as the amount of cooling required, the size and weight of plant and type of the cooling media. Due to elimination of the secondary cooling water loop, air-cooled condensers are preferred over the water-cooled condensers.

3.5 Control of the ORC

The research about adopting the ORC for harvesting energy from internal combustion engines is mostly dedicated to choosing the best architecture [113], working fluid and expander selection [88] and modelling [114, 115]. Publications about thermal management and control of the ORC are scarce, and not usually supported by experimental results. Furthermore, control of high-pressure part of the ORC adopted for recovering energy in automotive applications is not a trivial task. First, the heat source transient behaviour (in terms of mass flow rate and temperature) makes the operation of the cycle very different from a typical steam Rankine cycle. Second, automotive regulations impose several constraints for working fluid selection. Third, the size and weight of components are constraints that should be addressed at the design stage of the ORC. Lastly, a reliable control system is required to ensure the safety of the system by keeping the system parameters within the limits and maximise the heat recovery efficiency [116].

An important technical issue to address when designing the ORC system for mobile applications is the large range of operating condition and resulting thermal power fluctuation of the heat source due to driving conditions. For example, mass flow rates and temperatures of exhaust gases fluctuate with load condition and slope of the road [117]. In order to mitigate the effect of unsteady heat source in the ORC system, strategies such as controlling the vapour temperature at the evaporator outlet and using thermal energy storage (TES) devices can be considered to prevent the component damage and increase the efficiency of the WHR system [118]. In the ORC system, typical objectives of a control system in the high-pressure part of the cycle are to control the evaporator outlet temperature (superheating) by adjusting the pump speed and maintaining the required pressure by changing the expander speed [119].

In [74] the authors proposed three different control strategies to control superheating and evaporating temperature by adjusting pump speed and expander speed as the manipulated variables, respectively. Two independent PI controllers deployed to examine the performance of the control strategies. The best performance achieved from the optimized evaporating temperature strategy; however, the performance of the controller drops as the operating condition changes from the nominal condition.

Endo et al. [120] studied a distributed control system using two proportional controllers with feed-forward pressure and temperature terms from the evaporator outlet for an ORC system. In their study, the outlet temperature of evaporator manipulated using the pump speed and vapour pressure adjusted by changing the expander speed. In [121], Peralez et al. designed a gain scheduled PID controller combined with a nonlinear feed-forward action computed from a reduced-order model of the high-pressure region of the ORC system to control superheating at the evaporator outlet. More recently, authors in [122] deployed offline dynamic programming and online optimization techniques to maximise the power production of a diesel-electric railcar. Hou et al. [123] applied a generalized minimum variance controller (GMVC) to a 100 kW ORC system to control the outlet temperature of evaporator, power, condenser outlet temperature and throttle pressure. However, the stochastic disturbances in the system have not been considered in their proposed control scheme.

Zhang et al. [110] investigated a multi-variable linear quadratic regulator (LQR) coupled with a PI controller and an extended observer. This control scheme is developed based on the linear state-space model of the ORC system. Liu et al. [124] developed adaptive linear model predictive control (LMPC) and nonlinear model predictive control (NMPC) . The controllers in their study are designed based on a reduced-order moving boundary (MB) model of the

ORC system using ethanol as the working fluid. The authors pointed out the superiority of both control methods in terms of set-point tracking and disturbance rejection as compared to a tuned PID controller, but it should be noted that this improvement is achieved at the price of higher online computations, because both LMPC and NMPC require the online iterative solution of optimal control problem.

Despite high potential of employing the ORC for increasing the efficiency of internal combustion engines, implementation challenges such as developing non-toxic and non-corrosive organic fluids, designing high efficiency expander capable of withstanding high pressures and obtaining safe and efficient system operating points by utilising an effective control system have limited the commercial usage of this technology. Therefore, to adopt the ORC for mobile applications, the study of agile and efficient real-time controllers for the cycle should be emphasized to ensure the safety of system and maximise its performance in simulation before the experimental stage.

In order to address the objectives of this thesis the rest of this study is organized as follows: In chapter 4, the model for all components of the ORC is presented. Since the evaporator unit dominates the dynamic response of the ORC cycle, in chapter 5, a novel neuro-fuzzy model of this unit is presented and its performance is compared to the conventional numerical models. The neuro-fuzzy model of the evaporator is integrated with the model of other components of the ORC and in chapter 6, an agile neuro-fuzzy controller based on the inverse dynamics of the ORC cycle is developed to ensure the safety of the cycle and maximise its performance.

3.6 Summary

In this chapter initially various architectures of ORC are reviewed and their suitability for integration as a bottoming technology for waste heat recovery in internal combustion engines is discussed. Furthermore, the criteria for selection of the appropriate ORC working fluid for waste heat recovery are investigated. Moreover, selection of the main components of the ORC and their applicability for mobile applications is discussed. The findings of this chapter are summarised as follows:

- The superior conversion efficiency and compatibility with low to medium temperature heat sources are among the advantages of the ORC that makes it a viable option for waste heat recovery in mobile application.
- The reviews suggest that selection of the cycle architecture mostly depends on the heat source characteristics. In applications of WHR from internal combustion engines, SRORC, DRORC and RORC due to the complexity of the expander are not generally suitable architectures. However, ORC with recuperator architecture can be deployed to preheat the working fluid entering evaporator. This cycle will be beneficial as it reduces the amount of heat required for vaporizing the working fluid in the evaporator.
- Despite the broad range of available substances, there is not a single optimal working fluid for all applications of the ORC and only a few of the available substances are deployed in commercial ORC applications. The desired properties of working fluid include adequate temperature profile match with the heat source, low boiling point, high auto-ignition temperature, chemical stability, high flash point, low ODP and GWP.

- In automotive applications of the ORC, the size and weight of the components should be taken into account at the design stage since excessive weight or size has a negative impact on the fuel consumption of the vehicle.
- Selection of the pump depends on the pressure and flow rate demands of the cycle. In mobile applications compatibility with working fluid and being leak proof are extra features that are required. Since the flow rate of pump is usually used to control the superheating at the evaporator outlet, the pump needs to be able to deliver the organic fluid in low flow rates while keeping the pressure at the required level.
- Due to the high thermal inertial, the evaporator dominates the dynamic response of the system. Plate heat exchangers are highly compact and have a large heat transfer area, hence, they are able to recover maximum amount of heat from the heat source. Furthermore, minimum pressure drop, minimum risk of internal leakage and straightforward maintenance are the features that make plate heat exchanger a proper choice for ORC in mobile applications.
- Selection of the expander type plays a vital role in the overall performance and cost of the ORC for small scale ORC applications. Scroll expanders are the most widely used volumetric expanders for small-scale ORC applications with maximum reported expander output of 12 kW.
- The condenser selection depends on factors such as the amount of cooling required, the size and weight of plant and type of the cooling media. Air-cooled condensers are preferred over the water-cooled condensers since they do not require a secondary cooling water loop.

- In the ORC system, typical objectives of a control system in the high-pressure part of the cycle are to control the evaporator outlet temperature (superheating) by adjusting the pump speed and maintaining the required pressure by changing the expander speed.

Chapter 4: Modelling the components of ORC

In this chapter models of components in the ORC system are presented. The objective is to create an agile control-oriented ORC model that can be used for real-time control purposes. It should be noted that while the model of some components such as pumps and expanders are readily available in the literature, the correct representation of the components which determine the dynamic response of the ORC (i.e., heat exchangers) is a challenging task. Therefore, the modelling techniques for these components will be emphasized in this study.

4.1 Pump model

In the ORC waste heat recovery system, the pump is responsible for pressurizing the working fluid and providing the required mass flow rate through the cycle. Depending on the mass flow rate and pressure requirements centrifugal and volumetric-type pumps such as diaphragm and piston pumps can be utilized. However, in automotive applications, other requirements such as being leak-proof, ability to deliver lower mass flow rate at higher pressures and compatibility with the organic working fluid should be met. In this study, among the available options a diaphragm pump is selected for the ORC system. The enthalpy of working fluid at the evaporator outlet $H_{p,o}$ and the pump work W_p are given by:

$$H_{p,o} = \frac{\overline{v}_p(P_{p,o}-P_{p,i})}{\eta_p} + H_{p,i} \tag{4.1}$$

$$W_p = \frac{\dot{m}_p\overline{v}_p(P_{p,o}-P_{p,i})}{\eta_p} \tag{4.2}$$

where $P_{p,o}$ and $P_{p,i}$ are the inlet and outlet pressures of the pump, respectively. $H_{p,i}$ is the working fluid enthalpy at the pump inlet, $\dot{m}_p$ is the pump mass flow rate in kg/s; $\overline{v}_p$is the average specific volume of the working fluid in m^3/kg and η_p is the pump efficiency.

4.2 Expander model

The expander selection plays a vital role in the performance of ORC. In small-scale ORC systems, volumetric-type expanders are usually preferred over velocity-type expanders, because of their reliability, availability, reduced number of moving parts and ability to operate at the higher pressures and lower mass flow rates [125]. Selection of the expander type depends on many factors such as type of working fluid and expansion process pressure ratio. Moreover, the dynamic response of expander is much faster than the heat exchanging components in the cycle. Therefore, a detailed dynamic model of the expander is unnecessary for the simulation and a steady-state model is sufficient for this purpose. In this study, a volumetric scroll type expander is used. A zero-dimensional thermodynamic model for the expander based on the state enthalpies is formulated. The expander output work W_{exp} is given by:

$$W_{exp} = \dot{m}_{exp}\,\eta_{exp}(H_{exp,o} - H_{exp,i}) \tag{4.3}$$

where $\dot{m}_{exp}$ is the working fluid mass flow rate passing through the expander, $H_{exp,o}$ and $H_{exp,i}$ are the inlet and outlet enthalpies of working fluid in kJ/kg, and $\eta_{exp}$is the expander efficiency.

4.3 Condenser model

The heat exchanging elements are determining the dynamic response of the ORC system due to their slower response time. Nevertheless, since the ORC system is operating under the supercritical pressures, prediction and control of the high-pressure side of the ORC system is much more important. This is due to complex heat transfer behaviour in the evaporator under supercritical pressures and transient heat source. In this study, it is assumed that there

is enough cooling capacity on board to remove the excessive heat from the working fluid in the condenser. This task can be achieved by using a separate fan to cool down the condenser or utilizing the engine cooling fan to reduce the temperature of organic fluid. Therefore, the working fluid at the outlet of condenser is considered to be subcooled and a zero-order thermodynamic model according to the inlet and outlet working fluid enthalpies describes the condenser power Q_{con} as follows:

$$Q_{con} = \dot{m}_{cond}(H_{exp,o} - H_{con,o}) \tag{4.4}$$

where $\dot{m}_{cond}$ is the mass flow rate of refrigerant through the condenser and $H_{exp,o}$ and $H_{con,o}$ are the enthalpies at the expander outlet and condenser outlet, respectively.

4.4 Valve model

A three-way control valve in the ORC configuration is responsible for bypassing the excessive mass flow rate of working fluid. The valve provides an extra degree of freedom in the ORC configuration to regulate the work output of the expander by adjusting the percentage of working fluid mass flow rate passing through the expander. The working fluid mass flow rate passing through the valve is as follows:

$$\dot{m}_{r,v} = \alpha A_v \sqrt{2\rho\Delta P} \tag{4.5}$$

where α is the percentage of the valve opening, A_v is the valve cross-section area in m^2 and ΔP is the pressure drop between the evaporator outlet and the valve inlet calculated using the Darcy-Weisback pressure drop correlation [126] as follows:

$$\Delta P_{pipe} = \frac{f_D \rho L_p v^2}{2D_h} \tag{4.6}$$

$$\frac{1}{\sqrt{f_D}} = -1.8 \log \left[\left(\frac{\in_p / D}{3.7} \right)^{1.11} + \frac{6.9}{Re} \right] \quad (4.7)$$

where D_h and L_p are the pipes hydraulic diameter and length of pipe in m, respectively and $\in_p$ and $\in_p / D$ denote the absolute and relative roughness of the pipe in m.

4.5 Liquid receiver model

Liquid receiver is a storage vessel used in thermodynamic cycles to temporarily hold the excessive working fluid which is not in circulation and reduce the fluctuation of working fluid level occurring due to the dynamic operation of the cycle. The performance of ORC system can be influenced by the amount of working fluid charge circulating in the system. Similar to refrigerant systems, during the dynamic operation of the ORC, the excessive working fluid can accumulate in the condenser and reduce the effective condensing heat transfer area [127]. Furthermore, supplying the pump with two-phase mixture flow may result in formation of cavity which can damage it. Therefore, improper charge within the cycle can reduce its efficiency and compromise its reliability.

In order to prevent the accumulation of excessive charge in the condenser and ensure that the pump is only supplied with saturated liquid a liquid receiver needs to be installed between the condenser and pump within the cycle. The size of liquid receiver should be large enough to absorb the refrigerant fluctuations caused by dynamic operation of the system and prevent liquid back up in the condenser that can impair the ORC performance [127]. By assuming a properly sized liquid receiver installed between the condenser and pump in the cycle, in a dynamic model of ORC system, the effect of two-phase mixture flow on the pump and liquid back up in the condenser can be neglected. The behaviour of liquid receiver can be modelled by deploying the following conservation equations:

$$\frac{d\Psi}{dt} - \frac{\dot{m}_{r,lr,i} - \dot{m}_{r,lr,o}}{\rho_{r,l} V_{ac}} = 0 \quad (4.8)$$

$$\frac{dH_{lr}}{dt} - \frac{\dot{m}_{r,lr,o}(H_{lr,i} - H_{lr,o})}{\rho_{r,l} V_{lr}} = 0 \quad (4.9)$$

where Ψ denotes the liquid receiver's relative liquid refrigerant level, $\dot{m}_{r,lr,i}\ and\ \dot{m}_{r,lr,o}$ are the mass flow rate of working fluid at the receiver's inlet and outlet, respectively. $\rho_{r,l}$ is the density of liquid working fluid, and V_{lr} represents the total volume of the liquid receiver tank. $H_{lr,i}\ and\ H_{lr,o}$ are the enthalpy of working fluid at the inlet and outlet of liquid receiver.

4.6 Evaporator model

Designing an effective and reliable control system for the ORC relies on accurate modelling of all components in the system. The evaporator is the most critical component of the ORC system, responsible for the energy transfer from heat source to working fluid. When dealing with a low-capacity heat source in kW range found in ICEs, the governing dynamics of the system is dominated by the behavior of the evaporator. Moreover, due to highly dynamic engine conditions the conventional methods of evaporator modelling such as the single-segment lumped method leads to poor off-design performance of the ORC system for a variety of driving conditions since they do not model the dynamic nature of the heat source and the phase change of working fluid is not considered in them. Several methods including, intermediary thermal fluid loop, exhaust gas mixture recirculation, thermal energy storage (TES) have been developed to dampen or reduce the fluctuation of heat source and optimize it around a certain steady-state point [128]. Addition of these systems to ORC system has several drawbacks, including reducing the efficiency potential in the loop, increasing the exergy loss of the system and increasing the size, cost and weight of the system which can reduce the feasibility potential of the system [128]. Although these methods can help to

reduce the chance of decomposition of the organic working fluid, none of them is able to eliminate the fluctuations of the heat source completely. Therefore, it is necessary to create a dynamic model of the evaporator that is capable of handling transient conditions in an ORC waste heat recovery system. Among different modelling techniques of the evaporator, Finite Volume (FV) [129, 130] and Moving Boundary (MB) [131-134] techniques are the most widely used approaches to model evaporator in the ORC for cycle optimisation, working fluid selection and testing the response of different control strategies.

Quoilin et al. [74] modelled the ORC for low-grade source heat (120-300 °C) to investigate the behaviour of three different control strategies using the steady-state and dynamic FV method for the evaporator. In steady-state model all the time derivatives are set to zero, while in the dynamic model the time derivatives are taken into account. The authors discretized the whole length of evaporator into 10 segments and used the steady-state model in Engineering Equation Solver software to optimize the working condition of evaporator for 31 different working points. The heat transfer coefficient for hot fluid side considered to be constant whereas a variable heat transfer coefficient for the working fluid side. The optimized working points then used to derive the equations for control strategies. The dynamic model is deployed to compare the performance of the control strategies. The authors concluded that this method cannot be used as a predictive model to precisely evaluate the energy recovery potential of the system, due to the various simplification that are considered in the hypothesis, including evaporation pressure of the working fluid considered to be constant and the assumption of a constant pinch value.

Wei et al. [115] presented a comparison between the FV and MB methods for a stationary, industrial-sized 100 kW ORC system. For the FV method they discretized the evaporator to

5 segments and assumed the linear pressure drop in whole evaporator length. The authors concluded that the MB method is the preferred method over the FV method since both of the models simulate the system correctly during transients and MB method is less computationally demanding which results in a faster model.

Benato et al. [135] modelled a horizontal circular finned-tube evaporator using the FV method. The authors investigated the decomposition of the working fluid during transients in an ORC waste heat recovery system used for a gas turbine power plant. Furthermore, it is worth mentioning that due to the higher thermal inertia in power plants' evaporators, the obtained response time of the system was about 60 minutes which is much higher than the response time of the mobile ORC systems.

Jiménez-Arreola et al. [136] modelled two type of compact evaporator in order to compare their dynamic behaviour in applications with fluctuating heat sources at the design stage. The authors used the 1-D FV method and discretized both fin-and-tube and louver fin and multi-port flat tubes evaporators to 20 segments and considered the pressure drop in the whole length of evaporators according to the correlation of flow inside the pipes. The commercial TIL library of Dymola and REFPROP were deployed to simulate the system and calculate the thermodynamic properties, respectively. Based on their simulation results the authors concluded that the response time for fin-and-tube evaporator is almost double the louver fin multi-port flat tubes evaporator.

Desideri et al. [137] provided a comparison between the MB and FV methods for modelling low capacity (5-150 kW) evaporators in terms of model integrity and accuracy. The Authors used the mathematical formulation of 1-D mass and energy conservation laws to develop the equations for the evaporators. Both models are available in open-source ThermoCycle Modelica library. Pressure drop across the whole length of evaporator is neglected in both

modelling techniques. The models are used to develop a low-capacity ORC system and are validated using the experimental data from an 11 kW ORC power unit. Moreover, the open-source CoolProp software is utilized to calculate the thermodynamic properties of the working fluid. The obtained simulation time for the steady-state FV model of evaporator with 100 control volumes is 625s and one-third of this time is reported for MB model simulation. Rongqi Shi et al. [128] used the MB approach to model the dynamics of the evaporator in order to investigate the effect of Exhaust Gas Mixture Recirculation (EGMR) loop on the ORC system. The mass, energy and momentum conservation equations are derived to model the dynamic behaviour of evaporator. Furthermore, the authors utilized the Active Disturbance Rejection Control (ADRC) as the control scheme. The mass flow rate of exhaust gas and the evaporating pressure of working fluid is considered as the control input and output, respectively. According to the simulation results the cycle efficiency of 7% is reported. The overall efficiency of system is increased from 0.9% for conventional ORC system to 1.5% for EGMR-ORC system.

4.6.1 Finite Volume model

In most of the ORC investigations, FV and MB methods have been used to model the evaporator behaviours under steady or transient heat sources. In the FV technique, the evaporator volume is discretised to a finite number of equally spaced and constant control volumes. The governing equations of evaporator are calculated by integrating the 1-D mass, energy and momentum conservation equations over the control volumes. Output of each cell is input to the next cell and by formulating the governing equations the final outputs can be calculated by utilising an iteration process. **Fig. 4.1** represents the discretisation of the evaporator with length L to N control volumes.

As the number of the control volumes increases, the accuracy of the model improves. Selection of the number of control volumes is a compromise between accuracy and total computational time of the model [137]. If the number of control volumes is high enough to capture the transients, since the temperature variations within the cells is considered to be low, the thermo-physical properties of working fluid within the cells can be assumed constant.

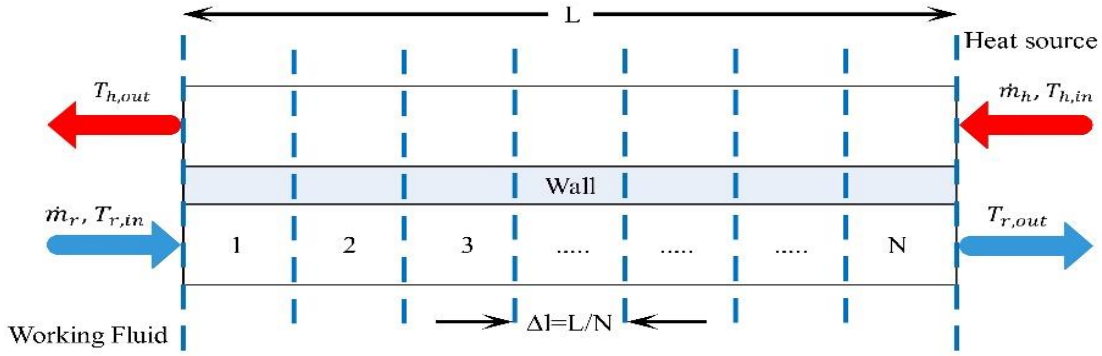

Fig. 4.1. *Discretisation of evaporator to N control volumes*

The mass, energy and momentum conservation equations for each cell J of refrigerant side of the evaporator will be derived hereunder.

The mass conservation equation representing the evaporator behaviour is:

$$\frac{dM}{dt} = \dot{m}_{r,in} - \dot{m}_{r,out} \tag{4.10}$$

Definition of mass and its relation with volume and density results in the following equation:

$$\frac{dM}{dt} = V_r \frac{\partial \rho_r}{\partial t} \tag{4.11}$$

Substituting the term $\frac{dM}{dt}$ from equation (4.10) in equation (4.11) results in:

$$\dot{m}_{r,in} - \dot{m}_{r,out} = V_r \frac{\partial \rho_r}{\partial t} \tag{4.12}$$

The pressure drop across the evaporator is neglected; therefore, the momentum conservation equation is in form of equation (4.13).

$$P_{in} = P_{out} \tag{4.13}$$

The energy balance for the evaporator can be represented as (4.14), where $H_{r,in}$ and $H_{r,out}$ are the input and output enthalpy of refrigerant for each cell J, Q_r is the evaporator heat input and W_r is the work done by the evaporator which by assumption is considered to be zero.

$$\frac{dU}{dt} = \dot{m}_{r,in}\, H_{r,in} - \dot{m}_{r,out}\, H_{r,out} + Q_r + W_r - P\frac{dV_r}{dt} \tag{4.14}$$

By definition, the system energy U can be represented in form of total enthalpy, pressure and volume as follows:

$$U = \overline{H_r} - PV_r \tag{4.15}$$

$$\overline{H_r} = H_r \cdot m_r \tag{4.16}$$

$$U = H_r \cdot m_r - PV_r = H_r \cdot \rho_r\, V_r - PV_r \tag{4.17}$$

Applying the chain rule differentiation to equation (4.17) results in equation (4.18). Since the pressure drop across the evaporator is neglected the term $V_r\frac{dP}{dt}$ in equation (4.18) becomes zero.

$$\frac{du}{dt} = V_r\,\rho_r\frac{\partial H_r}{\partial t} + V_r\,H_r\frac{\partial \rho_r}{\partial t} - V_r\frac{dP}{dt} \tag{4.18}$$

By substituting the term $\frac{dU}{dt}$ from equation (4.18) in equation (4.14), equation (4.19) can be written as:

$$V_r\,\rho_r\frac{\partial H_r}{\partial t} + V_r\,H_r\frac{\partial \rho_r}{\partial t} = \dot{m}_{r,in}\, H_{r,in} - \dot{m}_{r,out}\, H_{r,out} + Q_r \tag{4.19}$$

Combining equation (4.11) and equation (4.19) results in equation (4.20).

$$V_r\,\rho_r\,\frac{\partial H_r}{\partial t} + \left(\dot{m}_{r,in} - \dot{m}_{r,out}\right)H_r = \dot{m}_{in}\,H_{r,in} - \dot{m}_{out}\,H_{r,out} + Q_r \tag{4.20}$$

By rearranging the terms, the general term of balance equation for refrigerant side can be written as equation (4.21).

$$V_r\,\rho_r\,\frac{\partial H_r}{\partial t} = \dot{m}_{in}\left(H_{r,in} - H_r\right) - \dot{m}_{out}\left(H_{r,out} - H_r\right) + Q_r \tag{4.21}$$

Equation (4.21) can be represented in general form for each cell J as follows:

$$V_r\,\rho_r\,\frac{\partial H_r}{\partial t} - \dot{m}_r\left(H_{r,J} - H_{r,J-1}\right) - Q_r = 0 \tag{4.22}$$

Since the procedure for deriving the equations for the hot fluid side is the same as refrigerant side, the derivation is not presented here. Equation (4.23) represents the general balance equation for cell J in the hot fluid side.

$$V_h\,\rho_h\,C_{p,h}\,\frac{\partial T_h}{\partial t} + \dot{m}_h\,C_{p,h}\left(T_{h,J} - T_{h,J+1}\right) + Q_h = 0 \tag{4.23}$$

Equation (4.24) represents the energy conservation principle across the evaporator's wall.

$$m_{wall}\,C_{p,wall}\,\frac{\partial T_{wall}}{\partial t} - Q_h + Q_r = 0 \tag{4.24}$$

where Q_r and Q_h are the heat input in the refrigerant side and hot fluid side, respectively, and are given by equation (4.25) and (4.26).

$$Q_r = A_r\,h_r(T_{wall} - T_r) \tag{4.25}$$

$$Q_h = A_h\,h_h(T_h - T_{wall}) \tag{4.26}$$

Equation (4.22), (4.23) and (4.24) are the three equations representing the behaviour of the evaporator. In order to solve these equations, they are discretized numerically according to the finite volume theorem and equations (4.27), (4.28) and (4.29) are achieved.

$$H_{r,J}^{t+1} = H_{r,J}^{t} + \frac{\Delta t}{V_{r,J}\,\rho_{r,J}^{t}}\left(A_{r,J}\,h_{r,J}^{t}\left(T_{wall,J}^{t} - T_{r,J}^{t}\right) - \dot{m}_{r,J}^{t}\left(H_{r,J}^{t} - H_{r,J-1}^{t}\right)\right) \quad (4.27)$$

$$T_{h,J}^{t+1} = T_{h,J}^{t} + \frac{\Delta t}{V_{h,J}\,\rho_{h,J}^{t}\,C_{ph,J}^{t}}\left(\dot{m}_{h,J}^{t}\,C_{ph,J}^{t}\left(T_{h,J+1}^{t} - T_{h,J}^{t}\right) - A_{h,J}\,h_{h,J}^{t}\left(T_{h,J}^{t} - T_{wall,J}^{t+1}\right)\right) \quad (4.28)$$

$$T_{wall,J}^{t+1} = T_{wall,J}^{t} + \frac{\Delta t}{m_{wall,J}\,C_{pwall,J}}\left(A_{h,J}\,h_{h,J}^{t}\left(T_{h,J}^{t} - T_{wall,J}^{t}\right) - A_{r,J}\,h_{r,J}^{t}\left(T_{wall,J}^{t} - T_{r,J}^{t}\right)\right) \quad (4.29)$$

4.6.1.1 Stability criteria and numerical time step calculation

According to the finite volume method of discretization, for obtaining a stable solution and prevent instability of numerical calculations the coefficients of $H_{r,J}^{t}$ and $T_{h,J}^{t}$ in equations (4.27) and (4.28) respectively, must be greater than zero.

Therefore, from equation (4.27) the time step can be written as:

$$1 - \frac{\Delta t \cdot \dot{m}_{r,J}^{t}}{V_{r,J}\,\rho_{r,J}^{t}} \geq 0 \quad (4.30)$$

$$\Delta t \leq \frac{V_{r,J}\,\rho_{r,J}^{t}}{\dot{m}_{r,J}^{t}} \quad (4.31)$$

And from equation (4.28) time step can be calculated as:

$$1 + \frac{\Delta t}{V_{h,J}\,\rho_{h,J}^{t}\,C_{ph,J}^{t}}\left(-\dot{m}_{h,J}^{t}\,C_{ph,J}^{t} - A_{h,J}\,h_{h,J}^{t}\right) \geq 0 \quad (4.32)$$

$$\Delta t \leq \frac{V_{h,J}\,\rho_{h,J}^{t}\,C_{ph,J}^{t}}{\dot{m}_{h,J}^{t}\,C_{ph,J}^{t} + A_{h,J}\,h_{h,J}^{t}} \quad (4.33)$$

Since stability criteria for equations (4.27) and (4.28) result in two different time steps, in order to choose a unique time step that guarantees the stability of model, the minimum value of Δt from equation (4.31) and (4.33) will be calculated and used as numerical time step as follows:

$$\Delta t = min\left(\frac{V_{r,J}\,\rho_{r,J}^{t}}{\dot{m}_{r,J}^{t}}, \frac{V_{h,J}\,\rho_{h,J}^{t}\,C_{ph,J}^{t}}{\dot{m}_{h,J}^{t}\,C_{ph,J}^{t}+A_{h,J}\,h_{h,J}^{t}}\right) \tag{4.34}$$

This method can be used to produce accurate simulations; however, it is computationally expensive and is not appropriate for control purposes. The computational time of a super-critical FV model is reported to be over three times more than the actual number of operating hours of evaporator [138]. FV method is robust, accurate and widely used in the literature [72, 74, 139], but this method is not suitable for real-time control purposes.

4.6.2 Moving Boundary model

The MB method divides the whole length of evaporator into three control volumes (liquid, two-phase mixture, vapour) with intermediate moving boundaries that vary with time, thus, the number of states is less than that of FV models [115]. In the MB model, if any of three phases disappears, this creates a singularity that causes numerical problems. Therefore, the MB model is not appropriate for situations where all three distinct phases of working fluid do not exist such as start-up and shut-down. Unfortunately, most of the ORC components failure occurs in such conditions [115]. Therefore, in such situations, a switching mechanism is required to switch between Two-Phase and vapour region mode (TP-V) and Two-Phase region mode (TP) [140]. Comparisons between both models have been made in [115, 137, 141] that show, in terms of accuracy, the FV models are slightly more accurate since they have a finer spatial discretisation, but due to the lower number of state variables,

MB models are less computationally expensive. Wei et al. [115] represented two FV and MB models for the evaporator and compared the mass flow rate and outlet temperature of evaporator of both models with the experimental data available by UTRC (United Technology Research Center) for a 100 kW ORC system. From their simulation results, it is observable that the accuracy of FV model with five cells is better than the MB model.

4.7 Summary

In this chapter mathematical representation of the ORC components are presented. The objective is to create a model of the ORC which is fast enough to be used for real-time control purposes. As opposed to the model of some components such as pump and expander which can be easily obtained, deriving a model of evaporator which determines the dynamic response of the system is challenging. Most of studies in the literature deployed the moving boundary and finite volume methods to formulate the evaporator model. The FV is a robust and accurate model which is able to handle the supercritical pressures. However, this method utilises a numerical iteration process for mimicking the evaporator behaviour. Therefore, this model is computationally expensive. The accuracy of the finite volume model in influenced by number of the control volumes and as the number of control volumes increases the computational time of the model increases too. To overcome this issue the moving boundary evaporator model can be utilised which is slightly less accurate but is computationally less expensive. In the moving boundary model just three control volumes based on the phase of the fluid are considered. This model suffers from singularity when any of distinct phases disappear that could cause numerical issues. Therefore, this model is not appropriate for conditions such as start-up or shut-down which are responsible for most of the ORC components failure.

The numerical methods of evaporator modelling are useful at the design stage of the ORC system to find the best components of the cycle and the optimal working fluid selection, but a more traceable model is required for the real-time control of the ORC with transient heat source. In the next chapter a novel data-driven neuro-fuzzy approach is deployed to reduce the computation burden of the evaporator model.

Chapter 5: Neuro-fuzzy modelling of evaporator

5.1 Artificial intelligence modelling

Artificial intelligence (AI) has emerged as a powerful tool for modelling and control of nonlinear and challenging problems. As machines become increasingly capable, intelligent modelling and control has been increasingly applied in many disciplines for a wide range of applications. The ability of AI technologies to deal with cognitive tasks such as learning, adaptation and optimization makes them adequate candidates for overcoming the limitations arising in modelling and control of challenging plants using conventional methods. Intelligent systems mainly consist of technologies such as expert systems, artificial neural networks, fuzzy systems and evolutionary computation. Given the superior predicative potential of AI techniques, they became popular for modelling and control of complex systems. In order to mitigate the drawbacks of traditional AI methods, hybrid techniques are developed to join their advantages by combining different methods. This chapter aims to provide an overview of some major AI techniques and model the highly nonlinear behaviour of an evaporator used in the ORC applications using the input-output data gathered from a conventional FV model.

5.2 Artificial neural network modelling

The human brain capabilities have always fascinated researchers and motivated them to replicate its function. Artificial Neural Networks (ANN) are developed to mimic the remarkable ability of biological neural network to reason and learn in an uncertain and imprecise environment. The elementary unit of an ANN is called neuron. The ANN resembles the biological neural network in two respects [142]:

- The network requires a learning process to acquire knowledge from its environment.
- The acquired knowledge is stored in the interneuron connection strengths known as synaptic weights.

The fundamental information processing unit of an ANN is called a neuron. A neuron is a mathematical function that mimics the function of a biological neuron. **Fig. 5.1** represents the model of neuron which is a basis for designing various types of neural networks. Each neuron comprises three basic elements: weighted connecting links which are also known as synapses, the summing junction for adding the input signals and an activation function to limit the neurons output amplitude.

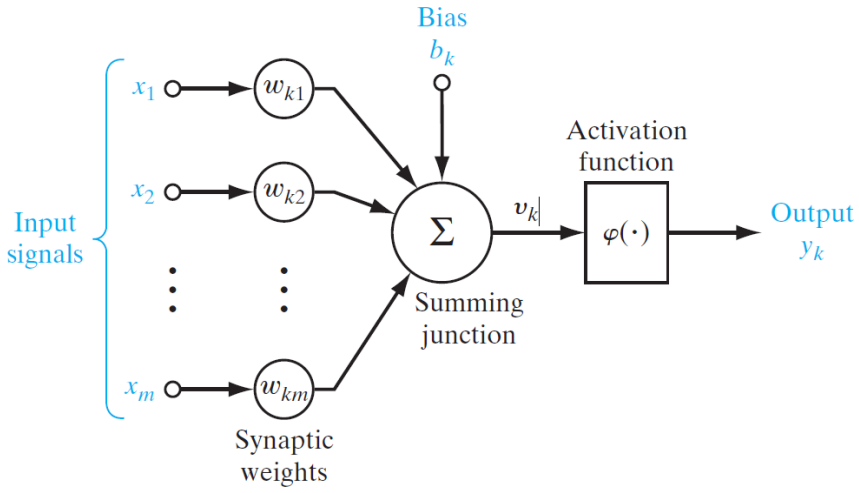

Fig. 5.1. Nonlinear model of a neuron [142]

In mathematical terms, the model of a neuron can be formulated as follows:

$$v_k = \sum_{j=0}^{m} w_{kj} x_j \tag{5.1}$$

$$y_k = \varphi(v_k) \tag{5.2}$$

where x_j represents the input signal, w_{kj} denotes the respective synaptic neuron weight, $\varphi(.)$ is the neurons activation function, and y_k is the output signal of the neuron.

A layer is formed by employing one or more neuron which perform parallel operation. An ANN comprises an input layer, an output layer and one or more hidden layers. The neurons in the hidden layer are connected to neurons in input and output layers using directional connections with adaptive weights. The neurons can process the signal and then transmit it to the other connected nodes. The connection between these neurons determines the function of network. The ANN method is categorised as a data-driven non-parametric technique in which requires data for mapping the input variables to the output variables [143].

After forming the architecture of network, it needs to be trained to perform the required task. The process of tuning the weights in a network in order to perform the adequate mapping between the input and output variables is called training the network. The weights are initially selected randomly and the data is presented to the network. In the next step, optimisation algorithms are employed to adjust the network weights in order to minimise the error between target data and the network-calculated data.

5.2.1 Implementation of ANN evaporator model

In this study two Multi-Layer Perceptron (MLP) neural networks are trained using 1000 data points collected from the FV model of the evaporator to model the heat source outlet temperature and refrigerant outlet temperature of the evaporator. The inputs to the model are mass flow rate and temperature of heat source and mass flow rate of refrigerant.

To train the ANN model, the FV model of evaporator is excited by changing the heat source mass flow rate ($\dot{m}_h$), the heat source temperature (T_h) and the mass flow rate of refrigerant

($\dot{m}_r$) in the range of 0.07-0.29 kg/s, 412-523 K and 0.03-0.22 kg/s, respectively. The heat source mass flow rate and temperature data are randomly selected according to the range of a generic heat source in ICE of heavy-duty trucks. Details of the FV model used for collecting the data can be found in [129]. In total, 1000 data points collected and each data point represents one second of actual evaporator input-output behaviour. The input and output data are shown in **Fig. 5.2**.

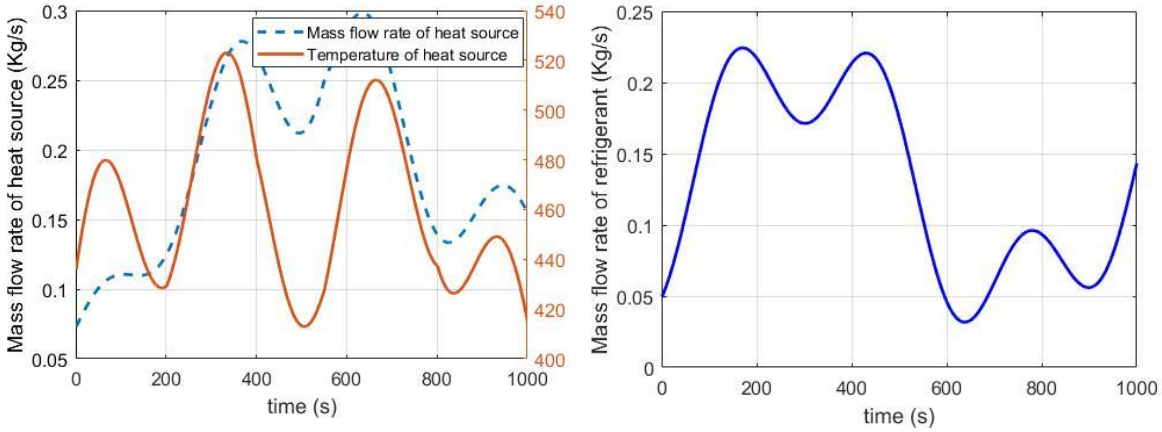

(a) (b)

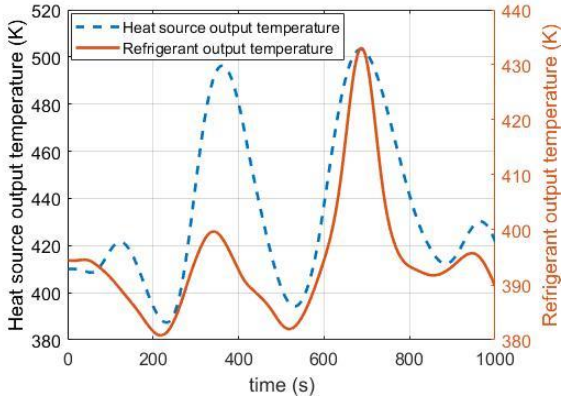

(c)

Fig. 5.2. *Input-output data gathered from FV model of evaporator (a) Mass flow rate and temperature of generic heat source (b) Mass flow rate of refrigerant (c) Refrigerant and heat source temperatures at the evaporator outlet*

When training the network, it is important to prevent overfitting the network. If the model is overfitted it would perform well for predicting the outputs of training dataset, but its performance on other datasets is not satisfactory. A very common approach to overcome the overfitting issue is to use a validation and a test data set. The network is trained using the training dataset, the validation dataset is used to avoid the overfitting during the training process and finally the test dataset is deployed to check the generalization ability of the network for an unseen data set. Therefore, the dataset is randomly divided into three subsets: training dataset (70%), validation dataset (15%) and test dataset (15%). The architecture of the network is shown in **Fig. 5.3**. As illustrated, the network consists of a hidden layer with 10 neurons and an output layer with one neuron. The activation function of the hidden layer is Tansig function and Purelin function is used in the output layer. The Levenburg-Marquardt algorithm is deployed for training the network and the number of iterations is set to 500. Moreover, the MSE and RMSE are used to evaluate the performance of the network.

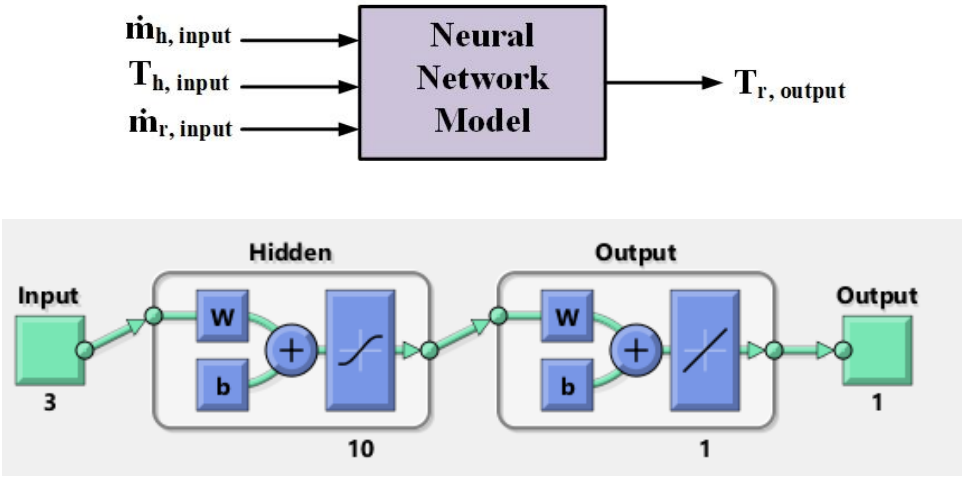

Fig. 5.3. *MLP neural network architecture and refrigerant outlet temperature model input output variables*

As illustrated in **Fig. 5.4**. for the outlet refrigerant temperature prediction, the best validation performance is reached at iteration 426 with MSE equal to 0.0014. The comparison of the

performance of MLP neural networks model and FV model for the training and test datasets is presented in **Figs. 5.5** and **5.6**, respectively. **Table 5.1** represents the performance of the MLP neural networks model in predicting the refrigerant outlet temperature for training and test datasets.

Table 5.1 *– Network performance for prediction of refrigerant outlet temperature*

	MSE	**RMSE**	**R**
Training data	0.0014	0.038	0.9999
Test data	0.0019	0.043	0.9999

The results indicate acceptable generalisation performance for prediction of outlet temperature of refrigerant with RMSE equal to 0.038 and 0.043 for training and test datasets, respectively. Furthermore, the linear correlation coefficient (R) of 0.99 obtained for both training and test datasets which indicates the high accuracy of the trained network in prediction of the evaporator data.

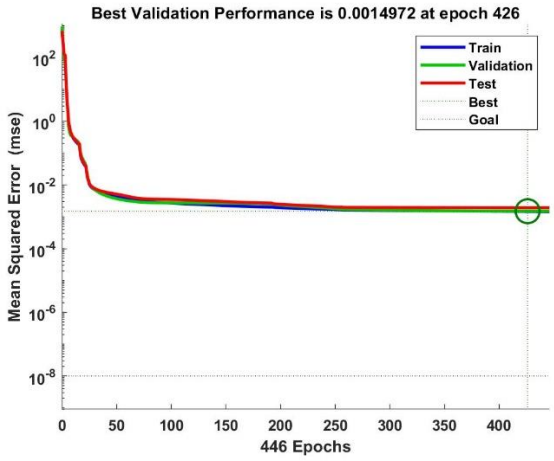

Fig. 5.4. *Mean square error during the network training*

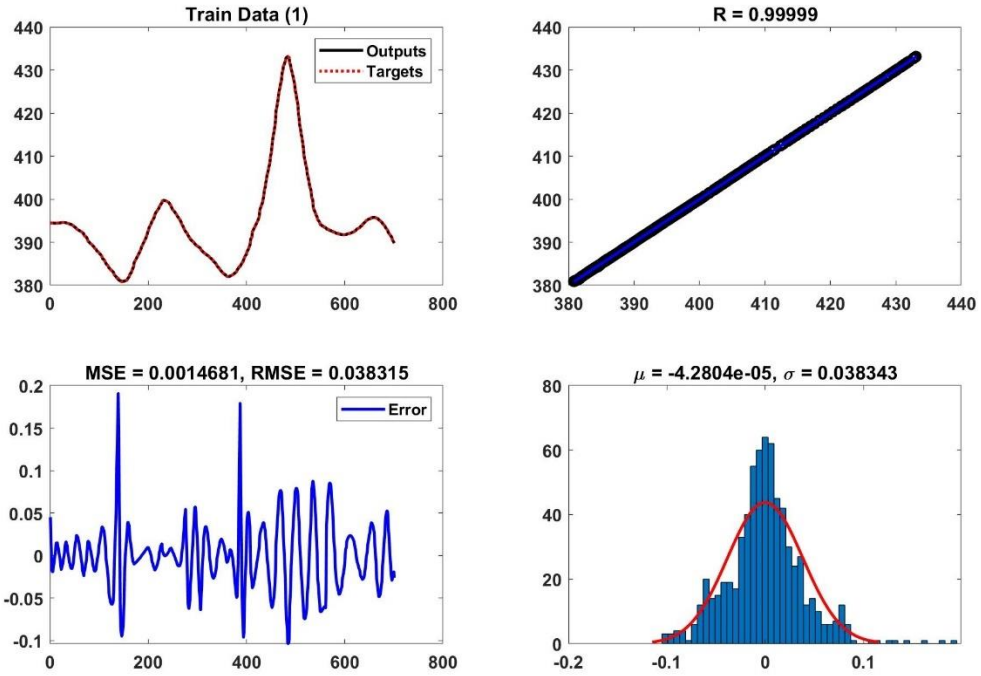

Fig. 5.5. *Performance of the network in predicting the evaporator outlet temperature (training data)*

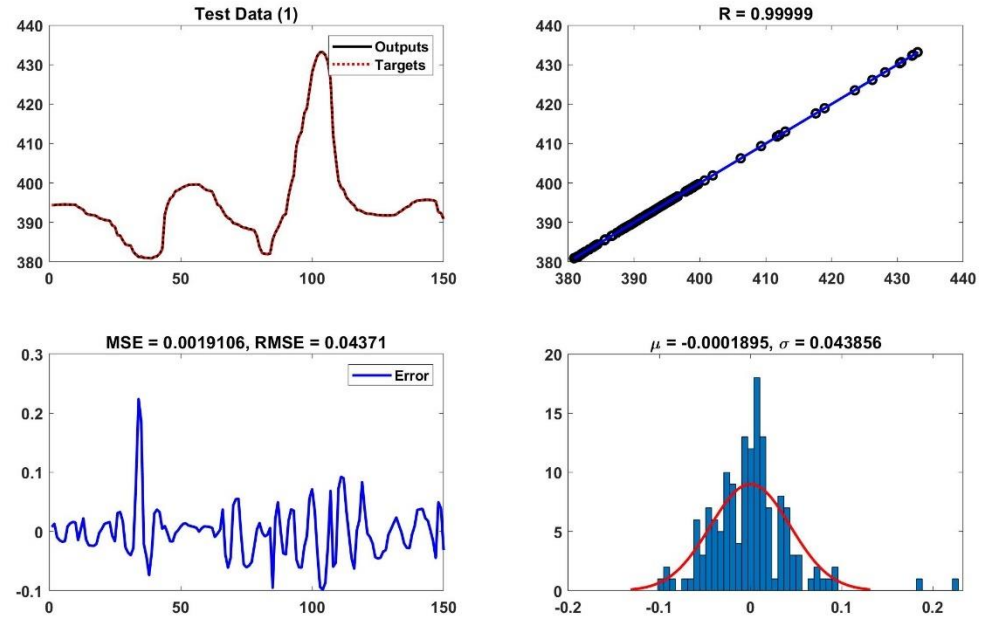

Fig. 5.6. *Performance of the network in predicting the evaporator outlet temperature (test data)*

Similar to the network trained for prediction of refrigerant outlet temperature, an MLP neural network with the same parameters is trained for modelling the heat source outlet temperature. The network architecture and model's input and output variables are shown in **Fig. 5.7**.

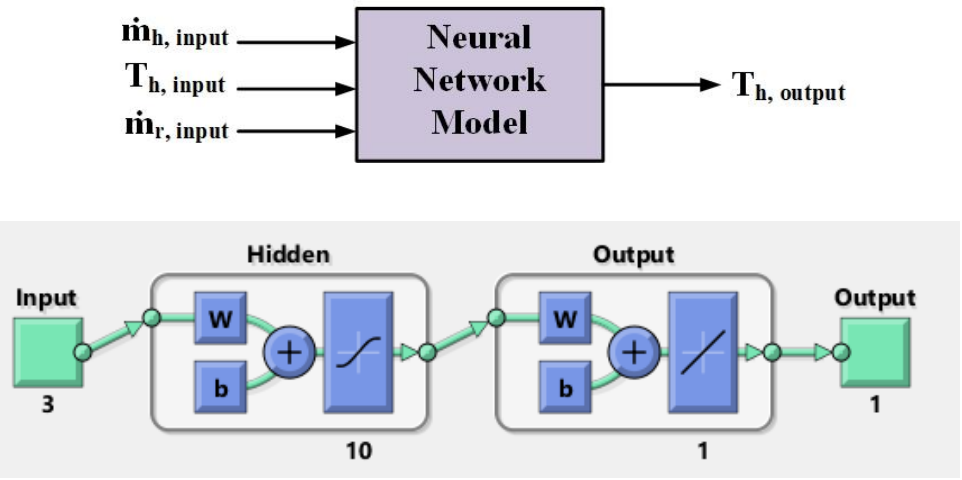

Fig. 5.7. *MLP neural network architecture and heat source outlet temperature model input output variables*

The reduction of mean square error during the training phase of the network is represented in **Fig. 5.8**. For this network, the best validation performance equal to 0.023 reached at epoch 500.

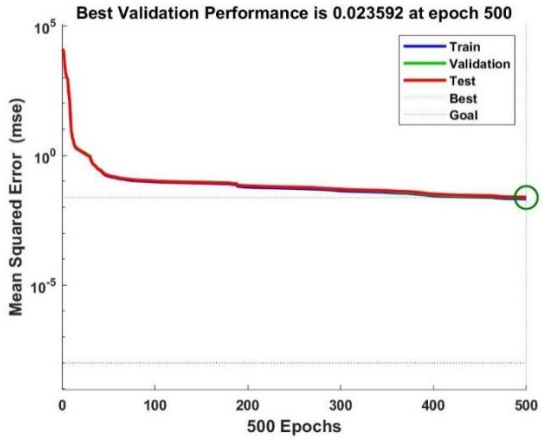

Fig. 5.8. *Mean square error during the network training*

Figs. 5.9 and **5.10** represent the comparison of the trained MLP neural networks model and FV model outputs in prediction of heat source outlet temperature for training and test datasets, respectively. The performance of the network in prediction of training and test datasets is compared in **Table 5.2**.

Table 5.2 *– Network performance for prediction of refrigerant outlet temperature*

	MSE	**RMSE**	**R**
Training data	0.021	0.145	0.9999
Test data	0.024	0.157	0.9999

The comparison of obtained results from FV model and MLP neural networks model indicated an acceptable agreement between both model outputs. The RMSEs obtained for the training dataset and test dataset are equal to 0.145 and 0.157, respectively. Furthermore, the MSE of training dataset is 0.021 and 0.024 achieved for the test dataset. Both obtained R values are close to 1 which indicate acceptable generalisation ability of the network.

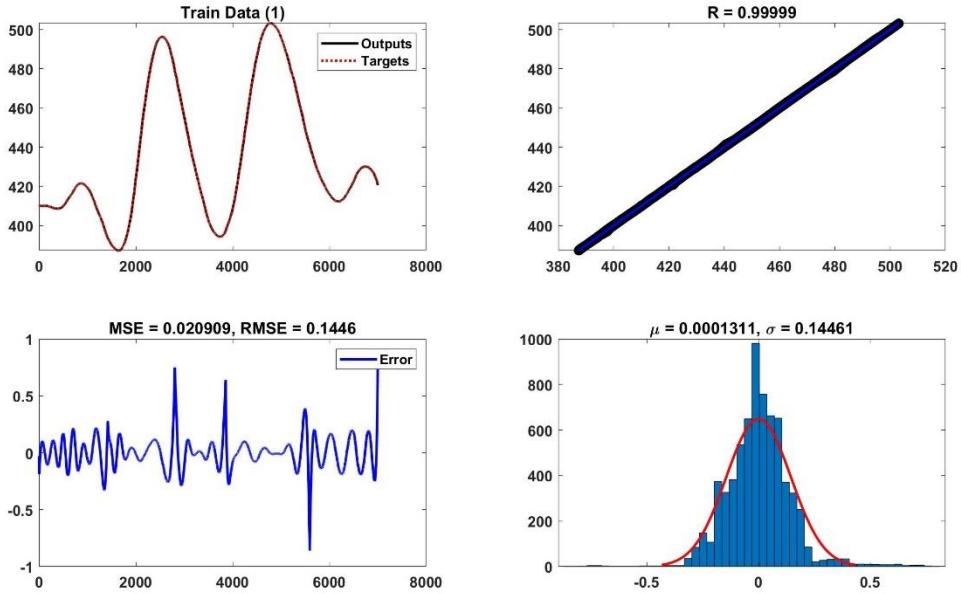

Fig. 5.9. *Performance of the network in predicting the heat source outlet temperature (training data)*

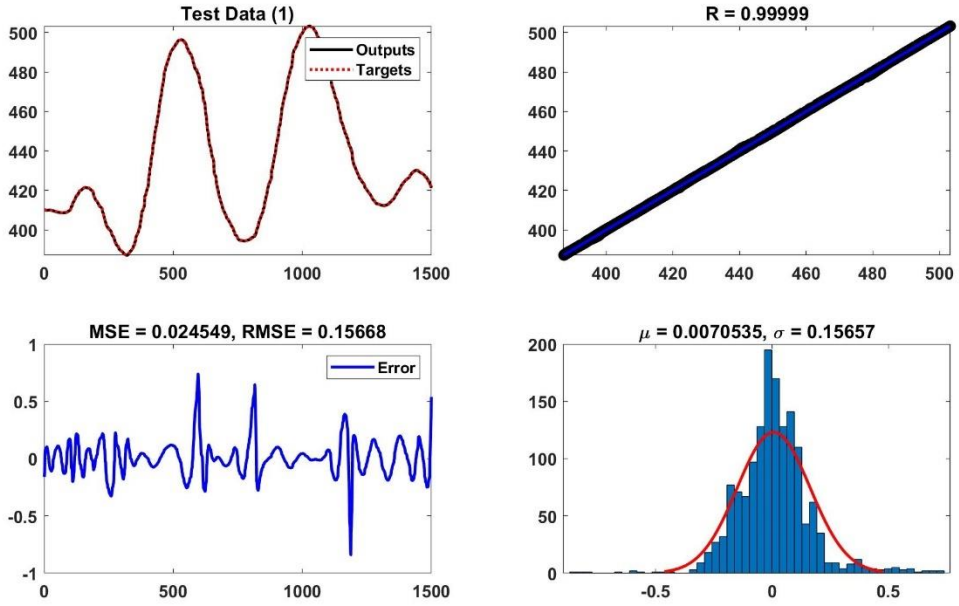

Fig. 5.10. *Performance of the network in predicting the heat source outlet temperature (test data)*

Although the performance of both MLP neural networks trained for predicting the outlet temperature of heat source and outlet temperature of refrigerant are acceptable, these models are referred to as black-box models. As opposed to the principle-based models, in black-box models the mathematical relations are unknown to the designer and have no physical meaning. Furthermore, these models require proper training in order to perform efficiently. Therefore, since the model performance depends on the design parameters such as model architecture, number of neurons in hidden layers, activation function of neurons, optimisation algorithm and learning rate parameter, deploying the ANN technique and its training involves a trial-and-error task.

5.3 Fuzzy theory and fuzzy modelling

Fuzzy systems are knowledge-based and rule-based systems introduced by Zadeh in 1965 [144]. Since the introduction of fuzzy systems, it has been gradually developed and applied in a variety of fields such as control, signal processing, communications, medicine, psychology, etc. Fuzzy logic can be considered as an extension of Boolean logic. While the Boolean logic assigns the value of 0 for “false” and 1 for “true” to the variables, fuzzy logic allows the variables to take any value in the interval [0, 1]. Therefore, fuzzy logic can handle the vague or uncertain data similar to the way that humans often think or communicate.

A common issue of the traditional mathematical modelling techniques is inability to incorporate the extra information provided by engineers or operator due to the vague and imprecise nature of this information. The fact that humans are able to manage complex tasks with high uncertainty has motivated the researches to search for alternative modelling and control approaches. Fuzzy modelling and control are an example of incorporation of human knowledge and deductive processes. Fuzzy models are considered as logical models that deploy “if-then” rules to establish qualitative relationships among the model variables.

Fuzzy modelling approach is usually chosen where the system is complex, ill-defined or uncertain and conventional modelling techniques could not provide satisfactory results. The rule-based nature of fuzzy models makes them transparent to interpretation and allows the use of information which is expressed in form of natural language [145]. Nonetheless, similar to neural network models, the fuzzy models are referred to as flexible mathematical structures which are able to approximate a large class of complex nonlinear systems to a desired degree of accuracy [145].

5.3.1 Fuzzy sets and membership function

The essential component of any fuzzy system is the concept of fuzzy sets. Unlike the Boolean logic that the truth values of variables can only be 0 or 1, in fuzzy sets the truth values can be any real number ranging between 0 and 1. Consider evaporator temperature as an example. In order to identify a temperature (x) as "high", the degree of membership of this temperature $\mu_{A_i}(x)$ to the set A (high) could be defined as follows:

$\mu_A(x) = 1$, if x is completely in A

$\mu_A(x) = 0$, if x is not in A

$0 < \mu_A(x) < 1$, if x is partially in A (5.3)

If we consider evaporator temperatures more than 450K as high, we can define the set of evaporator high temperatures using the classical sets as follows:

$$A = \{x | x \geq 450K\} \quad (5.4)$$

As depicted in the **Fig. 5.11**, this classical set imposes a sharp boundary at 450K, and a temperature would have to be either high or not. Using the classical set theory, an evaporator with temperature = 449 K does not belong to this set and is not considered high. In the fuzzy set methodology, a fuzzy set can be defined whose elements have a degree of membership. A fuzzy set allows gradual assessment of membership of elements in a set. A fuzzy set of a universe of discourse X (the range of variable change) is defined using the membership functions $\mu_A(x) : X \rightarrow [0, 1]$. This membership function assigns a degree of membership to all elements (x) in the universe of discourse in the interval [0, 1]. The membership function could be a curve (e.g., Gaussian membership function) which defines how each point in the input space is mapped to a degree of membership. The fuzzy set of evaporator high

temperatures is represented in **Fig. 5.12**. Since the assessment of membership using the membership function is gradual the boundary is no longer crisp. In selection of appropriate type of membership function, factors such as simplicity, speed, convenience and efficiency should be considered [146].

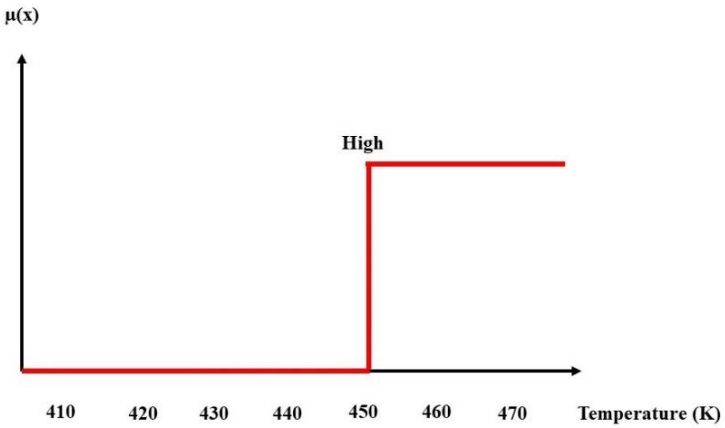

Fig. 5.11. *Crisp set of a high temperature*

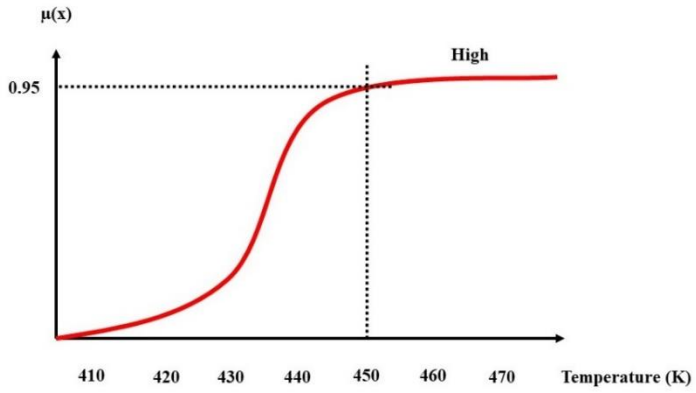

Fig. 5.12. *Fuzzy set of high temperature*

5.3.2 Linguistic variables and fuzzy rules

The concept of linguistic variables was introduced by Lotfi A. Zadeh in 1975 and it allows the variables to take linguistic expressions (words, sentences) instead of numerical values

[147]. The motivation for using the linguistic variables instead of numerical values rely on the fact that they are, in general, less specific. Temperature is a linguistic variable if the values are expressed in linguistic form rather than numerical. For example, freezing, cool, warm and hot instead of -10°C, 10°C, 20°C and 40°C, may imply the same meaning but are less precise, and thus, are less informative. Therefore, the terms freezing, cool, warm and hot could be considered as the linguistic values of the linguistic variable temperature. Fuzzy sets of freezing, cool, warm and hot are represented in **Fig. 5.13**.

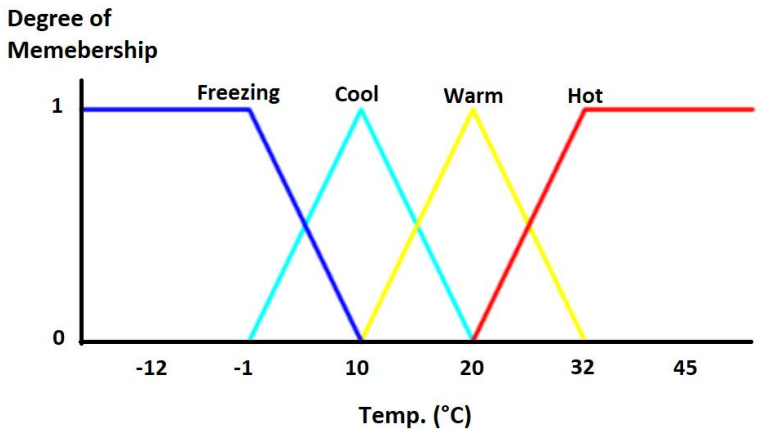

Fig. 5.13. *Fuzzy sets of freezing, cool, warm and hot*

More specifically, a linguistic variable can be characterised using a quintuple as follows [147]:

(L, T(L), U, G, M) (5.5)

where L denotes the variable name, T(L) is referred to as term-set of L which contains the linguistic values, U is universe of discourse, G is a syntactic rule for generating the terms in T(L) and M is a semantic rule which associates meaning to the each linguistic value X. Linguistic variables help to approximately characterise various phenomena that are ill-

defined or too complex to be susceptible of description in precise terms (numerical values) and, therefore, could be used in a wide variety of practical applications [147]. Nonetheless, the level of precision of the system can be adjusted by the number of linguistic terms and shape and overlap of membership functions.

Linguistic fuzzy rules can be formed using the IF-THEN statements, where the fuzzy sets are expressed in form of linguistic expressions. The general form of a fuzzy rule can be defined in the form:

R_i: **IF** x is A_i **THEN** y is B_i, i = 1, 2, 3, …, K (5.6)

where input of the fuzzy system is x (also referred to as antecedent variable). The output of fuzzy system (or consequent variable) is y. A_i and B_i are fuzzy sets (linguistic variables) defined by multi-variable membership functions $\mu_{A_i}(x): X \rightarrow [0,1]$ and $\mu_{y_i}(y): Y \rightarrow [0,1]$, respectively, and K is the number of rules.

The antecedent proposition is usually formed by combining simple fuzzy propositions of the individual components (x_i) of the system input (x). logical operators such as conjunction, disjunction and negation can be used for creating a compound proposition such as:

R_i: **IF** x_1 is A_{i1} **OR** x_2 is A_{i2} **AND** x_3 is **NOT** A_{i3} **THEN** y is B_i, i = 1, 2, 3, …, K (5.7)

Moreover, the t-norm, t-conorm and complement operators can be used to compute the degree of fulfilment of a rule, e.g., [145]:

$$B_i = \mu_{A_{i1}}(x_1) \cup \mu_{A_{i2}}(x_2) \cap (1 - \mu_{A_{i3}}(x_3)) \quad (5.8)$$

where the maximum operator (∪) and minimum operator (∩) represent disjunction (OR) and conjunction (AND), respectively, and $1 - \mu_{A_{i3}}(x_3)$ represents negation.

The intersection or disjunction of two fuzzy sets can be defined as:

$$\mu_{A\cap B}(x) = \min(\mu_A(x), \mu_B(x)) \tag{5.9}$$

The union or conjunction of two fuzzy sets can be defined as:

$$\mu_{A\cup B}(x) = \max(\mu_A(x), \mu_B(x)) \tag{5.10}$$

And the complement or negation of the fuzzy set A can be represented as:

$$\mu_{\bar{A}}(x) = 1 - \mu_A(x) \tag{5.11}$$

By combining these operators, the antecedent space can be partitioned as required.

5.3.3 Fuzzy inference system

Given the inputs and rules of the fuzzy system, fuzzy inference system (FIS) is referred to the process of deriving the output of fuzzy set. **Fig. 5.14** represents a fuzzy inference system with five functional blocks.

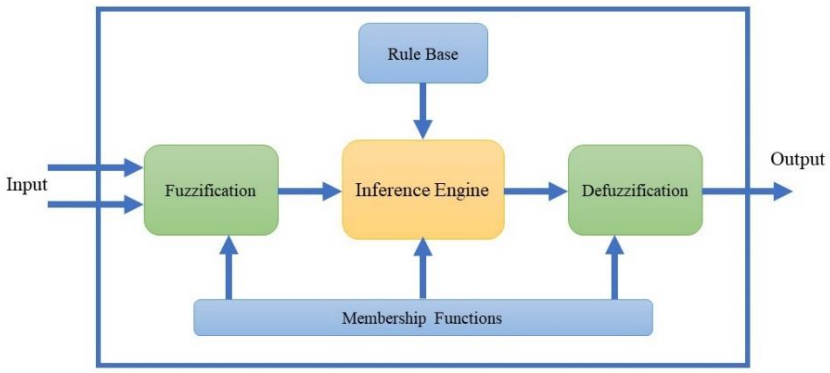

Fig. 5.14. *Fuzzy inference system*

The fuzzification block is responsible for assignment of a membership grade to each crisp input according to the defined type of membership function. In the next step the inference engine applies appropriate fuzzy operators in order to conduct the fuzzy reasoning process. Then, the defuzzification block transforms the output fuzzy set of inference engine to a crisp output by using appropriate defuzzification method. The centre of gravity (COG) and mean of maxima (MOM) are the most common defuzzification methods for generating a crisp output.

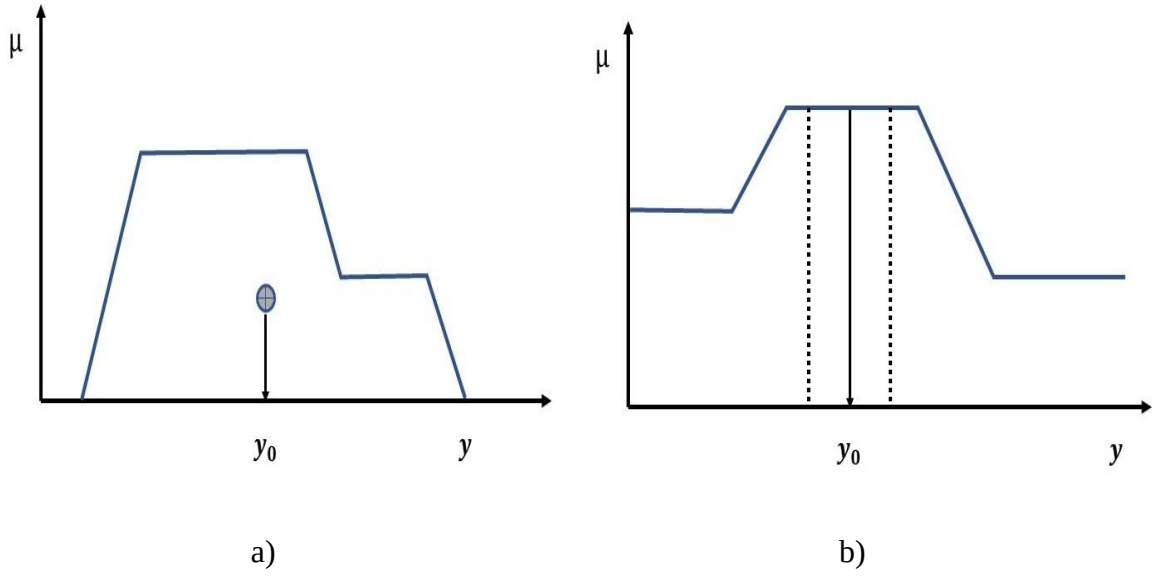

Fig. 5.15. *Defuzzification methods a) center of gravity b) mean of maxima*

The COG and MOM methods are graphically represented in **Fig. 5.15**. for the fuzzy set A, COG method numerically calculates the y coordinate of the fuzzy set as follows [145]:

$$COG(A) = \frac{\sum_{q=1}^{N_q} \mu_A(y_q) y_q}{\sum_{q=1}^{N_q} \mu_A(y_q)} \tag{5.11}$$

where N_q is the number of discretised values y_q in Y.

The MOM method calculates the mean value of interval with the largest membership value as follows:

$$MOM(A) = mean\,\{y \mid \mu_A(y) = max\,\mu_A(y)\} \tag{5.12}$$

Mamdani and Sugeno (TSK) methods are the most commonly used methods of fuzzy inference system [148]. Although both methods share some common features, their difference is in the specification of the consequent part. In the Mamdani inference system the consequents are fuzzy sets which are transformed to a crisp output using the defuzzification methods. In contrast, the consequents in the TSK method are not in the form of membership functions. The consequents are either constant or a linear (weighted) mathematical expression. The crisp result (also known as singleton output) is obtained using weighted average of the rules' consequent. The rules of first-order TSK fuzzy inference system represented in **Fig. 5.16** are as follows:

R_i: **IF** x is A **AND** y is B **THEN** $z = px + qy + r$ (5.13)

where A and B denote the fuzzy sets of antecedent and p, q, and r are the parameter set of linear consequent functions.

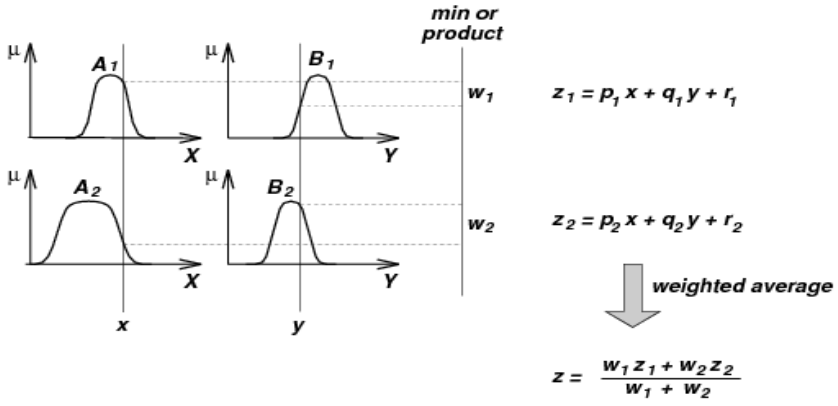

Fig. 5.16. *First-order TSK fuzzy inference system [149]*

5.3.4 Fuzzy based evaporator model

The numerical methods of evaporator modelling are useful at the design stage of the ORC system to find the best components of the cycle and the optimal working fluid selection, but a more traceable model is required for the real-time control of the ORC with transient heat source. The concept of a real-time control-oriented evaporator model has been investigated in Chowdhury et al. studies [138, 150] demonstrating fuzzy steady-state and dynamic models of evaporator. In their study, the nonlinear relationship between the input and output is mapped using the linguistic rules based on the expert knowledge about the evaporator behaviour.

Inputs of the Mamdani fuzzy system in their study are the mass flow rate and temperature of the hot fluid ($\dot{m}_h, T_h$) and mass flow rate of the organic working fluid ($\dot{m}_r$). The desired outputs are the working fluid and heat source output temperatures ($T_{r,o}, T_{h,o}$). By deploying membership functions the input and outputs of the fuzzy model are classified into different linguistic levels. Three linguistic levels of Low, Medium and High are assigned to describe the input variables. For the first output variable ($T_{r,o}$) five linguistic variables of Very Low, Low, Medium, High and Very High are selected. The second output variable ($T_{h,o}$) has an extra linguistic variable called Medium to High. **Figs. 5.17** and **5.18**, represent the normalised membership functions and their assigned linguistic level for input and output parameters.

A set of twenty-seven IF-THEN rules listed in **Table 5.3** were applied to model the behaviour of evaporator. The format of the rules is defined as follows:

R_i : **IF** $\dot{m}_r$ is α_i **AND** $\dot{m}_h$ is β_i **AND** T_h is γ_i **THEN** $T_{r,o}$ is δ_i **AND** $T_{h,o}$ is Ψ_i

where i = 1, 2, 3, ..., n, is the number of fuzzy rules, α_i, β_i, γ_i, δ_i, Ψ_i are the ith fuzzy sets of the input and output variables of the fuzzy system.

From the simulation results the authors concluded that compared to the previous computational methods of evaporator modelling, the fuzzy logic evaporator model is much faster and can calculate the outputs in 5.19 seconds compared to 3820.6 seconds for the FV model. Furthermore, the governing nonlinear partial differential equations of the evaporator does not need to be calculated and fuzzy system estimates the behaviour of evaporator using the previous knowledge of the system behaviour.

Comparison of the fuzzy and FV models of the evaporator for calculating the outlet refrigerant temperature and the heat source outlet temperature are presented in **Figs. 5.19** and **5.20**. The RMSE, fitness percentage and MAPE are used to evaluate the performance of fuzzy model in predicting the FV evaporator data. The reported RMSE for the outlet refrigerant temperature model and the heat source outlet temperature are 1.10 K and 3.09 K, respectively. Moreover, the MAPE obtained for the outlet refrigerant temperature model is reported 0.19%, and for the heat source outlet temperature, MAPE of 0.58% is obtained. The fitness percentage achieved are 90.32% and 91.24% for the outlet refrigerant temperature model and the heat source outlet temperature, respectively.

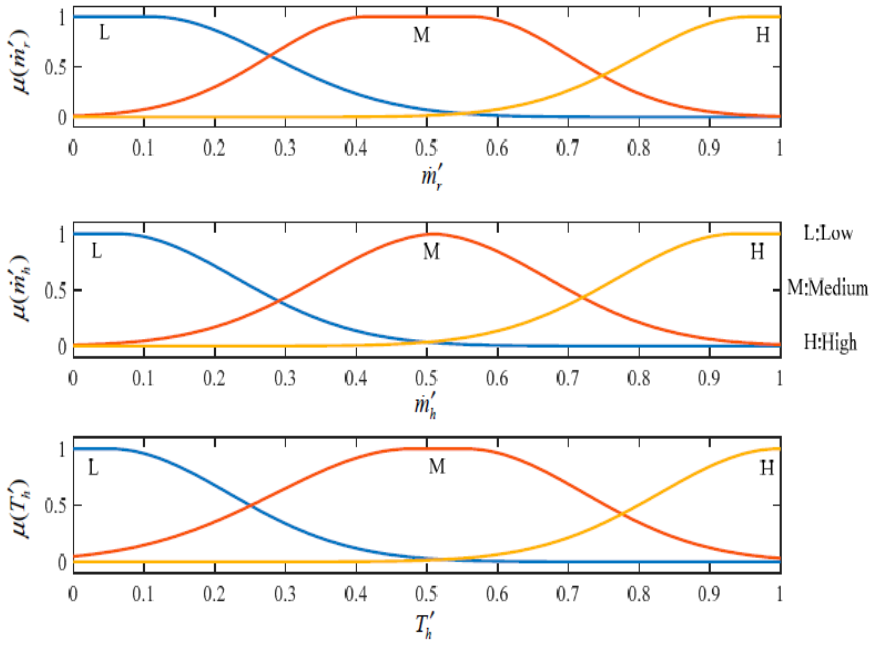

Fig. 5.17. *Normalized membership functions of input variables [150]*

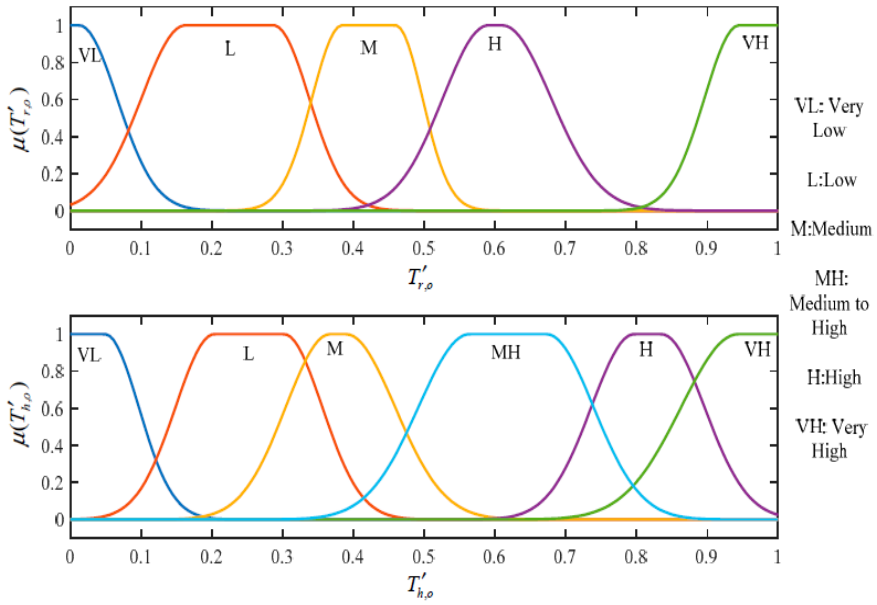

Fig. 5.18. *Normalized membership functions of outlet variables [150]*

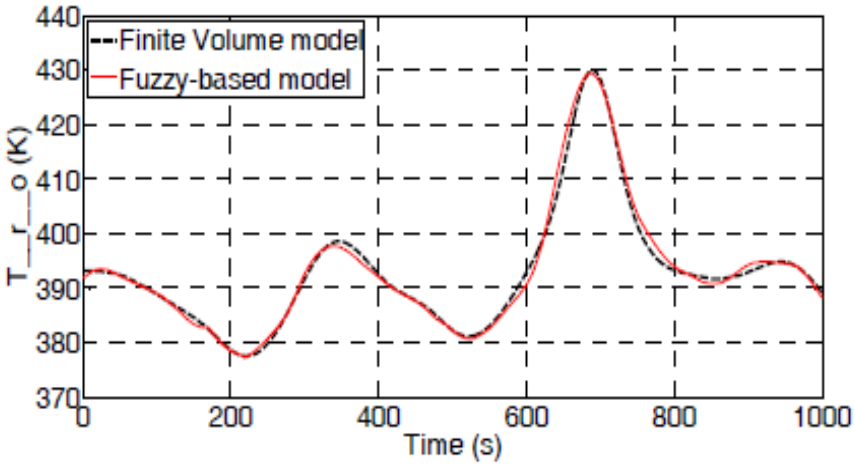

Fig. 5.19. *Comparison of refrigerant outlet temperature between Fuzzy model and FV model [150]*

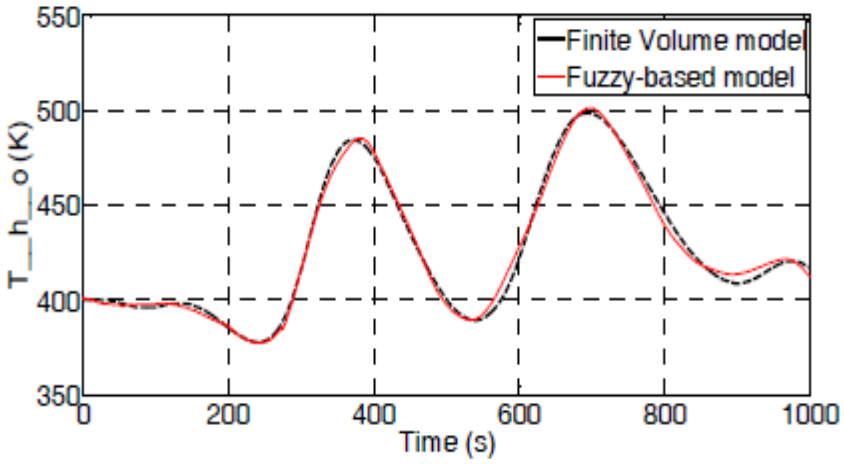

Fig. 5.20. *Comparison of heat source outlet temperature between Fuzzy model and FV model [150]*

Table 5.3 *– Fuzzy rules of fuzzy evaporator model [150]*

Rule number	IF $\dot{m}_r$ is	AND $\dot{m}_h$ is	AND T_h is	Then $T_{r,o}$ is	AND $T_{h,o}$ is
1	L	L	L	L	VL
2	L	L	M	M	L
3	L	L	H	M	L
4	L	M	L	L	L
5	L	M	M	L	LM
6	L	M	H	VH	M
7	L	H	L	M	LM
8	L	H	M	H	M
9	L	H	H	VH	MH
10	M	L	L	VL	VL
11	M	L	M	L	L
12	M	L	H	L	L
13	M	M	L	VL	LM
14	M	M	M	L	M
15	M	M	H	M	MH
16	M	H	L	VL	M
17	M	H	M	L	MH
18	M	H	H	M	VH
19	H	L	L	VL	VL
20	H	L	M	VL	L
21	H	L	H	VL	L
22	H	M	L	VL	LM
23	H	M	M	L	M
24	H	M	H	L	MH
25	H	H	L	VL	M
26	H	H	M	L	H
27	H	H	H	L	VH

This model can expeditiously be used for real-time modelling of the control system due to its lower computational time. Although the fuzzy method is agile, if any of evaporator design parameters such as size or evaporator layout change, the fuzzy rules and the membership functions of the fuzzy system need to be adjusted accordingly. Moreover, the parameters of membership functions and fuzzy rules are not tuned using the available adaptive techniques; therefore, setting the rules for manually tuning the evaporator behaviour is an adversely time-consuming task.

The lack of learning capability in this Mamdani model can be addressed by deploying hybrid modelling techniques such as neuro-fuzzy approach. Hybrid modelling techniques combine the techniques with learning capability such as neural networks with the fuzzy system in order to provide learning ability for the model while keep the transparency of the fuzzy system. Furthermore, inadequacies of both techniques can be covered and a better balance between credibility and understandability can be attained. Therefore, to reduce the modelling effort, increase the accuracy of models and eliminate the dependency of fuzzy models on expert knowledge about the system, the adaptive neuro-fuzzy system (ANFIS) modelling technique is represented in the next section for modelling the input-output behaviour of the evaporator.

5.4 Adaptive neuro-fuzzy inference system modelling

ANFIS is a systematic hybrid input-output mapping technique introduced by Jang [149] in 1993 and since its introduction has been applied in a wide range of engineering problems. This method combines feedforward neural network and Takagi-Sugeno fuzzy inference system. The optimal distribution of membership functions in the fuzzy system is determined using this technique, independent of expert knowledge of the system. The neural network is

particularly adequate for pattern recognition in nonlinear systems and the fuzzy technique is a powerful approach for modelling nonlinear systems. The model obtained using the ANFIS method is not regarded as a completely black-box model, because the fuzzy-logic capabilities of the model makes it interpretable in terms of the linguistic variables [151].

Despite the desirable capabilities of the ANFIS modelling technique, to the best of the author's knowledge, it has not been used to model the evaporator's behaviour in the literature. Therefore, this study aims to provide a model of evaporator using the ANFIS technique for the first time.

5.4.1 ANFIS architecture

The architecture of ANFIS consists of five layers and each layer has multiple nodes that are described by node functions as shown in **Fig. 5.21**.

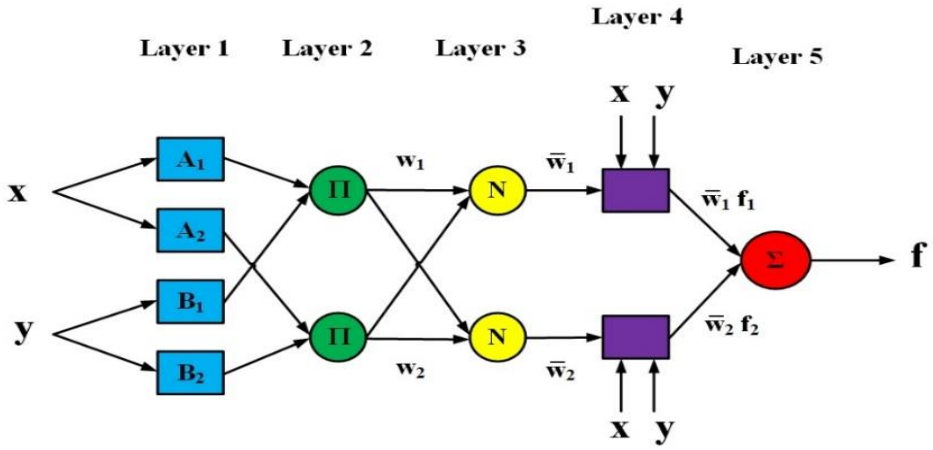

Fig. 5.21. *ANFIS architecture*

For simplicity, a system with two inputs and one output is considered here to illustrate the ANFIS procedure by assuming two Takagi-Sugeno type fuzzy IF-THEN rules for the ANFIS system rule base. The proposed defined rules are:

Rule 1: If x is A_1 and y is B_1, then $f_1 = p_1x + q_1y + r_1$

Rule 2: If x is A_2 and y is B_2, then $f_2 = p_2x + q_2y + r_2$ (5.14)

where x and y are input variables, f_i is the output and A_i and B_i represent the fuzzy sets which are defined over the input domain, and p_i, q_i and r_i are the parameters of linear polynomial in the fourth layer of ANFIS network. There are two types of nodes in the ANFIS architecture: adaptive and fixed. The adaptive nodes contain tuneable parameters, whereas the fixed nodes which can only perform a specific task. The function of the nodes in each layer is described as follows:

Layer 1: The nodes in first layer of ANFIS are adaptive nodes with the node function:

$O_{1,i} = \mu_{A_i}(x)$ for $i = 1,2$, or

$O_{1,i} = \mu_{B_{i-2}}(y)$ for $i = 3,4$ (5.15)

where x and y are the inputs to the node i, A and B are the linguistic labels and $\mu(x)$ and $\mu(y)$ are Gaussian membership functions with the range between 0 and 1, as follows:

$$\mu(x) = \exp(-\frac{(C_i - x)^2}{2{\sigma_i}^2}) \quad (5.16)$$

In equation (5.16), c_i and σ_i determine the centre and width of the fuzzy set, respectively. The parameters in the first layer of ANFIS are referred to as premise parameters. Selection of shape and number of membership functions has a substantial influence on the complexity and accuracy of ANFIS-based models [152]. Therefore, Gaussian membership functions due to their smooth representation of input space are selected.

Layer 2: Nodes in this layer are fixed and their outputs are determining the firing strength of the rules by multiplying all incoming signals, as follows:

$$O_{2,i} = w_i = \mu_{A_i}(x)\mu_{B_i}(y),\ i = 1,2 \tag{5.17}$$

Layer 3: The nodes in this layer are fixed and are responsible for normalizing the firing strengths. The output in this layer is calculated by dividing the i^{th} rule's firing strength to sum of all rules firing strengths:

$$\overline{w}_i = \frac{w_i}{w_1+w_2},\ i = 1,2 \tag{5.18}$$

Layer 4: All the nodes in this layer are adaptive with the node function:

$$O_{4,i} = \overline{w}_i f_i = \overline{w}_i(p_i x + q_i y + r_i) \tag{5.19}$$

where $\overline{w}_i$ is the normalized firing strength from previous layer and p_i, q_i and r_i are the parameters set referred to as consequent parameters.

Layer 5: The single node in this layer is a fixed node and calculates the summation of all incoming signals to produce a crisp output as follows:

$$O_{5,1} = \sum_i \overline{w}_i f_i = \frac{\sum_i w_i f_i}{\sum_i w_i} \tag{5.20}$$

5.4.2 Training algorithms of the network

The aim of training the ANFIS network is to adjust the premise and consequent parameters in the adaptive nodes to minimise a performance measure known as the error function. Despite outperforming other fuzzy methods, ANFIS requires an effective learning algorithm for training the parameters of the network. In the original ANFIS paper proposed by Jang [153] a hybrid gradient descent, least square estimate (GD-LSE) method is used to identify

the premise and consequent parameters of the network. In this method, because of utilising a gradient-based approach, the algorithm has a tendency to trap in local minima. Therefore, in search for a more effective training method for ANFIS, metaheuristic approaches have been investigated by researchers as an alternative for identifying the network parameters. Extensive literature review illustrates that various metaheuristic algorithms such as PSO, GA, ABC and their variants have been used for training the premise and consequent parameters of the ANFIS network for a range of engineering problems. **Table 5.4**, summarises some studies which have used metaheuristic methods for training the ANFIS network.

Table 5.4 *– Summary of studies which utilised metaheuristic algorithms for ANFIS training.*

	Premise	**Consequent**
Shoorehdeli, Teshnehlab [154]	AWPSO	FFRLS
Shoorehdeli, Teshnehlab [155]	AWPSO	EKF
Sargolzaei et al. [156]	PSO	PSO
Turki, Bouzaida [157]	PSO	PSO
Rini, Shamsuddin [158]	PSO	PSO
Karaboga, Kaya [159]	ABC	ABC
Soto, Melin [160]	GA	LSE
Cardenas, Garcia [161]	GA	GA

In this study, among many methods of minimising the performance measure, the particle swarm optimisation (PSO) and standard gradient descent, lest square estimate (GD-LSE) are chosen to train the ANFIS network. Moreover, their performance for matching training and test datasets is compared. The root mean square error (RMSE) is selected as the main performance indicator. The network output will better match the training target as the RMSE approaches zero.

5.4.2.1 Gradient descent least square estimate algorithm

ANFIS learns by updating the premise (c_i and σ_i) and consequent (p_i, q_i and r_i) parameters in the first and the fourth layers of network. The conventional method for finding the optimised premise and consequent parameters is hybrid, which combines the gradient descent (GD) and least square estimate (LSE) algorithms. This method consists of a forward and a backward pass. In the forward pass, the node outputs go forward until the fourth layer and the LSE algorithm identifies the consequent parameters. In the next step, by fixing the consequent parameters the error signals propagate backward through the network and the premise parameters in the first layer of ANFIS are updated by using the GD algorithm. Combination of a forward path and a backward path is called an epoch and with enough epochs the premise and consequent parameters of the ANFIS model can be set to adequately provide the prediction power for the model. **Table 5.5** illustrates the two-pass learning algorithm of ANFIS.

Table 5.5 *– Hybrid GD-LSE learning algorithm*

Parameter	**Forward Pass**	**Backward Pass**
Antecedent Parameters	Fixed	Gradient Decent
Consequent Parameters	Least Square Estimate	Fixed
Signals	Node Outputs	Error Signals

The data is presented to the network after fixing the premise parameters. The node outputs propagated forward through the network and, consequently, the network output is obtained as a linear combination of consequent parameters as follows:

$$f = \frac{w_1}{w_1+w_2} f_1 + \frac{w_2}{w_1+w_2} f_2$$

$$= \overline{w}_1 f_1 + \overline{w}_2 f_2 \tag{5.21}$$

Substituting the fuzzy if-then rules into equation (5.21) yields:

$$f = (\overline{w}_1 x)p_1 + (\overline{w}_1 y)q_1 + (\overline{w}_1)r_1 + (\overline{w}_2 x)p_2 + (\overline{w}_2 y)q_2 + (\overline{w}_2)r_2 \tag{5.22}$$

Equation (5.22) is linear in the consequent parameters $p_1,\ q_1,\ r_1,\ p_2,\ q_2$ and r_2.

$$f = XW \tag{5.23}$$

Therefore, if the X matrix is invertible:

$$W = X^{-1} f \tag{5.24}$$

Otherwise, W is calculated by deploying a pseudo-inverse as follows:

$$W = (X^T X)^{-1} X^T f \tag{5.25}$$

where X^T is transpose of X, and $(X^T X)^{-1} X^T$is pseudo-inverse of X if $X^T X$ is non-singular.

However, $X^T X$ may become singular during the iterations that makes the problem ill-defined. Moreover, although equation (5.26) is concise in notation finding the inverse of X is expensive in computation. Therefore, to overcome this issue the recursive LSE method proposed by Jang [149] can be employed as follows:

$$W_{i+1} = W_i + S_{i+1} x_{i+1} (f_{i+1}^T - x_{i+1}^T W_i) \qquad i = 0, 1, \dots, P-1 \tag{5.26}$$

$$S_{i+1} = S_i - \frac{S_i x_{i+1} x_{i+1}^T S_i}{1 + x_{i+1}^T S_i x_{i+1}} \tag{5.27}$$

where S_i is the covariance matrix and least square estimate of W is equal to W_P. x_i^T is the ith row vector of matrix X and f_i^T is the ith element of f.

After identifying the consequent parameters, the output of network can be calculated and the error measure of P^{th} entery of the training data can be obtained as follows:

$$E_P = (T_P - O_P)^2 \tag{5.28}$$

where T_P and O_P represent the desired output and ANFIS output, respectively. Therefore, the RMSE of whole training data set can be computed as follows:

$$RMSE = \sqrt{\frac{\sum E_P}{P}} \tag{5.29}$$

In the backwards pass, the consequent parameters are fixed and the error signals propagate through the network in the reverse direction. Accordingly, using the GD algorithm the premise parameters that are located in the first layer of the network are updated as follows:

$$c_{ij}(t+1) = c_{ij}(t) - \frac{\eta}{p} \cdot \frac{\partial E}{\partial c_{ij}} \tag{5.30}$$

where, c_{ij} is the membership function's adjustable parameter and η represents the learning rate. To obtain the partial derivative $\frac{\partial E}{\partial c_{ij}}$, the chain rule is applied as follows:

$$\frac{\partial E}{\partial c_{ij}} = \frac{\partial E}{\partial f} \cdot \frac{\partial f}{\partial f_i} \cdot \frac{\partial f_i}{\partial w_i} \cdot \frac{\partial w_i}{\partial \mu_{ij}} \cdot \frac{\partial \mu_{ij}}{\partial c_{ij}} \tag{5.31}$$

An important disadvantage of using the gradient-based techniques for tuning the membership functions of the ANFIS model is that they are likely to fall into local minima. Therefore, non-gradient methods of tuning the antecedent parameters of the model are recommended [162].

5.4.2.2 Particle swarm optimization

Particle swarm optimization (PSO) is a heuristic swarm intelligence technique first introduced by Eberhart and Kennedy [163]. This method is inspired by biological and sociological behaviour of birds and fish searching for their food. PSO is a population-based search method, which is applied in several studies to solve optimization problems [164, 165]. Each possible solution to the optimisation problem is called a particle. In this method an initial random position is assigned to each particle and particles move in the multidimensional search space and their position and flight speed is updated according to their best-known local position guided by other whole particles best known general position, until equilibrium is reached or the computational limitations is exceeded. Consider a swarm with population size of N, initial position of x and movement speed of v. The best local position of a particle is denoted as P_{best} and position of the particle in the swarm which better minimizes the performance measure is denoted as G_{best}. The speed and position of the i^{th} particle of the swarm in the next iteration can be formulated as follows:

$$v_i(k) = wv_i(k-1) + \rho_1(x_{Pbest} - x_i(k)) \; + \; \rho_2(x_{Gbest} - x_i(k)) \tag{5.32}$$

$$x_i(k) = \; x_i(k-1) + \; v_i(k) \tag{5.33}$$

where ρ_1 and ρ_2 are random variable defined as $\rho_1 = r_1 c_1$ and $\rho_2 = r_2 c_2$, with r_1 and r_2 ~ $U(0,1)$. The variables c_1 and c_2 are positive acceleration constants that satisfy the condition $c_1 + c_2 \leq 4$ [166] and w is the inertial weight that can be calculated using the inertial weight approach (IWA) as follows [167]:

$$w = w_{max} - \frac{w_{max} - w_{min}}{Itr_{max}} \; Itr \tag{5.34}$$

where w_{max} and w_{min} denote the initial and final weights, Itr represents the current iteration number and Itr_{max} is the maximum number of iterations.

Although metaheuristic algorithms such as PSO do not guarantee convergence to the optimal solution, they do not require the optimization problem to be differentiable as opposed to the gradient-based methods. Furthermore, for a given size of network the PSO ANFIS method has the advantage of being less computationally expensive [162]. In this study, the PSO algorithm is deployed to find the optimal parameters of antecedent and consequent parts of ANFIS and the results are compared with the hybrid GD-LSE learning algorithm.

5.5 ANFIS evaporator model implementation

In this section an ANFIS evaporator model is developed using the data collected from a FV model of evaporator available in the literature [129]. To train the ANFIS model, the FV model of evaporator is excited by changing the heat source mass flow rate ($\dot{m}_h$), the heat source temperature (T_h) and the mass flow rate of refrigerant ($\dot{m}_r$) in the range of 0.073-0.2985 kg/s, 412-523 K and 0.0318-0.2243 kg/s, respectively. The heat source mass flow rate and temperature data are randomly selected according to the range of a generic heat source in ICE of heavy-duty trucks. Outlet temperature of refrigerant (T_{rout}) and outlet temperature of the heat source (T_{hout}) are selected as the output parameters of the evaporator model. In total, 1000 data points collected form dynamic FV model and each data point represents one second of actual evaporator input-output behaviour. Details of the FV model used for gathering the data can be found in Ref. [138]. Input-output data used for the modelling is illustrated in **Fig. 5.22**. As recommended in several studies, the data is further divided randomly to 70% for training and 30% for testing the proposed PSO ANFIS and GD-LSE ANFIS models.

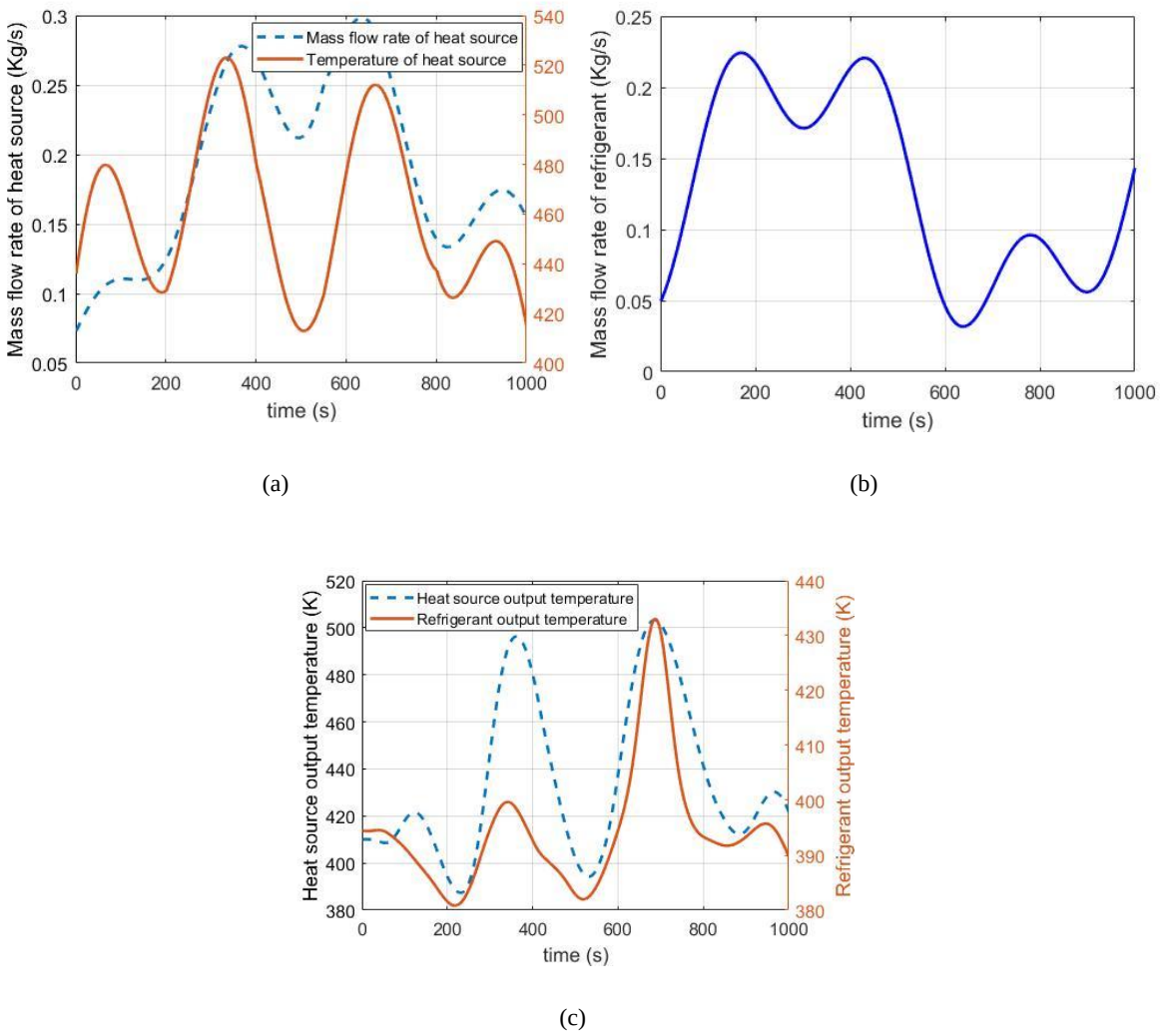

Fig. 5.22. *Input-output data gathered from FV model of evaporator (a) Mass flow rate and temperature of generic heat source (b) Mass flow rate of refrigerant (c) Refrigerant and heat source temperatures at the evaporator outlet*

In order to obtain a base FIS, the input search space needs to be clustered. Grid partitioning (GP), subtractive clustering (SCM) and fuzzy c-means (FCM) are the most widely used approaches in the literature for clustering the data. In this study, FCM clustering method due to its higher flexibility is implemented to obtain the base FIS.

5.5.1 Training ANFIS evaporator model using hybrid GD-LSE algorithm

The ANFIS method has been applied to train two multi-input single-output ANFIS models for prediction of the refrigerant output temperature (T_{rout}) and heat source output temperature (T_{hout}). Moreover, the GD algorithm is used to adjust the premise parameters and LSE algorithm is applied to update the consequent parameters. The ANFIS training parameters for both models are listed in **Table 5.6**. In **Figs. 5.23** and **5.24**, the trained membership functions for refrigerant and heat source output temperatures are represented, respectively. The fuzzy surfaces shown in **Figs. 5.25** and **5.26** indicate the effect of transient inputs on the heat source output temperature and refrigerant output temperature, respectively.

Table 5.6 *– GD-LSE ANFIS training parameters*

Parameters	**GD-LSE ANFIS model for heat source output temperature**	**GD-LSE ANFIS model for refrigerant output temperature**
Number of training data set	701×4	701×4
Number of test data set	300×4	300×4
Clustering method	FCM	FCM
Membership functions	Gaussian	Gaussian
Number of Clusters	7×3	8×3
Number of Epochs	3000	3000
Number of nodes	62	70
Number of linear parameters	28	32
Number of nonlinear parameters	42	48
Total number of parameters	70	80
Number of fuzzy rules	7	8

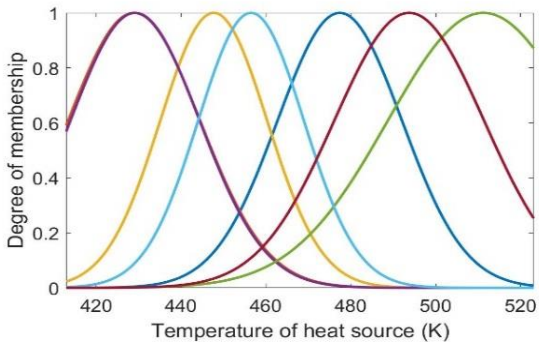

(a)

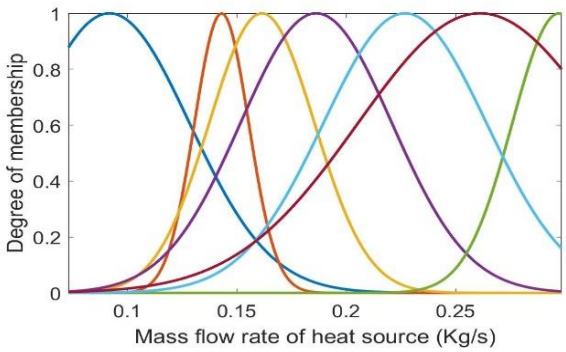

(b)

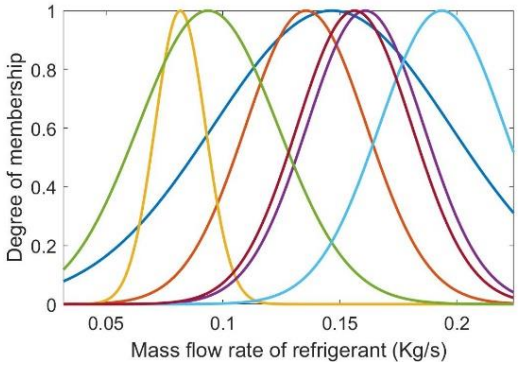

(C)

Fig. 5.23. *Trained membership functions of GD-LSE ANFIS model for predicting the heat source output temperature (a) temperature of heat source (b) mass flow rate of heat source (c) mass flow rate of refrigerant*

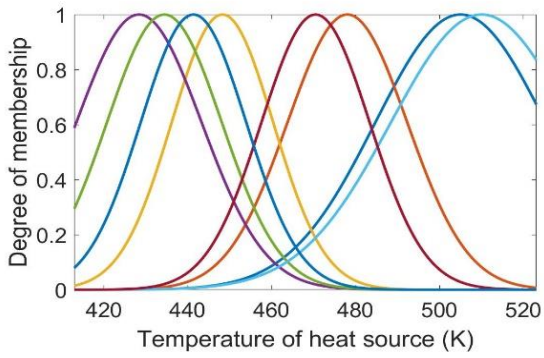

(a)

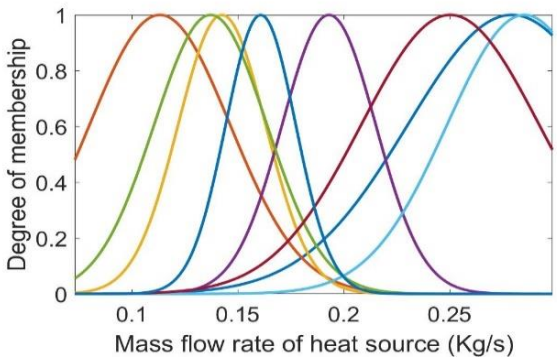

(b)

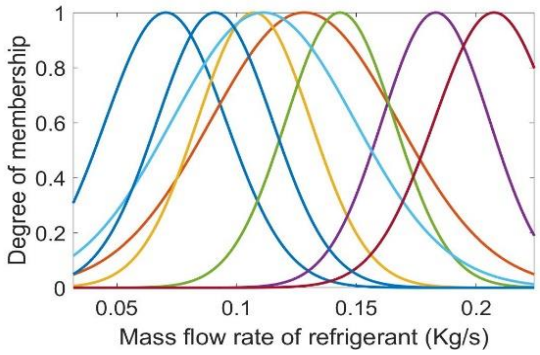

(c)

Fig. 5.24. *Trained membership functions of GD-LSE ANFIS model for predicting the refrigerant output temperature (a) temperature of heat source (b) mass flow rate of heat source (c) mass flow rate of refrigerant*

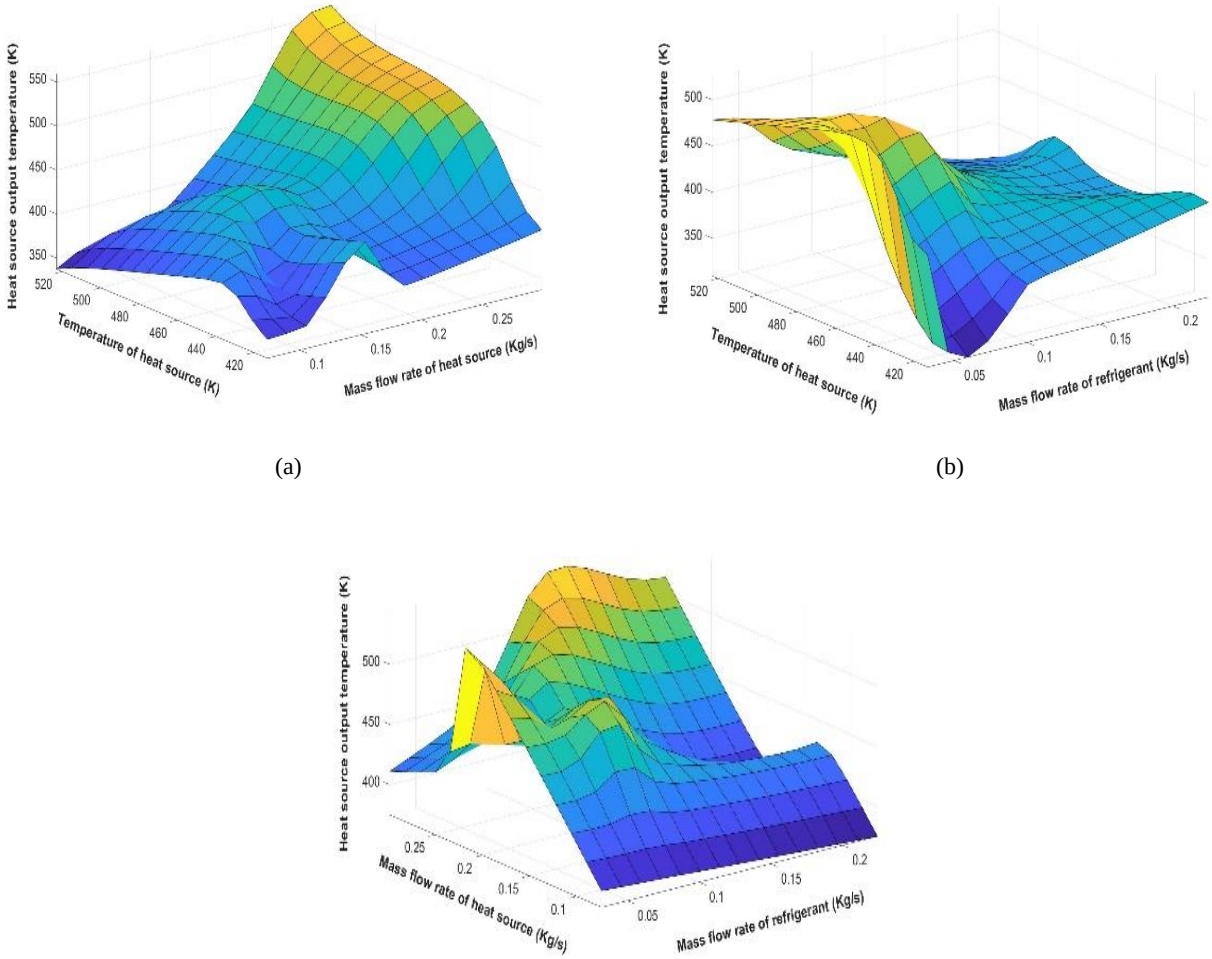

Fig. 5.25. *Fuzzy surfaces representing the Effect of changing the input parameters on the heat source output temperature in the GD-LSE ANFIS model*

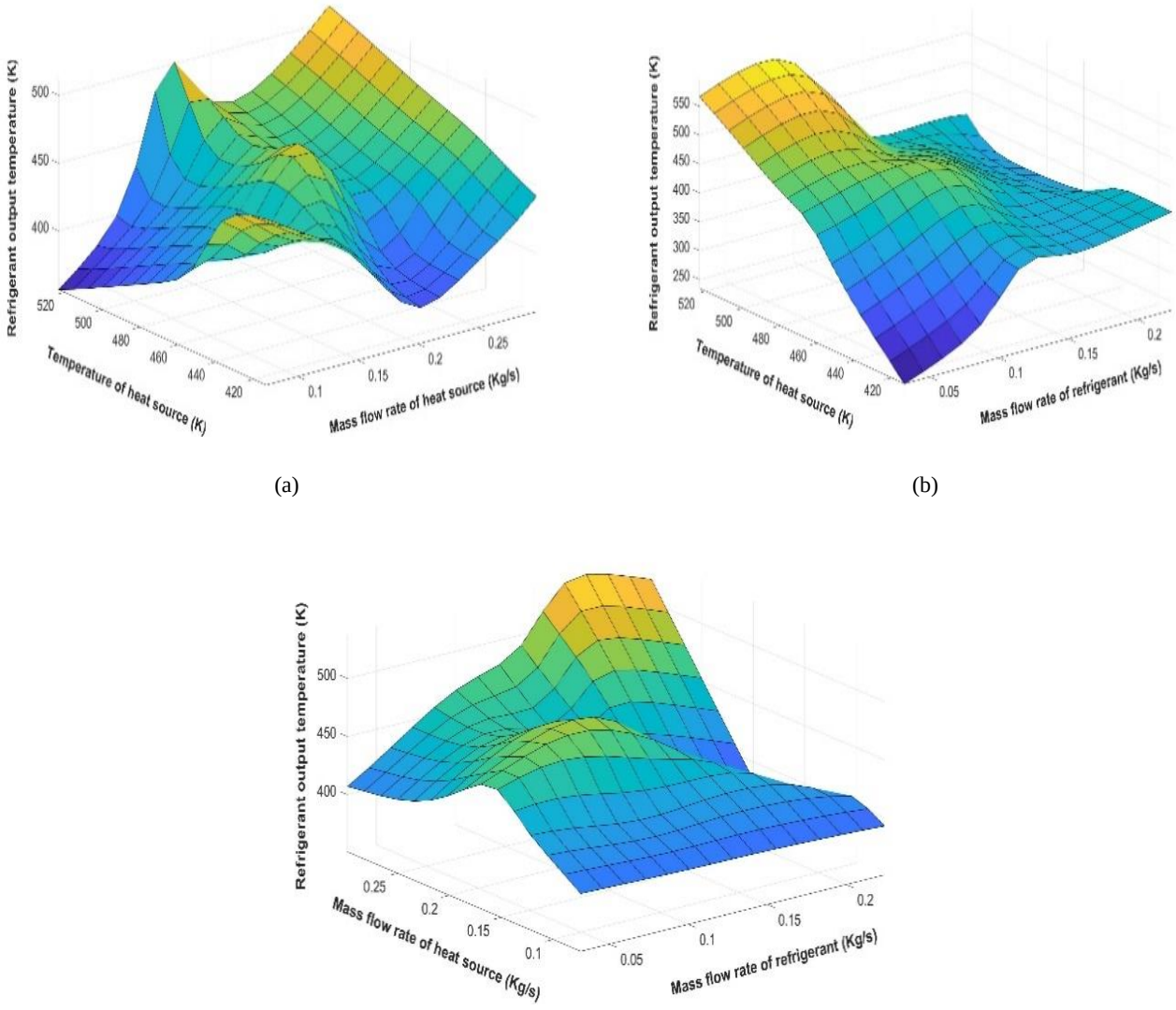

Fig. 5.26. *Fuzzy surfaces representing the Effect of changing the input parameters on the refrigerant output temperature in the GD-LSE ANFIS model*

5.5.2 Training ANFIS evaporator model using PSO algorithm

The standard two pass GD-LSE learning method of ANFIS is prone to get stuck in local minima, therefore, derivative-free metaheuristic algorithms such as PSO for training the parameters of ANFIS model are recommended [162]. In general, combining the ANFIS with PSO technique produces a model with more reliable results. The most influential parameters of PSO algorithm are: (1) the number of the population, (2) the personal and global learning coefficients (C_1 and C_2), and (3) the inertial weight (w).

For training the ANFIS using the PSO algorithm, the parameters of Gaussian membership functions in the antecedent and parameters of consequent linear polynomial of the base FIS obtained using the FCM algorithm are extracted. These parameters are optimized using the PSO algorithm in order to minimize the cost function defined as the RMSE between the target values and the ANFIS model output values as follows:

$$RMSE = \sqrt{\frac{1}{N}\sum_{i=1}^{N}(H_i^{Target} - H_i^{Output})} \tag{5.35}$$

The PSO parameters utilised for modelling the output temperature of refrigerant and output temperature of heat source are listed in **Table 5.7**. In **Figs. 5.27** and **5.28** the trained membership functions of the input variables for output temperature of heat source and output temperature of refrigerant models are depicted, respectively. **Figs. 5.29** and **5.30** indicate the interdependency of input variables for the output temperature of heat source and the output temperature of refrigerant prediction within the selected ranges, respectively.

Table 5.7 – Parameters of PSO ANFIS algorithm

Parameters	**PSO ANFIS model for heat source output temperature**	**PSO ANFIS model for refrigerant output temperature**
Number of training data set	701×4	701×4
Number of test data set	300×4	300×4
Clustering method	FCM	FCM
Membership functions	Gaussian	Gaussian
Number of Clusters	7×3	8×3
Maximum iteration	3000	3000
Inertial weight	1	1
Personal learning coefficient (C_1)	1	1
Global learning coefficient (C_2)	2	2
Number of optimized parameters	70	80
Number of fuzzy rules	7	8

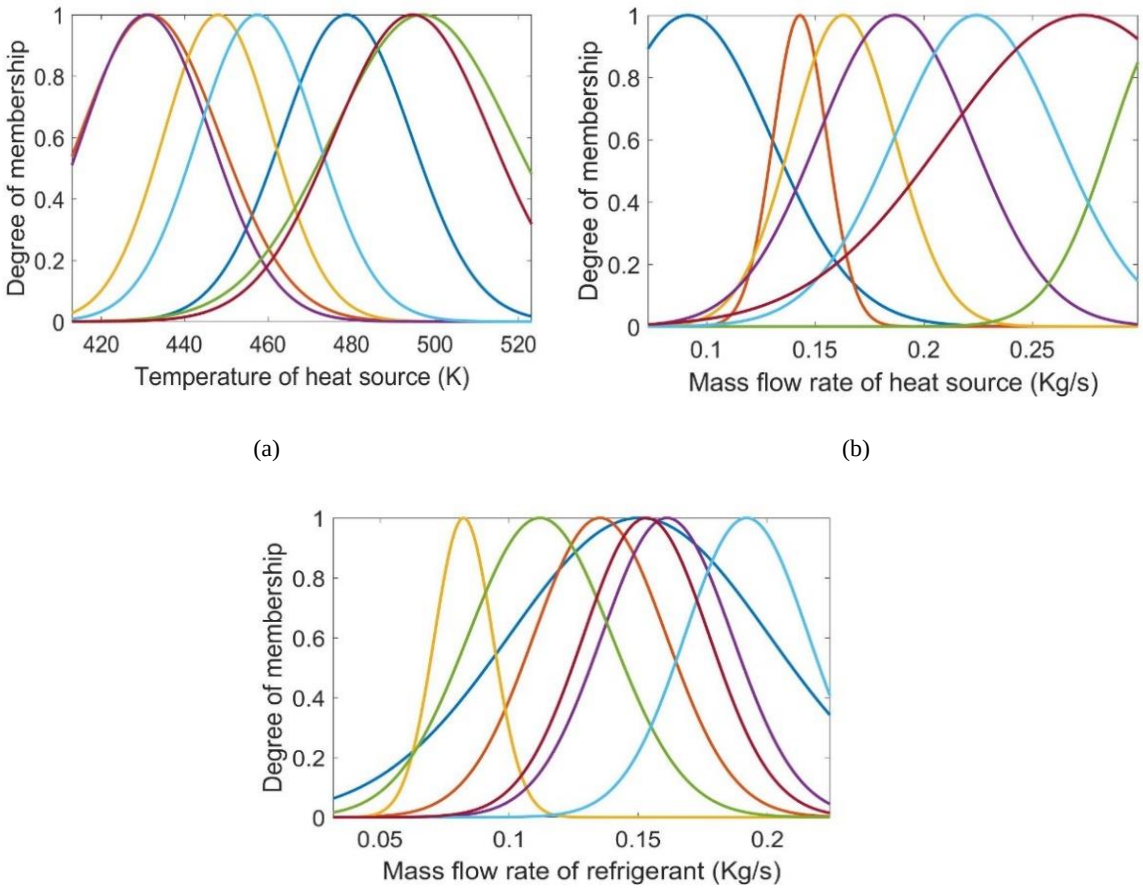

(a) (b)

(c)

Fig. 5.27. *Trained membership functions of PSO ANFIS model for predicting the heat source output temperature (a) temperature of heat source (b) mass flow rate of heat source (c) mass flow rate of refrigerant*

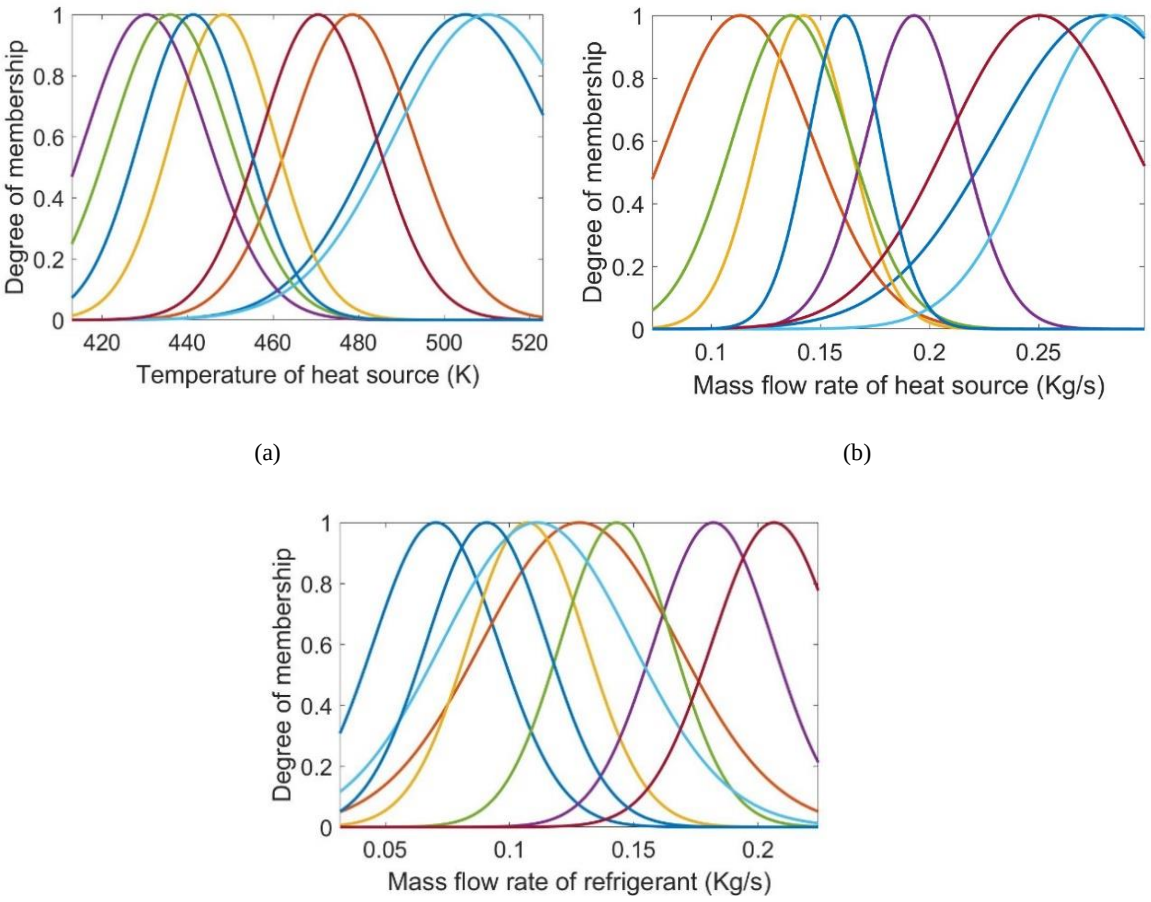

(a) (b)

(c)

Fig. 5.28. *Trained membership functions of PSO ANFIS model for predicting the refrigerant output temperature (a) temperature of heat source (b) mass flow rate of heat source (c) mass flow rate of refrigerant*

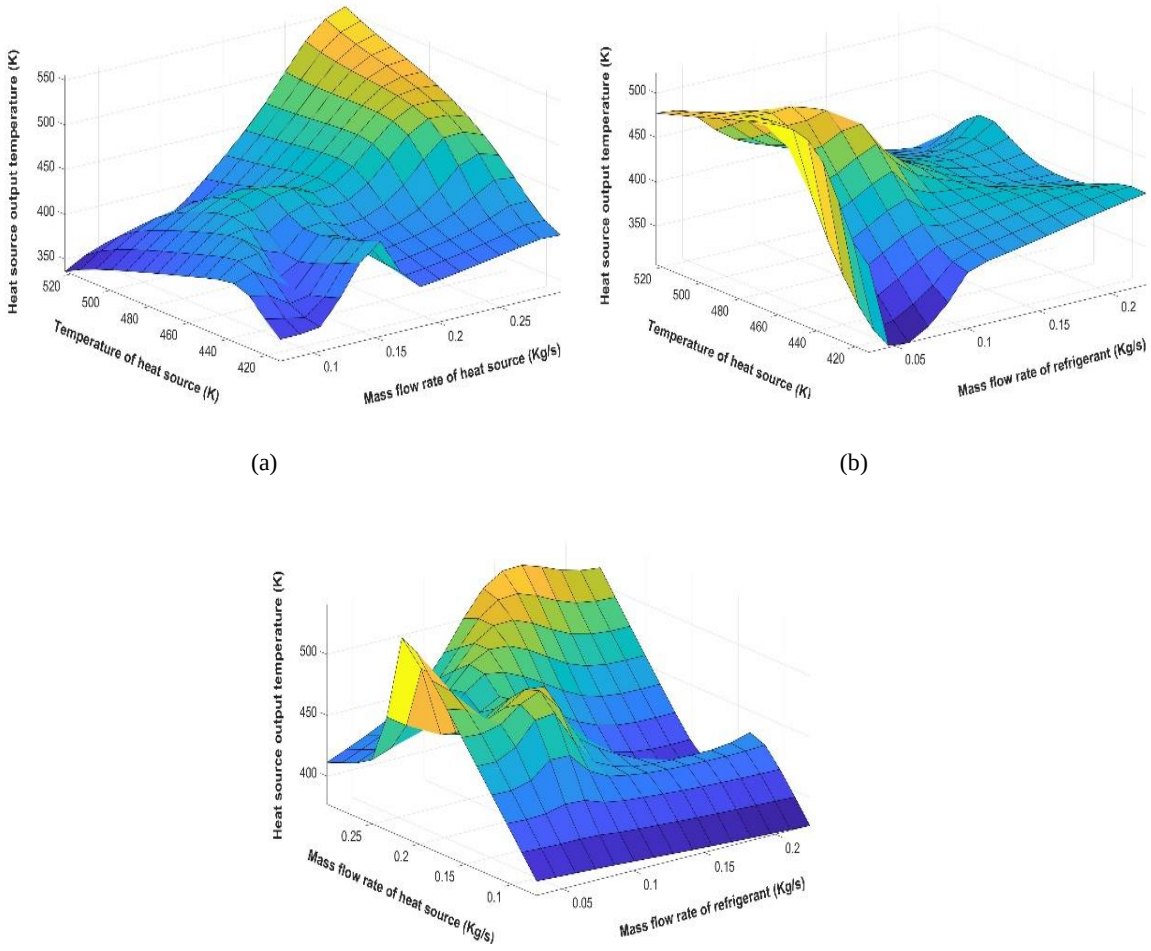

Fig. 5.29. *Fuzzy surfaces representing the Effect of changing the input parameters on the heat source output temperature in the PSO ANFIS model*

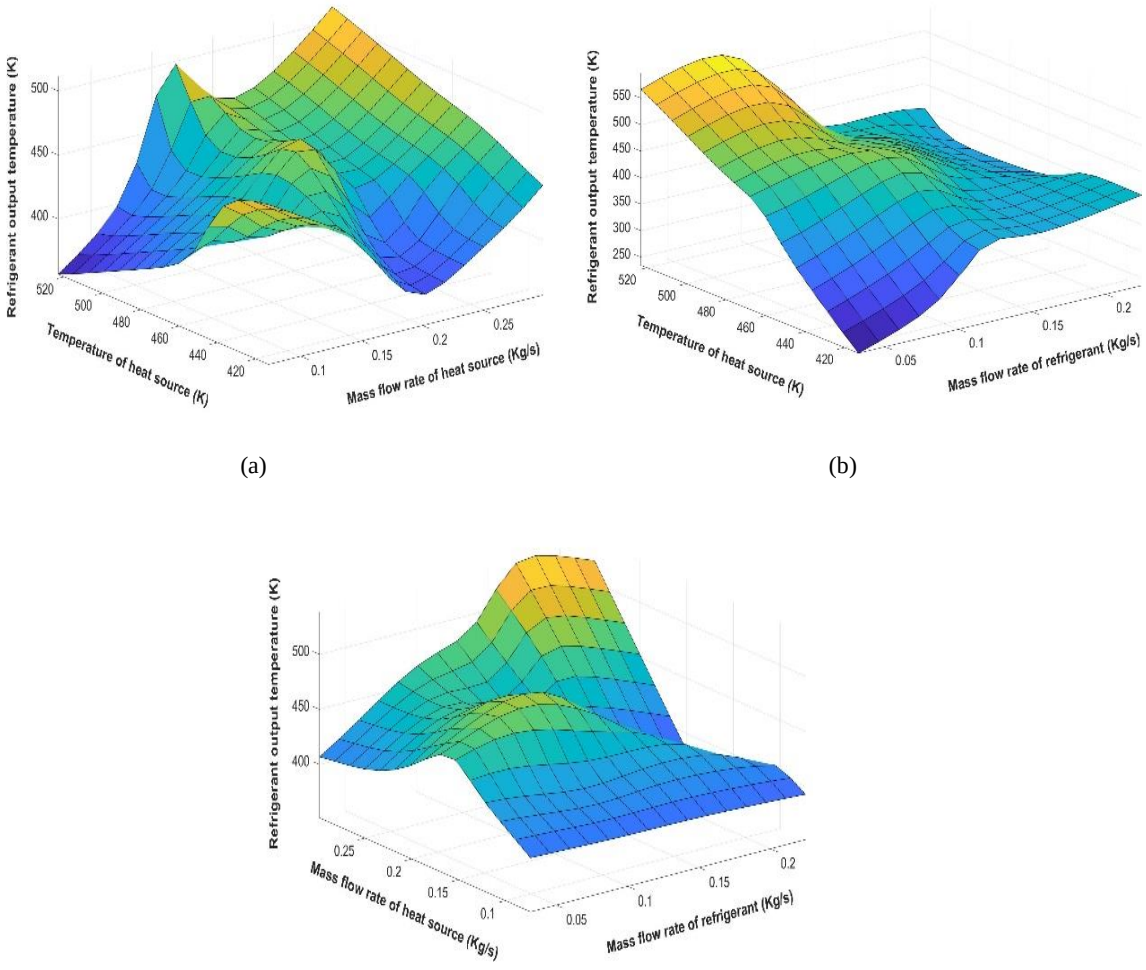

Fig. 5.30. *Fuzzy surfaces representing the Effect of changing the input parameters on the refrigerant output temperature in the PSO ANFIS model*

5.6 Comparison of training ANFIS model using GD-LSE and PSO

Two intelligent ANFIS approaches are applied to determine the output temperature of heat source and the output temperature refrigerant in a counter flow evaporator by considering mass flow rate and temperature of heat source and mass flow rate of refrigerant as input variables to the evaporator. A comparison between the prediction power of the GD-LSE ANFIS and PSO ANFIS models for the heat source output is illustrated in **Fig. 5.31**. As it can be seen, both training data and an unseen test data are applied to the trained models to evaluate the generalization power of the models. Additionally, a statistical criterion in terms of RMSE is considered to evaluate the accuracy of the models. For the training data, the RMSEs for PSO and GD-LSE trained ANFIS models are 0.241 and 0.327, respectively. The unseen test data RMSE is equal to 0.242 for the PSO ANFIS model and 0.336 for the GD-LSE model. It can be deduced that the output heat source temperature results obtained from PSO ANFIS model have a better agreement with the FV model as compared with the GD-LSE ANFIS model.

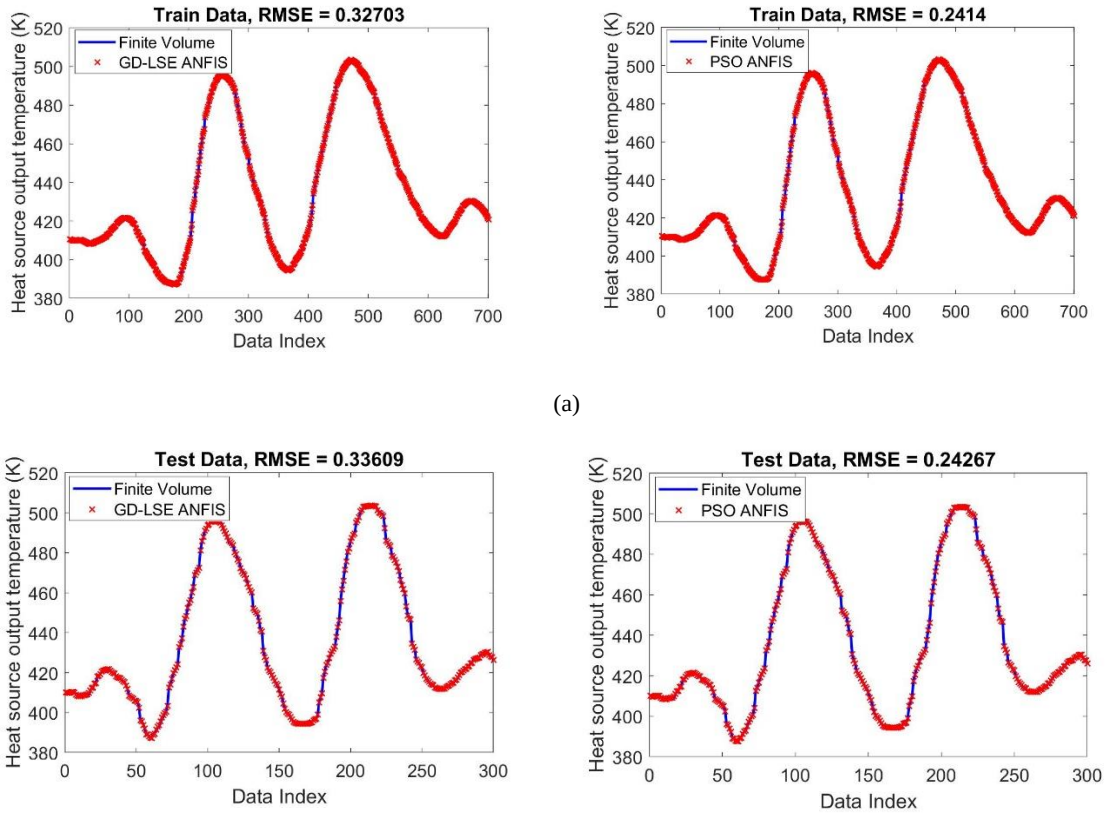

Fig. 5.31. *Comparison of heat source output temperature prediction between GD-LSE ANFIS model and PSO ANFIS model for (a) training data (b) test data*

Furthermore, to better illustrate the deviation of the predicted heat source output temperatures from the numerically simulated values, regression plots are shown in **Fig. 5.32**. The linear correlation coefficient (R) for both models clearly imply the high generalization power of the models since the R value for both training and test data are close to one.

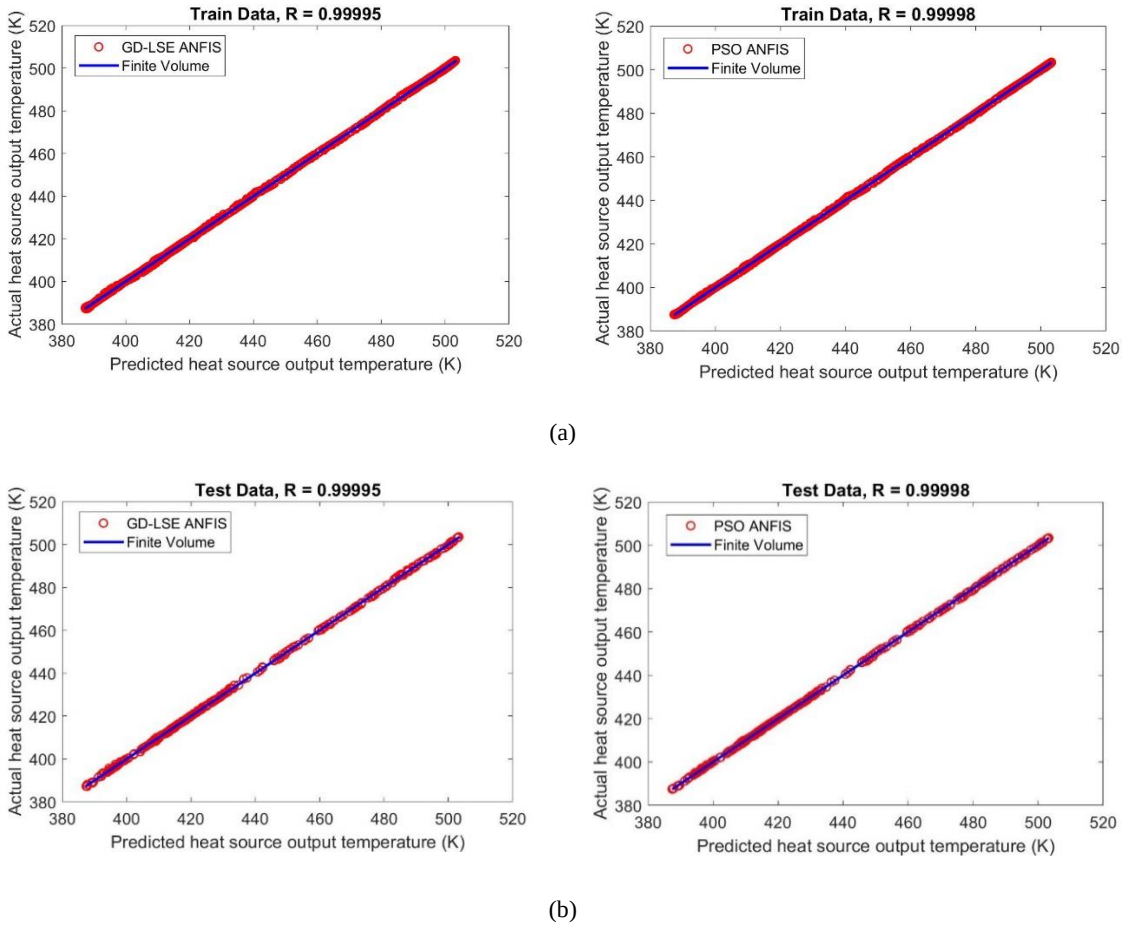

Fig. 5.32. *Comparison of regression plots for heat source output temperature prediction between GD-LSE ANFIS model and PSO ANFIS model for (a) training data (b) test data*

The predicted data of refrigerant output temperature by two aforementioned methods of GD-LSE and PSO ANFIS are plotted versus FV model data in **Fig. 5.33**. In order to assess the generalization ability of the trained models, as discussed earlier in the data preparation, a test dataset (30% of the whole dataset) is randomly selected, and applied to the model. The predicted values for test dataset versus FV is also showcased in **Fig. 5.33** for the GD-LSE and PSO ANFIS models. It can be concluded that the models are not overfitted since the RMSE for the test data and the training data have a subtle difference.

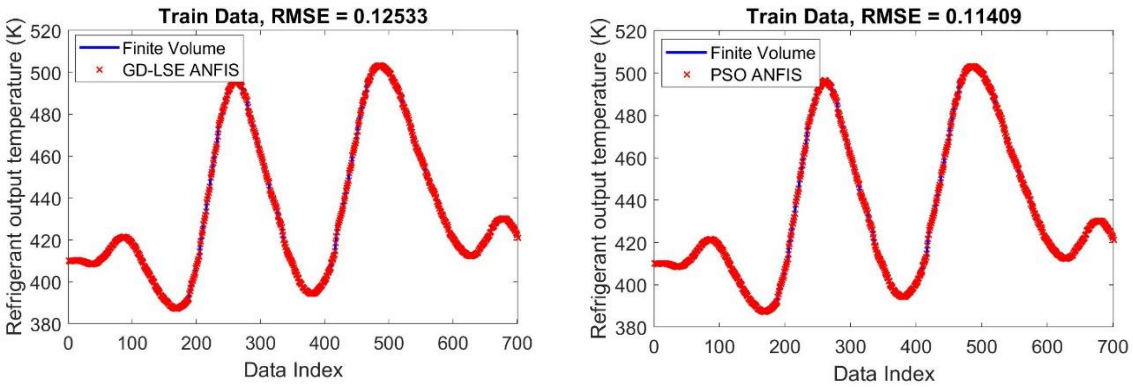

(a)

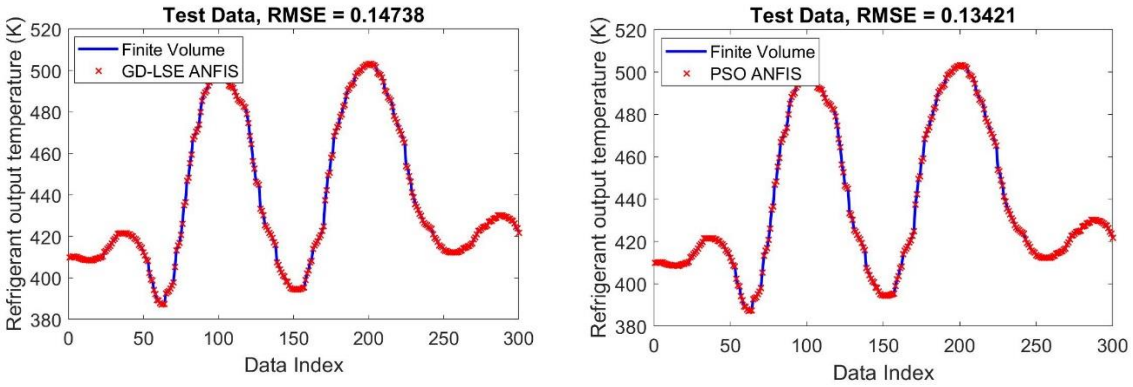

(b)

Fig. 5.33. *Comparison of refrigerant output temperature prediction between GD-LSE ANFIS model and PSO ANFIS model for (a) training data (b) test data*

Similarly, comparison of regression plots for refrigerant output temperature prediction between the GD-LSE and PSO trained ANFIS models is presented in **Fig. 5.34**. The obtained linear correlation coefficient (R) values of both models for training and test data are close to one. This indicates the low deviation of results as compared to numerically calculated FV model results. To better point out the accuracy of proposed ANFIS models, Statistical error analysis is summarized in **Table 5.8**. Referring to RMSE and MSE for heat source and refrigerant output temperature models, clearly the models trained with the PSO algorithm have higher accuracies. The highest accuracy is achieved for the refrigerant output temperature model trained using PSO algorithm with the RMSE of 0.114 and MSE of 0.013

for the training dataset, and respectively, 0.134 and 0.018 for the test dataset. Since in the application of ORC cycle for recovering waste heat from exhaust of ICEs safety of the system is vital, such an accurate prediction of refrigerant temperature at the evaporator outlet plays a prominent role in designing robust control systems. On the other hand, the highest improvement in RMSE is achieved by PSO trained ANFIS for the heat source output temperature prediction compared to the GD-LSE ANFIS model by approximately 27 percent for both training and test datasets.

Table 5.8 *– Statistical error analysis of the proposed models*

Model	**Target Output**	**Data set**	**RMSE**	**MSE**	**R**
GD-LSE ANFIS	Heat source output temperature	Train	0.327	0.1069	0.99995
		Test	0.336	0.1130	0.99995
PSO ANFIS	Heat source output temperature	Train	0.241	0.0583	0.99998
		Test	0.242	0.0589	0.99998
GD-LSE ANFIS	Refrigerant output temperature	Train	0.125	0.0157	0.99999
		Test	0.147	0.0217	0.99999
PSO-ANFIS	Refrigerant output temperature	Train	0.114	0.0130	0.99999
		Test	0.134	0.0180	0.99999

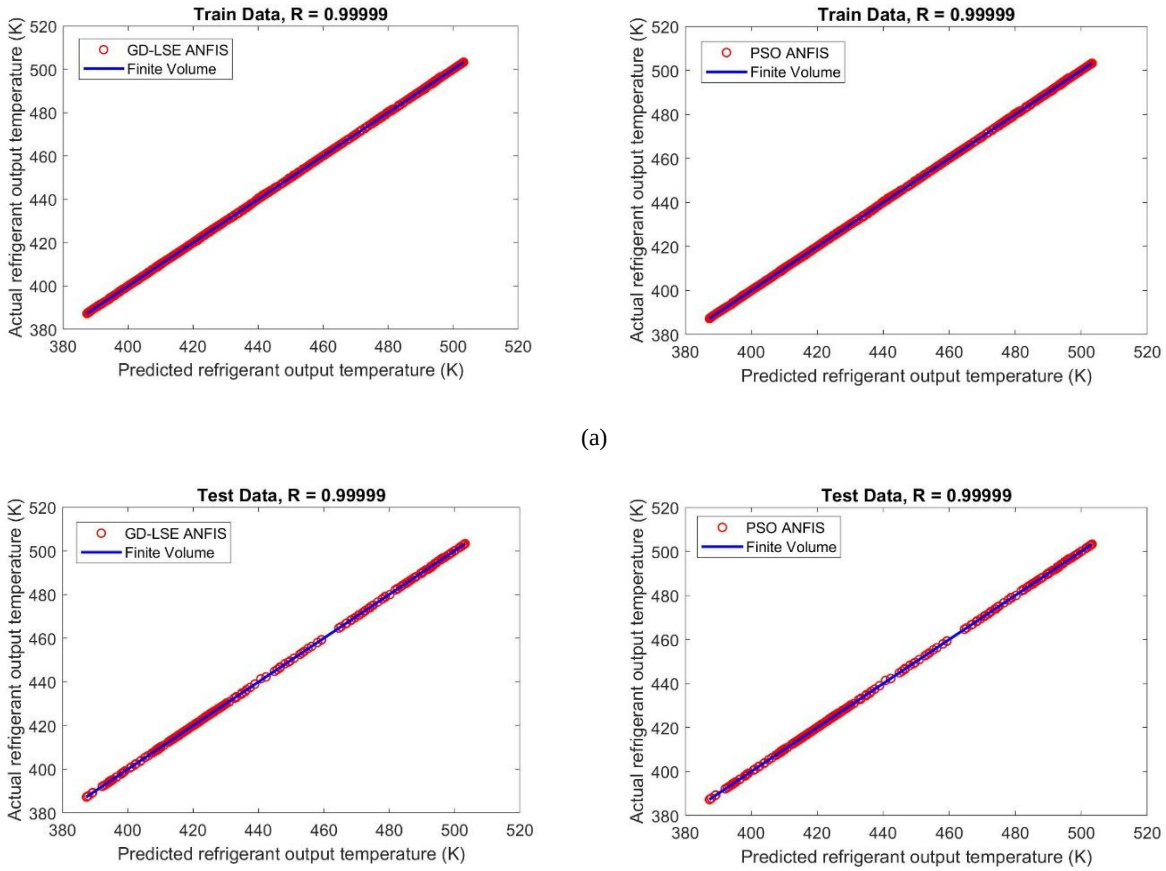

Fig. 5.34. *Comparison of regression plots for refrigerant output temperature prediction between GD-LSE ANFIS model and PSO ANFIS model for (a) training data (b) test data*

5.7 Case Study: 1kWe-Organic Rankine Cycle prototype

A case study of evaporator modelling using the proposed ANFIS technique is presented in this section to investigate the application of neuro-fuzzy techniques for modelling the evaporator in a 1-kWe ORC. The testing facility built in the Clean Energy Processes (CEP) Laboratory at Imperial College London, is composed of a rotary-vane pump, brazed-plate evaporator and condenser units and a scroll expander coupled magnetically to a generator with an adjustable resistive load.

The ORC prototype is operated with R245fa as a working fluid, which allows to maintain above-atmospheric pressure within the condenser and prevent non-condensable air to be sucked into the closed loop. The rotary-vane pump circulates the organic fluid through the cycle and allows adjustment of the flowrate. Shaft power is produced from the expansion of the high-temperature, high-pressure vapour exiting the evaporator down to the low pressure maintained in the condenser. The generator converts the mechanical energy into useful electrical energy, which is dissipated within a resistive load bank made of a set of adjustable resistors – with an equivalent overall resistance ranging from 10 to 60 Ω. This resistive load bank is able to dissipate safely up to 2 kW of heat without external ventilation.

The low-pressure vapour leaving the expander is then cooled down and fully condensed in the water-cooled condenser unit. To avoid cavitation in the pump and maintain zero sub-cooling at the condenser outlet, a liquid receiver is placed between the condenser and the pump. An 18-kW electric oil heater with adjustable delivery temperature is used as the heat source for the ORC, thus providing a controllable stream of hot Marlotherm SM oil. A detailed piping and instrumentation diagram (P&ID) of the testing facility is shown in **Fig. 5.35** and an actual picture of the test bench is presented in **Fig. 5.36**.

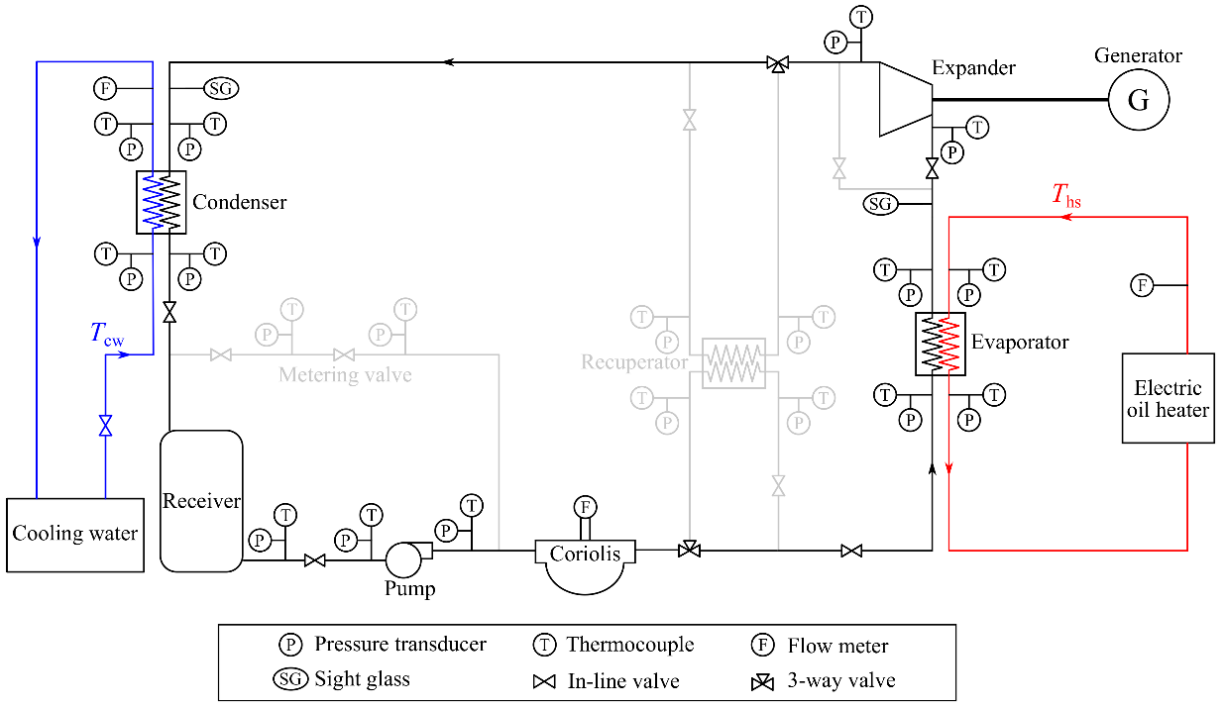

Fig. 5.35. *schematic of the ORC system (taken from [168])*

As shown in **Fig. 5.35,** pressure transducers and thermocouples (T-type) are placed at the inlet and outlet of each component to monitor the working fluid state throughout the cycle and provide informed measurements of the indicated and overall performance indicators. A DAQ970A data acquisition system is used to record time-resolved experimental data from the apparatus with a 1/2-Hz sampling rate. The detailed specification of the ORC components is listed in **Table 5.9**.

Table 5.9 *– Component specification of the ORC test rig*

		Mass flow rate	**Temperature range**	
Heat source thermal fluid	Marlotherm SM oil	[0.01– 1.4] kg/s	[93–142] °C	
Working fluid	R254fa	[14– 58] g/s	[70–136] °C	
Cooling fluid	Water	0.4 kg/s	18 °C	
	Model	**Type**	**Area**	**Specifications**
Pump	TMFR2 (Fluid-o-Tech S.R.L., Milano, Italy)	Magnet-driven rotary vane pump	_	[1100–3000] RPM
Condenser	CB60-30H-F (Alfa Laval Lund AB, Lund, Sweden)	Brazed-plate	1.62 m^2	_
Evaporator	B12Lx18 (SWEP, Didcot, United Kingdom)	Brazed-plate	0.45 m^2	_
Expansion machine	E15H22N4.25 (Air Squared Inc., Broomfield, USA)	Scroll expander	_	14.5 cm^3/rev, 1kWe
	Model			
Data acquisition system	DAQ970A (Keysight Technologies, Wokingham, UK)			
Pressure transducers	PXM309 (Omega Engineering, Manchester, United Kingdom)			
Coriolis flowmeter	Optimass 6000 (Krohne Ltd., Northamptonshire, UK)			

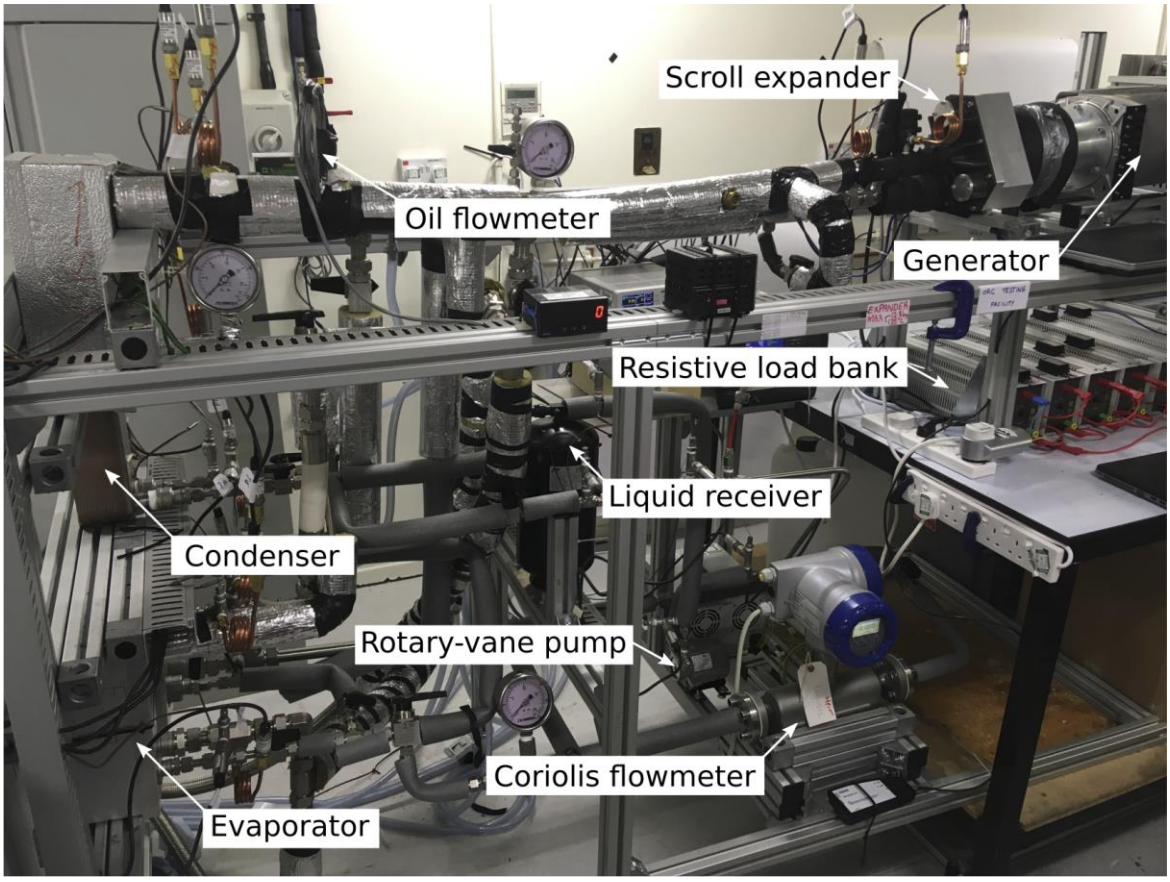

Fig. 5.36. *Experimental test rig (taken from [168])*

5.7.1 Data collection and evaporator model implementation

In this experiment, for modelling the evaporator, a set of 756 input-output data pairs are collected from the ORC test rig by varying the heat source mass flow rate and temperature and working fluid mass flow rate. For the heat source, the mass flow rate and temperature of supplied Marlotherm SM oil stream is altered using the electric heater in the range of 0.01 to 1.37 kg/s and 93 to 142 °C, respectively. Mass flow rate of the working fluid is also altered in the range of 14.4 to 57.8 g/s by manually changing the speed of pump. Four separate multi-input single-output sub-models are trained for prediction of evaporator output temperature (T_{rout}) and evaporator output pressure (P_{rout}). The inputs to sub-models are identical and

consist of mass flow rate of heat source ($\dot{m}_h$), temperature of heat source (T_h) and mass flow rate of the working fluid ($\dot{m}_r$). The recorded outputs for the sub-models are the evaporator outlet temperature (T_{rout}) and evaporator outlet pressure (P_{rout}). For evaluating the models, the data set is randomly divided to two subsets of training data set and test data set. The ANFIS network is optimised using the training data set whereas the test data set which is deployed for evaluating the model. In sub-models, 70% of data points are used for training the network and the remaining data points are deployed to test the constructed network. Among the available methods of clustering FCM algorithm because of its high flexibility is used for clustering the input space and generating the base FIS. The GD-LSE and PSO techniques are applied as the learning algorithm to optimise the base FIS. The training parameters for all four sub-models are listed in **Table 5.10**. The performance of both training methods is compared in terms of the RMSE and linear correlation coefficient for both sub-models.

Table 5.10 *– Summary of the R coefficient obtained for the evaporator outlet temperature sub-model*

Parameters	**GD-LSE ANFIS model for T_{rout}**	**GD-LSE ANFIS model for P_{rout}**	**PSO ANFIS model for T_{rout}**	**PSO ANFIS model for P_{rout}**
Number of training data set	529×4	529×4	529×4	529×4
Number of test data set	227×4	227×4	227×4	227×4
Clustering method	FCM	FCM	FCM	FCM
Membership functions	Gaussian	Gaussian	Gaussian	Gaussian
Number of Clusters	8×3	8×3	8×3	8×3
Number of Epochs	1000	1000	_	_
Number of linear parameters	32	32	32	32
Number of nonlinear parameters	48	48	48	48
Total number of parameters	80	80	80	80
Number of fuzzy rules	8	8	8	8
Maximum iteration	_	_	1000	1000
Population size	_	_	80	80
Inertial weight	_	_	1	1
Personal learning coefficient (C_1)	_	_	1	1
Global learning coefficient (C_2)	_	_	2	2

5.7.2 Learning Algorithm

To train the premise and consequent parameters of the network hybrid gradient descent, least square estimate and PSO algorithm discussed in sections 5.4.2.1 and 5.4.2.2, respectively, are deployed. The performance of both methods for matching training and test datasets are compared in terms of RMSE and the linear correlation coefficient.

5.7.3 Simulation results

Two neuro-fuzzy models of evaporator are developed to predict the evaporator outlet temperature and evaporator outlet pressure in a 1-kWe ORC test rig. **Fig. 5.37** represents the comparison between evaporator outlet temperature prediction in the models trained using GD-LSE and PSO techniques. As illustrated in **Fig. 5.37**, for the training dataset, RMSE of 3.48 and 2.46 achieved for GD-LSE and PSO, respectively. Furthermore, to evaluate the generalisation ability of the models, an unseen test dataset is applied to the models. For the test dataset, the obtained RMSEs are equal to 3.37 and 2.39 in the model trained using GD-LSE method and PSO technique, respectively. Comparison of RMSE values for training dataset indicates an improvement of 29% achieved for the evaporator outlet temperature model trained using the PSO technique. Moreover, this improvement in the test dataset equals 29%, which indicates better generalization capability of the model trained using the PSO technique.

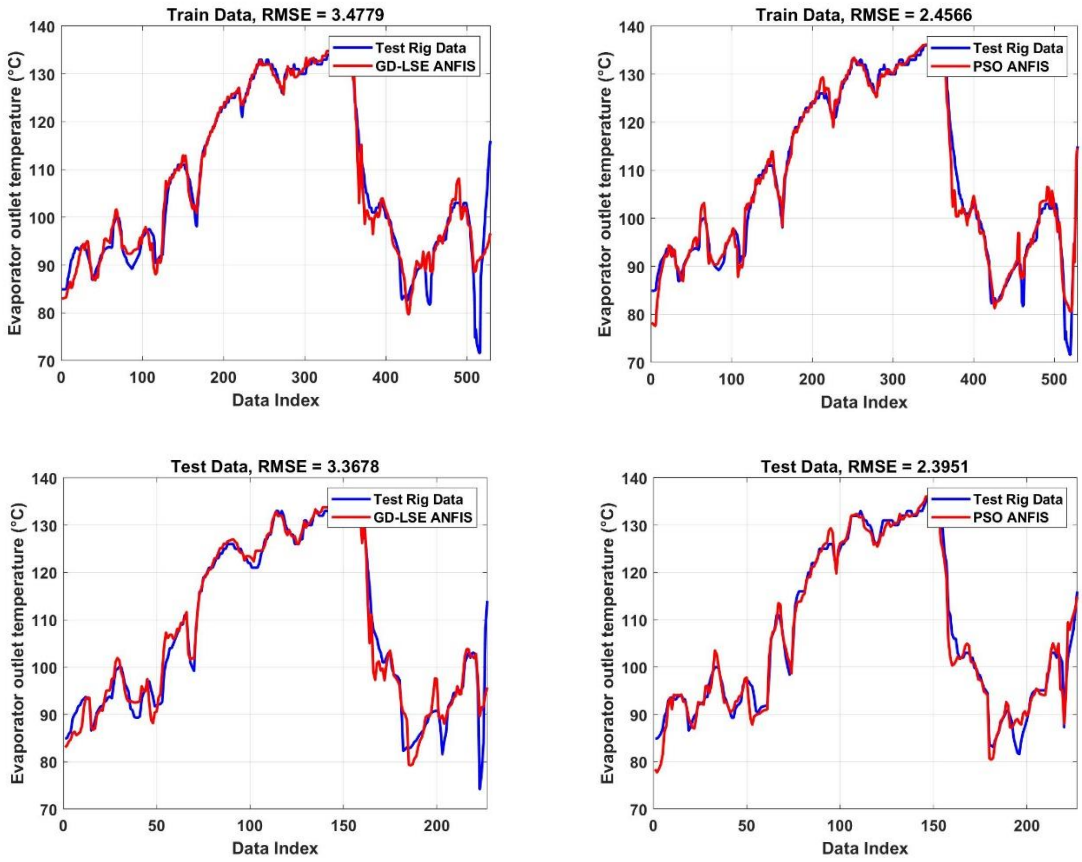

Fig. 5.37. *Comparison of GD-LSE ANFIS and PSO ANFIS models for prediction of* T_{rout} *using the training and test data*

Furthermore, regression plots are shown in **Fig. 38**, to illustrate the deviation of the predicted evaporator outlet temperatures from the experimentally obtained evaporator outlet temperatures. The linear correlation coefficient for both GD-LSE and PSO models are listed in **Table 5.11**. Comparison of the R values indicate an acceptable fit for training and test data for both models. However, the R coefficients in the PSO model are closer to one, which imply better fit and greater generalization ability of the model optimised by the PSO method. For the training and test datasets, the R coefficients improved 1.1% and 0.9%, respectively, by deploying the PSO method for training.

Table 5.11 *– Summary of the R coefficient obtained for the evaporator outlet temperature sub-model*

Training Method	Training data	Test data
GD-LSE	0.9798	0.9816
PSO	0.9902	0.9903

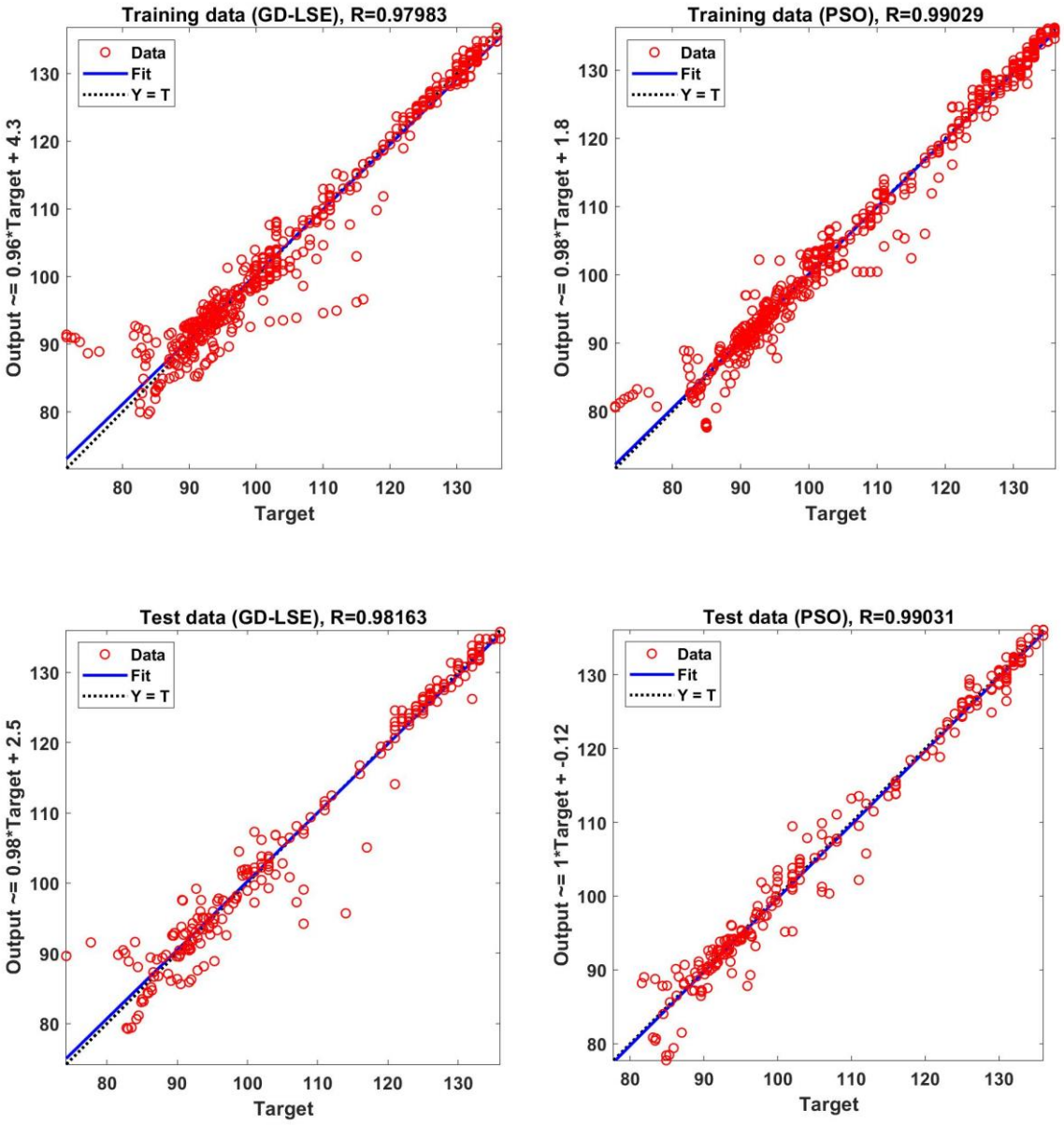

Fig. 5.38. *Comparison of regression plots between GD-LSE ANFIS and PSO ANFIS models for prediction of* T_{rout} *using the training and test data*

ANFIS model is applied to predict evaporator outlet pressure. The new sub-model is trained by deploying the GD-LSE technique and PSO technique. Comparison of the obtained RMSE values from both training and test dataset is presented in **Fig. 5.39**. For the training dataset RMSE of 0.42 and 0.35 are achieved from the models trained using GD-LSE technique and PSO technique, respectively. The obtained RMSE for the unseen test data is 0.45 for the PSO ANFIS model and 0.54 for the GD-LSE model. It can be inferred that the evaporator outlet pressure results achieved from the PSO ANFIS model have a better compliance with the experimental data as evaluated against the model trained by the GD-LSE technique. For the training data, deploying the PSO algorithm to train the neuro fuzzy model results in 15% improvement in the RMSE as compared with the GD-LSE method. Moreover, for the test data the RMSE of the model trained using the PSO technique enhanced by 18%, which illustrates better generalization ability in prediction of the evaporator outlet pressure.

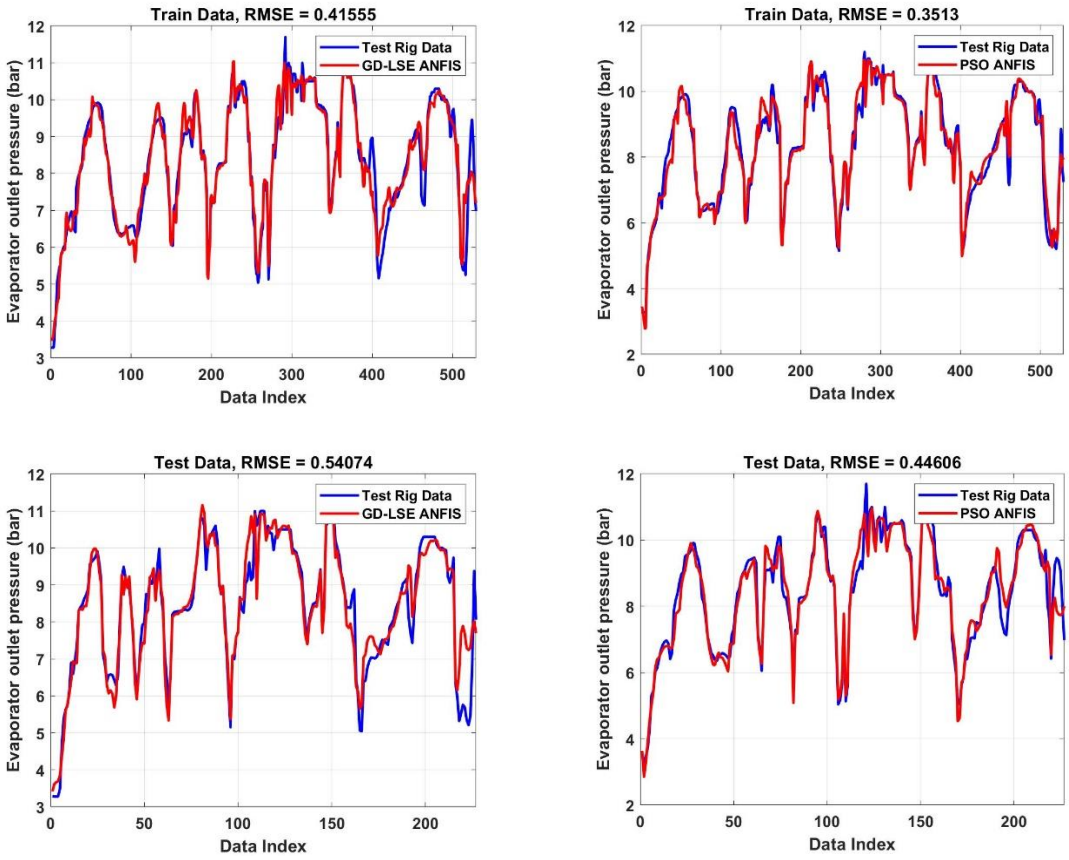

Fig. 5.39. *Comparison of GD-LSE ANFIS and PSO ANFIS models for prediction of* P_{rout} *using the training and test data*

Similarly, to examine the accuracy of the models, comparison of the regression plots for the models trained by GD-LSE and PSO methods are shown in **Fig. 40**. The R coefficient for the training and test data sets in both models are close to one, which indicates the agreement of models' outputs and experimentally measured evaporator outlet pressures. The obtained linear correlation coefficients are listed in **Table 5.12**. The R values achieved for the training and test data sets are higher in the PSO model. Furthermore, the highest obtained accuracy is for the refrigerant output pressure model optimised using PSO algorithm with the linear correlation coefficient of 0.9876 for the training dataset, and 0.9641 for the test dataset. These two sub-models for the evaporator outlet temperature and evaporator outlet pressure can be used to identify the phase of the working medium instantaneously. Therefore, in the

application of the ORC for recovery of the wasted heat in IC engines, this neuro-fuzzy model can be deployed to design an accurate control system to ensure the system safety and prevent decomposition of the working fluid by adjusting the pump speed.

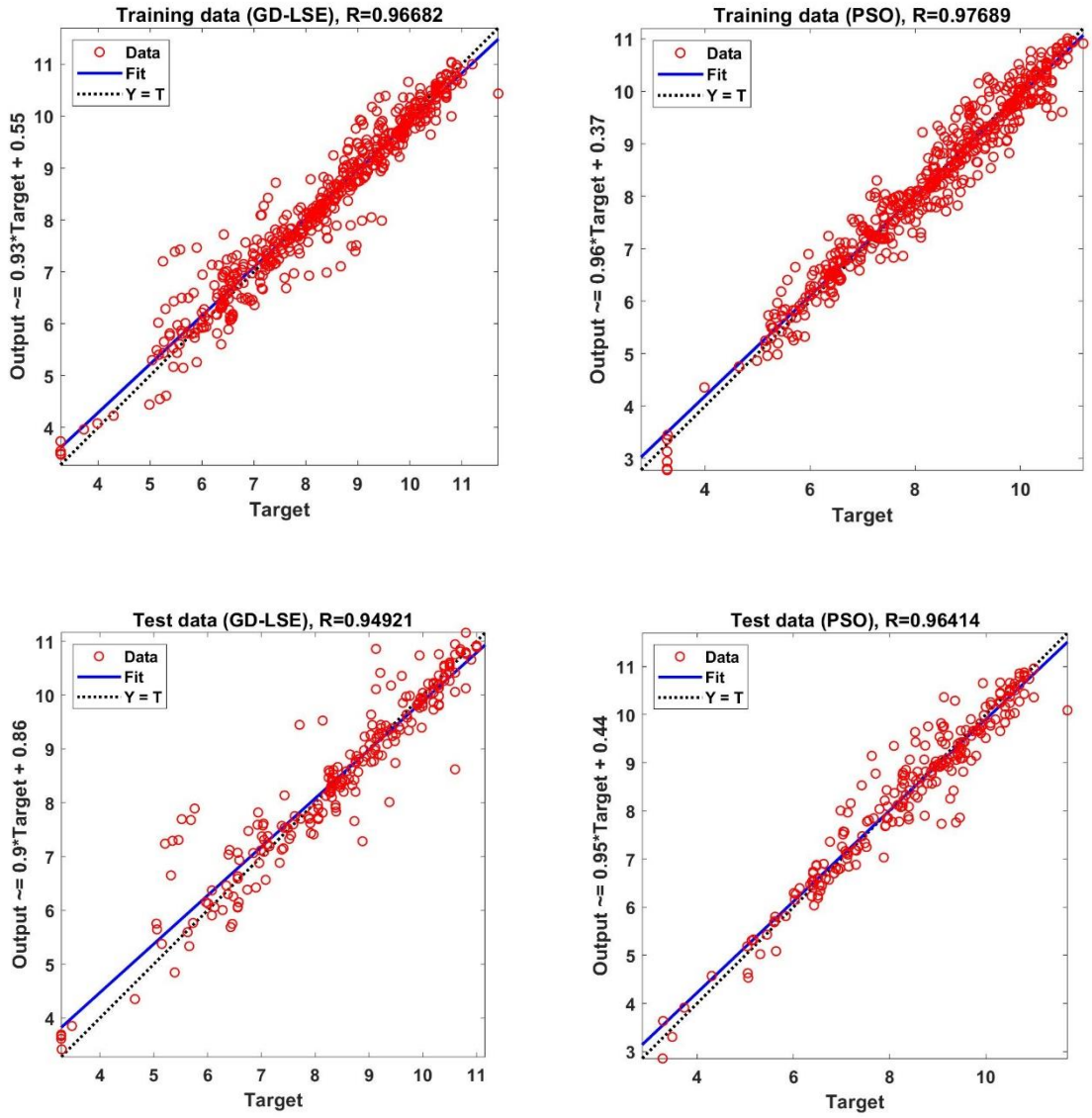

Fig. 5.40. *Comparison of regression plots between GD-LSE ANFIS and PSO ANFIS models for prediction of* P_{rout} *using the training and test data*

Table 5.12 *– Summary of the R coefficient obtained for the evaporator outlet pressure sub-model*

Training Method	Training data	Test data
GD-LSE	0.9668	0.9492
PSO	0.9768	0.9641

5.8 Investigation of the ORC cycle using the neuro-fuzzy evaporator

The overall model of the ORC cycle comprises evaporator, valve, expander, condenser, accumulator and pump as shown in **Fig. 5.41**. The individual component models developed previously in the chapter 4 are interconnected in commercial MATLAB/SIMULINK software to form the complete ORC cycle. The Simulink diagram of the ORC in shown in **Fig. 5.42**.

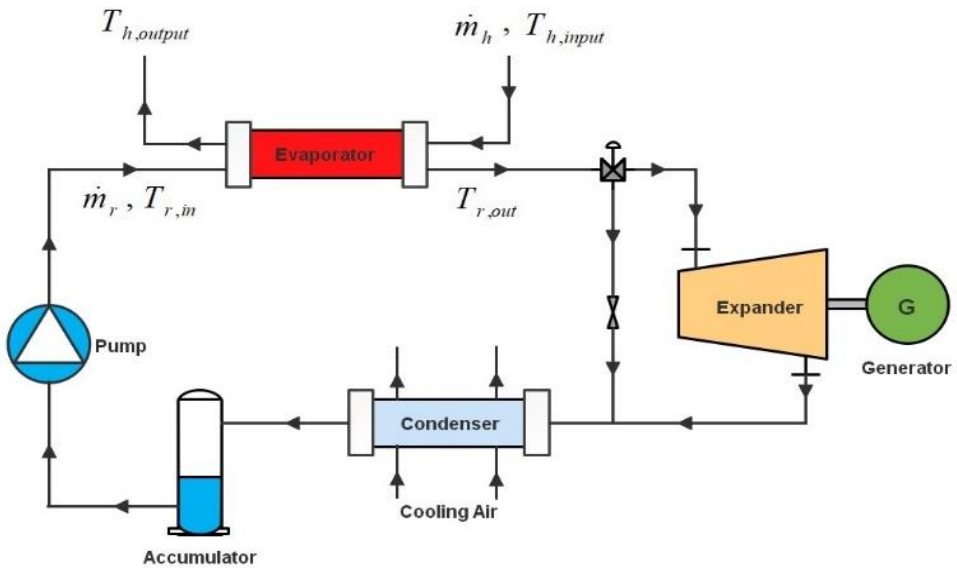

Fig. 5.41*. Overall model of the ORC*

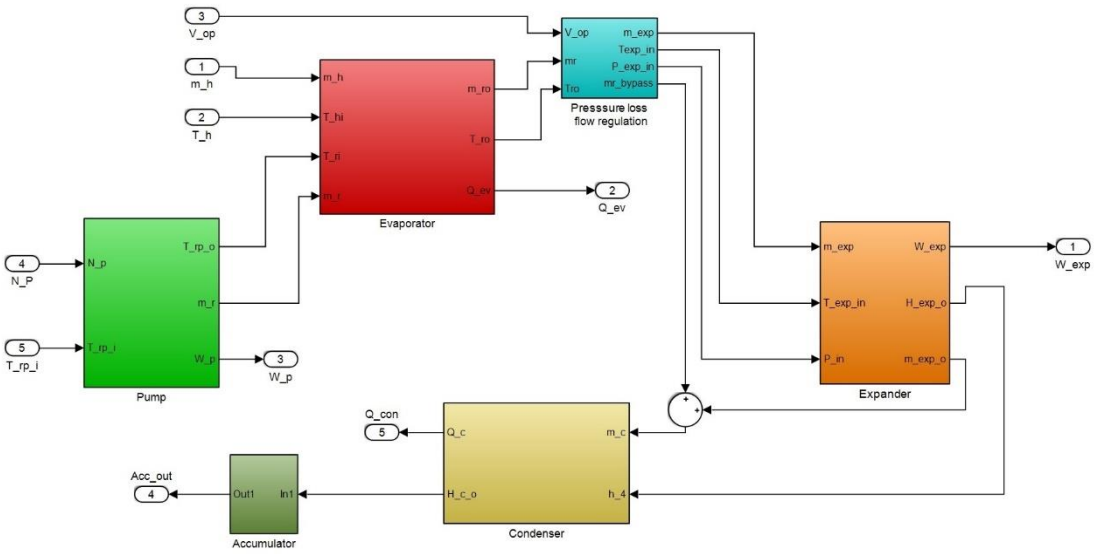

Fig. 5.42*. The open-loop Simulink diagram of the ORC*

The neuro-fuzzy evaporator model developed using FV evaporator data discussed in this chapter is deployed to model the outlet temperature of refrigerant (T_{rout}) and outlet temperature of the heat source (T_{hout}) due to its accuracy and superior computational speed. The following relationships describe the inlet and outlet of the components of the cycle:

- The mass flow rate of refrigerant is proportional to the pump speed. Since the high and low pressures are specified within the cycle, the temperature of the working fluid at the pump outlet and required power to drive the pump can be calculated.
- The enthalpy drop between the pump and the evaporator is considered negligible; therefore, the evaporator heat recovery is considered to be a function of working fluid pressure, mass flowrate of working fluid, mass flow rate and temperature of heat source.
- The speed of expander is not constrained and it can rotate freely. The expander's work output is a function of expander inlet and outlet enthalpy.

- The condenser outlet temperature is considered constant and to maintain the desired outlet temperature the model calculates the required cooling power.
- The liquid receiver maintains the working fluid level and its outlet enthalpy.

The piping pressure losses between the evaporator outlet and expander inlet in the high-pressure region of the ORC cycle need to be taken into account for achieving more accurate results. Hence, the Darcy-Weisbach correlation is adopted for modelling the total pressure losses of the piping as follows:

$$\Delta P_{Piping} = \frac{f_D \rho L_P v^2}{2D} \tag{5.36}$$

where f_D represents the friction factor, ρ denotes the pipes density, L_P is the length of pipe, D is the pipe's hydraulic diameter and v id the velocity of working fluid.

Furthermore, the Darcy friction factor in equation (5.36) is calculated using the Haaland's equation for friction factor in turbulent pipe flow [169] as follows:

$$\frac{1}{\sqrt{f_D}} = -1.8 \log\left[\left(\frac{\frac{\in_P}{D}}{3.7}\right)^2 + \frac{6.9}{Re}\right] \tag{5.37}$$

where $\in_P$ and $\frac{\in_P}{D}$ denote the absolute and relative pipe roughness, respectively.

For assessing the performance of the ORC model, a heat source with random mass flow rate and temperature in the range of 0.18 to 0.25 kg/s and 490 to 525 K, respectively is considered as shown in **Fig. 5.43**.

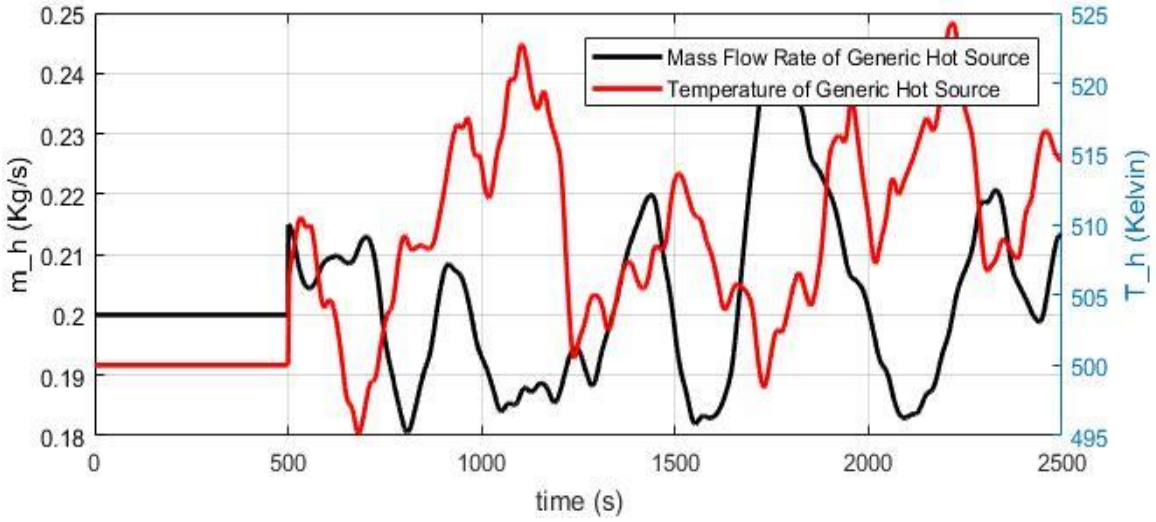

Fig. 5.43. *Random heat source temperature and mass flow rate*

The mass flow rate of working fluid is proportional to the pump speed. The open loop response of the ORC cycle is simulated for 2500 seconds by considering an arbitrary fixed pump speed equal to 850 RPM. The refrigerant temperature at the evaporator outlet is represented in the **Fig. 5.44**. As shown in **Fig. 5.44**. with an arbitrary fixed pump speed of 850 RPM and a random heat source, the refrigerant temperature at the evaporator outlet is fluctuating in the range of 380 to 408 K. These fluctuations in the working fluid temperature are caused by the transient nature of the heat source due to the different driving cycle. Furthermore, these fluctuations in temperature may result in decomposition of organic working fluid and deviation of expander work output from the nominal value. Therefore, for the safe and successful application of ORC in automotive applications other safety measures need to be considered to maintain this temperature at the desired value and maximise the work output of the system.

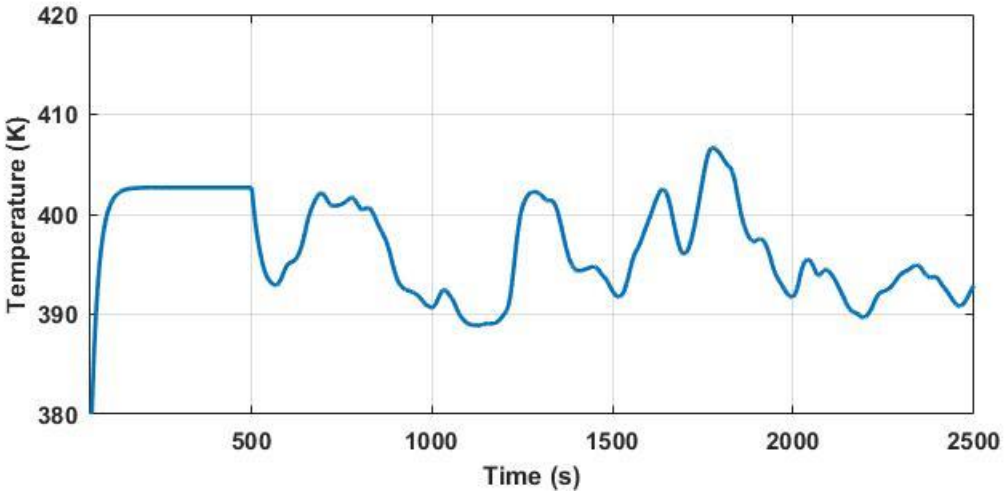

Fig. 5.44. *Working fluid temperature at the evaporator outlet*

The pressure at the expander inlet after considering the piping pressure losses is shown in **Fig. 5.45**. From **Fig. 5.45**, it is observable that the expander inlet pressure due to the piping friction fluctuates in the range of 5995 to 6000 kPa.

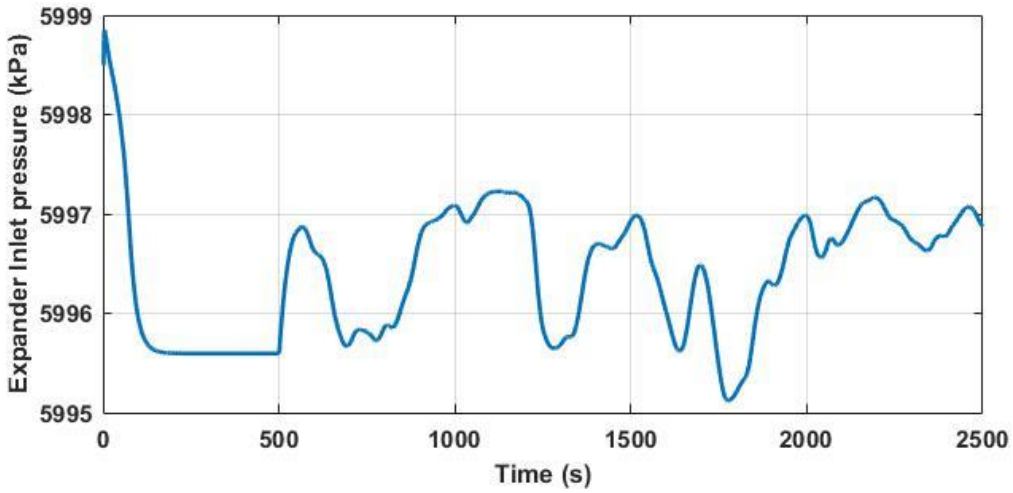

Fig. 5.45. *The pressure at the expander inlet after considering the piping pressure losses*

The performance of overall ORC model for calculation of the expander work output is shown in **Fig. 5.46**. The simulation of the expander work output is calculated by using the generic

heat source presented in **Fig. 5.43** and with a steady pump speed with $N_P = 850$ RPM. From **Fig. 5.46**, it can be observed that, since the pump speed is not regulated, the expander work fluctuates mostly between 2 to 3.25 kW. Given that the pump speed is not regulated and is fixed at $N_P = 850$ RPM, it can be inferred that the fluctuation in the expander work output is caused by the large range of operating conditions due to the transient nature of the heat source. Therefore, considering the fluctuations in the working fluid temperature at the evaporator outlet and expander work output, there is a vital need for a control scheme to simultaneously regulate the refrigerant temperature at the evaporator outlet and maintain the expander work output by regulating the pump speed.

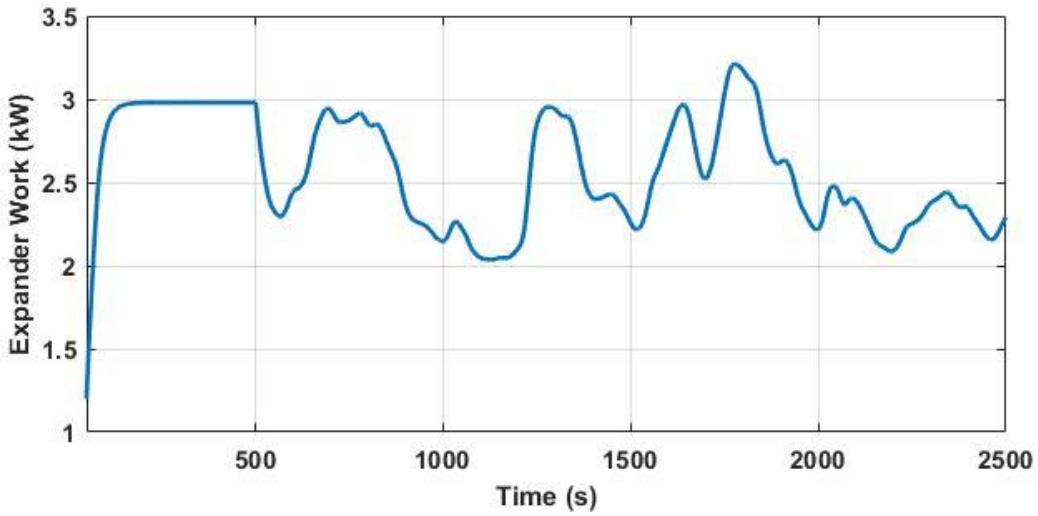

Fig. 5.46. *The expander work output*

5.9 Summary

In this chapter, an adaptive neuro-fuzzy inference system and its potential for modelling the highly nonlinear input-output behaviour of evaporator in an ORC subjected to a transient heat source is discussed. An ANFIS model of the evaporator is developed based on the data gathered from the FV evaporator model, which is computationally expensive for real-time

applications. Identifying the dynamics governing the behaviour of the evaporator can further result in proper control of the ORC in mobile applications. Furthermore, two intelligent learning algorithms are presented and their performances for training the ANFIS network are compared.

A case study is presented for prediction of the evaporator outlet temperature and pressure of a 1-kWe ORC prototype. As system safety is vital in ORC applications for the recovery of waste heat from the exhaust gases of IC engines, accurate modelling of the evaporator outlet temperature and pressure plays a pivotal role in the design of suitable control systems. Comparisons of experimentally gathered data and predictions from the neuro-fuzzy models reveal an acceptable accuracy in predicting the evaporator outlet temperature and pressure.

Based on the obtained results the main achievements of this study are as follows:

- The time and effort of identifying the antecedent and consequent parameters of the fuzzy model are decreased substantially by deploying the ANFIS method compared to the previous non-adaptive fuzzy models.

- The ANFIS models of evaporator for predicting the output temperature of heat source and refrigerant are trained using the hybrid GD-LSE and population-based PSO algorithms. The statistical analysis of the results indicates the higher accuracy and generalization ability of the ANFIS models trained using the PSO algorithm.

- The ANFIS models substantially outperformed the conventional numerical FV and MB methods in terms of real-time simulation time. Furthermore, the identified ANFIS models can be used for proper real-time control of the ORC cycle with transient heat source.

Chapter 6: Control of ORC

In this chapter different control strategies for a small-scale ORC are discussed. Controlling the ORC cycle operating under transient heat source conditions is always challenging. Excessive temperature of working fluid at the evaporator outlet beyond its nominal range could result in decomposition of the organic fluid, damage the components of the ORC and adversely affect the performance of the cycle. Moreover, if the working fluid temperature is reduced to temperatures below the nominal range, liquid droplets may form during the expansion process. Therefore, considering the pressure-enthalpy diagram of R134a presented in **Fig. 6.1**, the ideal temperature of $T = 405\ K$ is used as the nominal value for the refrigerant temperature at the evaporator outlet. Given the evaporator pressure is 6000 kPa, this temperature is the minimum temperature that prevents the formation of liquid droplets and corresponds to the enthalpy of 1.7 kJ/kg.K.

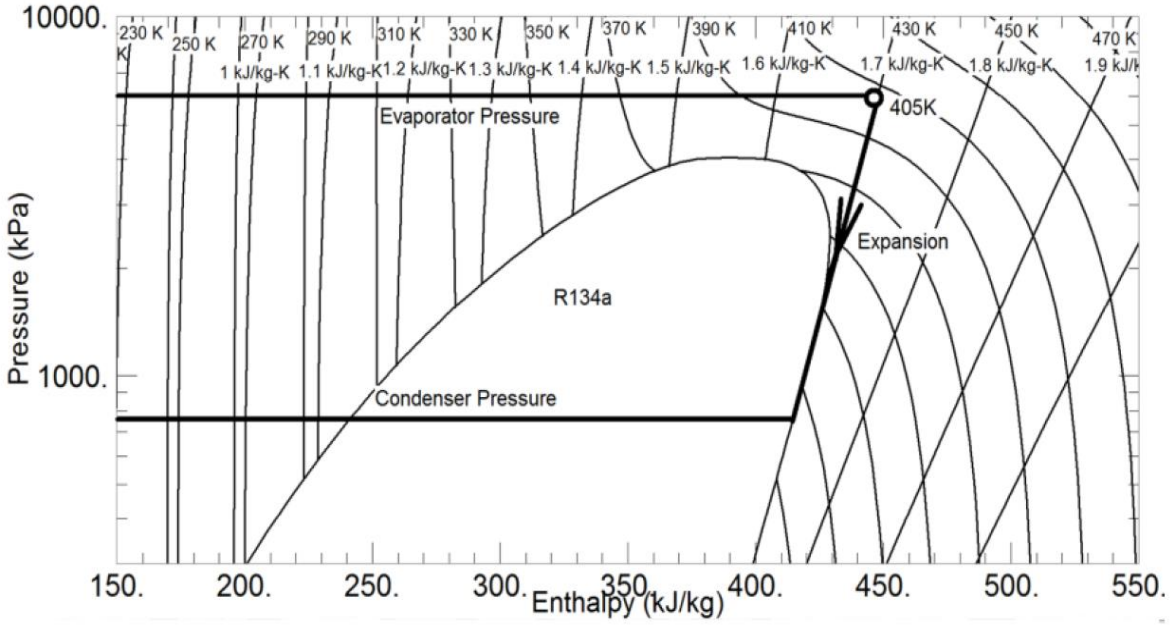

Fig. 6.1. *Selection of working fluid temperature at the evaporator outlet from the Pressure-Enthalpy diagram of R134a*

6.1 PID control

The Proportional, Integral, Derivative (PID) controller is a popular single-input single-output (SISO) control loop mechanism that is widely used in industry for variety of applications to regulate temperature, speed, flow or other process variables. PID employs the feedback of process variable y(t) and calculates the difference between the setpoint r(t) and the feedback value to form the error signal e(t). The objective is to minimise the error value by applying a correction based on proportional, integral and derivative terms. The block diagram of a PID controller is represented in **Fig. 6.2**.

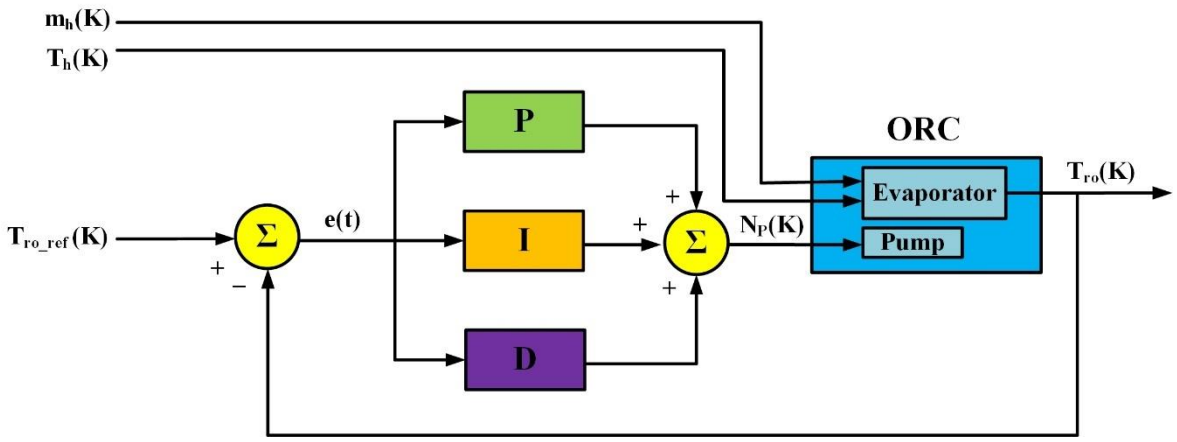

Fig. 6.2. *Block diagram of a PID controller*

In mathematical form the overall control function of a PID controller can be represented by the following transfer function:

$$u(s) = K_p + K_i\left(\frac{1}{s}\right) + K_d\left(\frac{zs}{s+z}\right) \tag{6.1}$$

where K_p is the proportional gain, K_i denotes the integral gain, K_d represents the derivative gain and z is the filter coefficient.

The advantage of PID controller lies in its easy implementation, good performance and simplicity of the controller design. Several methods such as Ziegler-Nichols, refined Ziegler-Nichols, Chien-Hrones-Reswick, etc., have been proposed for setting the gain parameters of the PID controller.

To control the ORC waste heat recovery system the pump speed needs to be adjusted in order to regulate the working fluid temperature at the evaporator outlet. However, the ORC is working under transient conditions and it has a wide range of operating conditions. Therefore, an operating point with the heat source mass flow rate and temperature equal to $m_h = 0.2\ kg/s\ T_h = 500\ K$, is selected in order to tune the PID controller gains. The K_p , K_i, K_d and z parameters, are tuned in order to obtain a suitable compromise between the time requirement and overshoot. The tuned PID controller gains are represented in **Table 6.1**.

Table 6.1 *– Tuned PID gains*

PID gains	**Tuned values**
$\boldsymbol{K_p}$	8.23
$\boldsymbol{K_i}$	2.51
$\boldsymbol{K_d}$	2.40
z	0.13

To assess the set-point tracking performance of the PID controller when the ORC is subjected to different heat source mass flow rate and temperature at the evaporator inlet, two more operating points are considered as follows:

Table 6.2 *– Operating points of the ORC for testing the PID controller*

	$\boldsymbol{m_h\ (\frac{kg}{s})}$	$\boldsymbol{T_h\ (K)}$
Case 2	0.185	520
Case 3	0.23	495

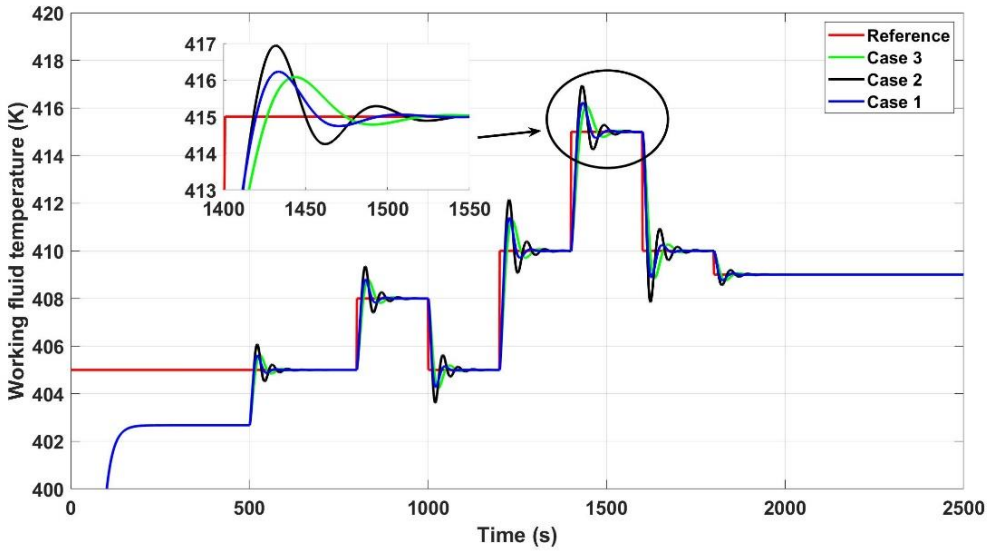

Fig. 6.3. *Setpoint tracking of PID controller at different operating points*

The set-point tracking performance of the PID controller for different operating points is represented in **Fig. 6.3**. Comparison of the set-point tracking for different input conditions indicates that the performance of the PID controller is reduced significantly as the input condition changes from the nominal value. The reason behind this performance drop lies in the fixed nature of the PID gains. In automotive applications, the ORC is exposed to a stream of hot exhaust gases with alternating temperature and mass flow rate. Therefore, utilising the PID controller may result in decomposition of the working fluid, formation of liquid droplets at the expander inlet and safety concerns. In order to obtain better control performance and

protect the components of the system a novel neuro-fuzzy controller based on the inverse dynamics of the ORC system is introduced in the next section.

6.2 Neuro-fuzzy system as direct inverse controller

Intelligent control has emerged as a powerful tool for nonlinear and challenging control problems. For plants with high nonlinearity, uncertainties and unknown variations in plant parameters utilizing intelligent control techniques instead of conventional control methods may improve the robustness of the controller [170]. Furthermore, various intelligent techniques (neural networks, fuzzy logic, evolutionary algorithms, etc.) could be merged in order to integrate benefits of different methods. One approach is the direct inverse neuro-fuzzy control, which utilises the learning ability of neural networks and approximate reasoning capability of fuzzy systems. This method assumes that the inverse model of plant can be obtained from the data obtained from the dynamics of the model which is not valid in general [170]. However, in case of the ORC, the inverse dynamics of the system can be realized using the data from the open-loop configuration.

In this study, a direct inverse neuro-fuzzy control strategy is proposed for an ORC waste heat recovery system deployed to recover the waste heat energy of internal combustion engines in heavy-duty trucks. This control strategy, potentially offers a highly effective control of superheating at the evaporator outlet accruing the benefit of safe operation of ORC system under highly dynamic heat source condition. Moreover, the control system maintains the expander work output at the desired value by regulating the vapour pressure at the expander inlet. The proposed control strategy has been developed to meet two main requirements: set-point tracking and disturbance rejection.

6.2.1 Development of inverse dynamic model

This control scheme is developed based on the inverse dynamics of the ORC model. The controller design process is performed in two phases: the learning phase and the implementation phase. The flowchart in **Fig. 6.4** illustrates the controller design procedure. The structure of inverse ANFIS controller during the learning phase is shown in **Fig. 6.5**. In the learning phase, the inverse model of the ORC is obtained based on the open-loop data and the goal is to minimize the error between the actual values of pump speed and its predicted values by the ANFIS structure. To achieve this goal, first, a random signal for the pump speed $N_p\ (k)$ ranging from 80 to 1750 RPM is produced. This signal is based on the typical range and rate of change of the low to medium grade waste heat ORC pump. Then, this signal alongside with the random signals for heat source mass flow rate $m_h\ (k)$ and temperature $T_h\ (k)$ applied to the ORC model in an open loop configuration. The range of heat source mass flow rate signal is equal to 0.073 to 0.2985 kg/s and the heat source temperature is ranging from 412 to 523 K. The temperature of the working fluid at the evaporator outlet $T_{ro}\ (k)$ and a unity-delayed temperature of working fluid at the evaporator outlet $T_{ro}\ (k-1)$ are recorded for 4500s. In the next step, the gathered data from the open-loop configuration is used to model the inverse dynamics of the ORC system offline. The data is further divided randomly to 70% for training and 30% for testing the proposed inverse ANFIS model. Consequently, 3150 and 1350 data points are used for training and testing the controller model, respectively. As illustrated in **Fig. 6.5**, the inputs for the inverse controller model in the learning phase are heat source mass flow rate $m_h\ (k)$ and temperature $T_h\ (k)$, working fluid temperature $T_{ro}\ (k)$ and unity-delayed working fluid temperature $T_{ro}\ (k-1)$ at the evaporator outlet. The output of the model is the pump speed $N_p\ (k)$. The ANFIS

parameters utilised for the inverse model during the learning phase of controller is listed in **Table 6.3**. The actual and predicted pump speeds for train and test data are shown in **Fig. 6.6**. As it can be seen, the training data and an unseen test data are applied to the trained models to evaluate the generalisation power of the models. Additionally, a statistical criterion in terms of RMSE is considered to evaluate the accuracy of the models. The training and test RMSE for prediction of pump speeds are 7.75 and 8.45, respectively. Furthermore, to better illustrate the deviation of the predicted pump speeds from the actual values, regression plots are also included in **Fig. 6.6**. The linear correlation coefficient (R) for training data set is 0.99972 and for test data set is 0.99968. The R value for training and test data clearly implies the high generalisation power of the model since the R value for both training and test data are close to one.

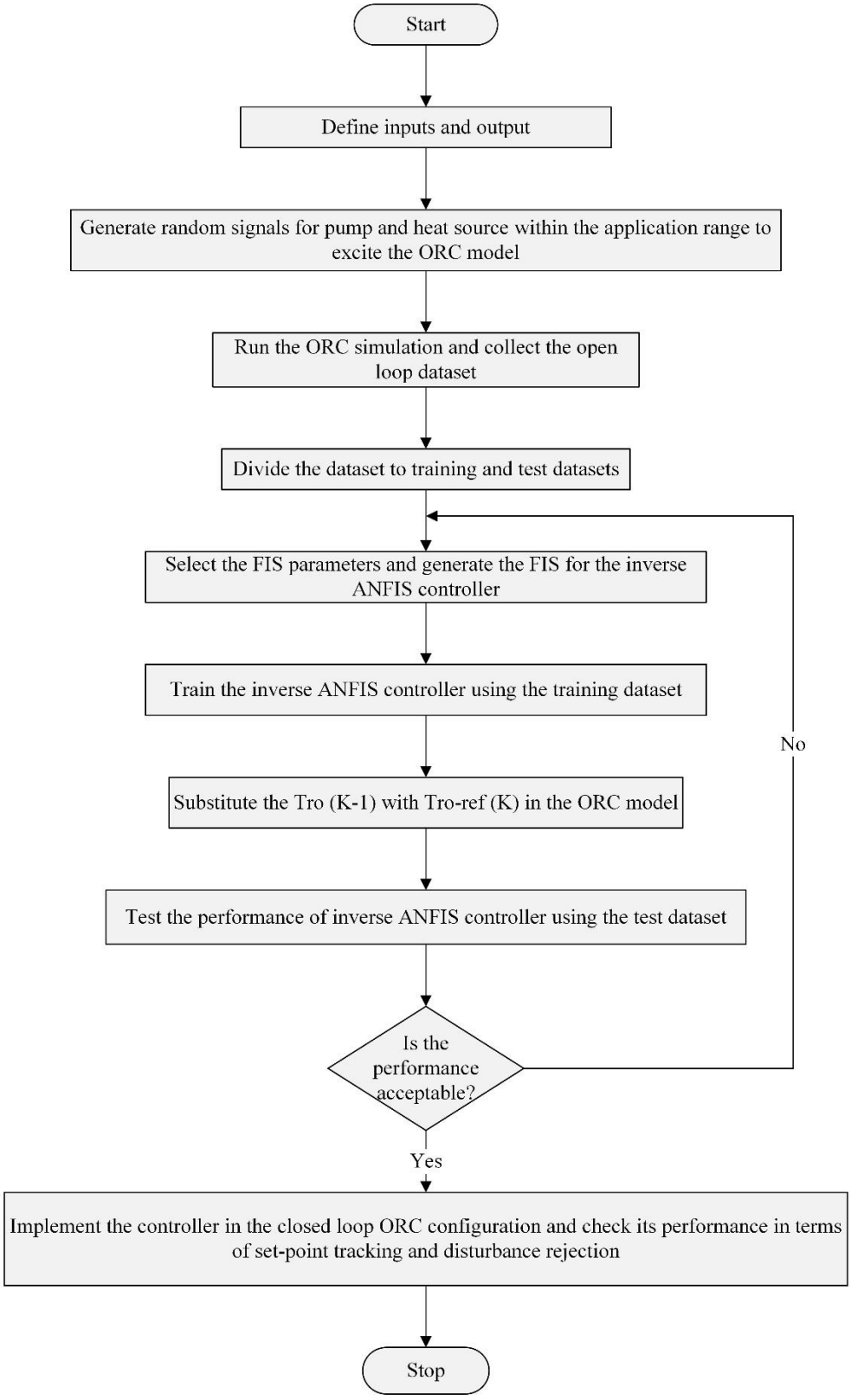

Fig. 6.4. *Inverse neuro-fuzzy controller design procedure*

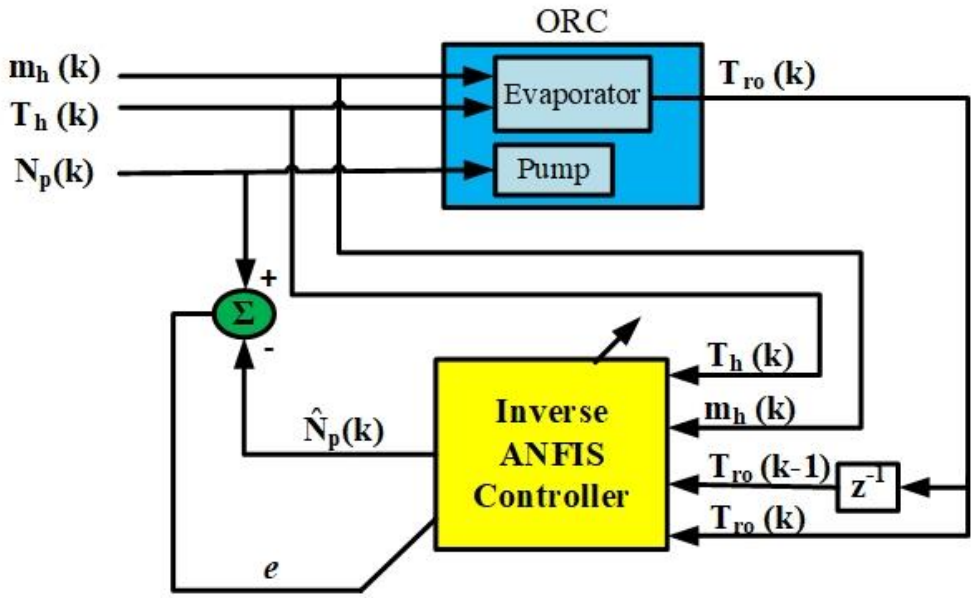

Fig. 6.5. *Structure of inverse ANFIS controller in the learning phase*

Table 6.3 *– Inverse ANFIS controller training parameters*

Parameters	**Inverse ANFIS controller**	**Parameters**	**Inverse ANFIS controller**
Number of training data set	3150×5	**Number of Epochs**	3000
Number of test data set	1150×5	**Number of linear parameters**	280
Clustering method	FCM	**Number of nonlinear parameters**	560
Membership functions	Gaussian	**Total number of parameters**	840
Number of Clusters	70×4	**Number of fuzzy rules**	70

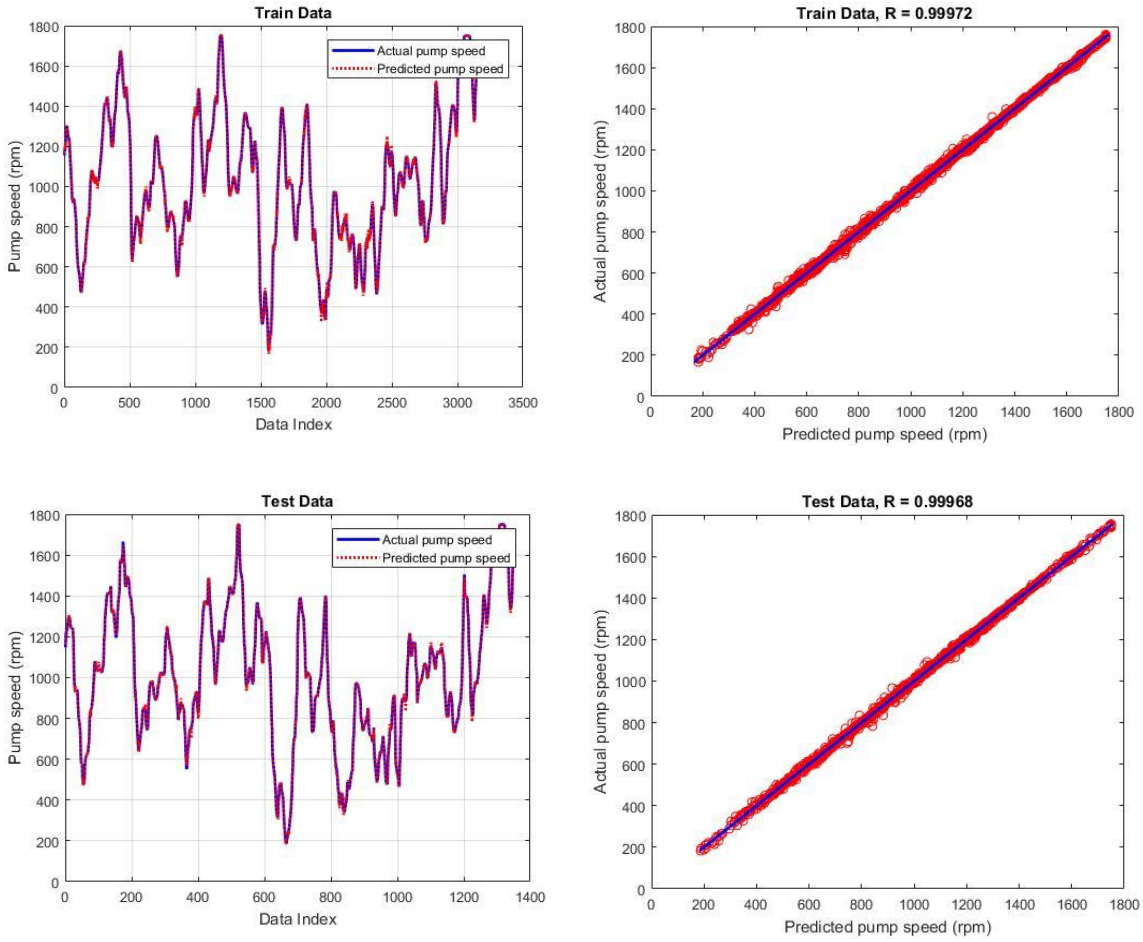

Fig. 6.6. *Comparison of actual and predicted pump speeds for training and test data sets*

6.2.2 Implementation of inverse neuro-fuzzy controller

Two closed loop ORC configurations are considered to assess the performance of the neuro-fuzzy controller developed in the previous section as shown in **Figs. 6.7** to **6.10**. The inputs to the controller in the implementation phase are the transient mass flow rate $m_h\ (k)$ and temperature $T_h\ (k)$ of the heat source, the temperature of working fluid at the evaporator outlet $T_{ro}\ (k)$ and the reference working fluid temperature $T_{ro\_ref}(k)$. In the second configuration, a single-input single-output (SISO) PID controller with fixed gains based on the error signal from the difference between reference working fluid temperature and the

evaporator outlet temperature is tuned to control the working fluid temperature at the evaporator outlet. The PID controller is combined with the inverse ANFIS controller to improve the chattering effect of pump signal and reduce the settling time and overshoot of the system response. The PID is tuned with the nominal heat source temperature of 500 K and mass flow rate of 0.2 kg/s. The PID gains achieved for this control scheme are $K_p = 8$, $K_i = 2.5$, $K_i = 2.5$ and $z = 0.13$, for the proportional, integral, derivative, and filter coefficient, respectively. In both configurations, the rate of change and range of pump speed are limited to $\pm 100\ RPM/s$ and 80-1750 RPM, respectively, according to the specifications of the deployed pump.

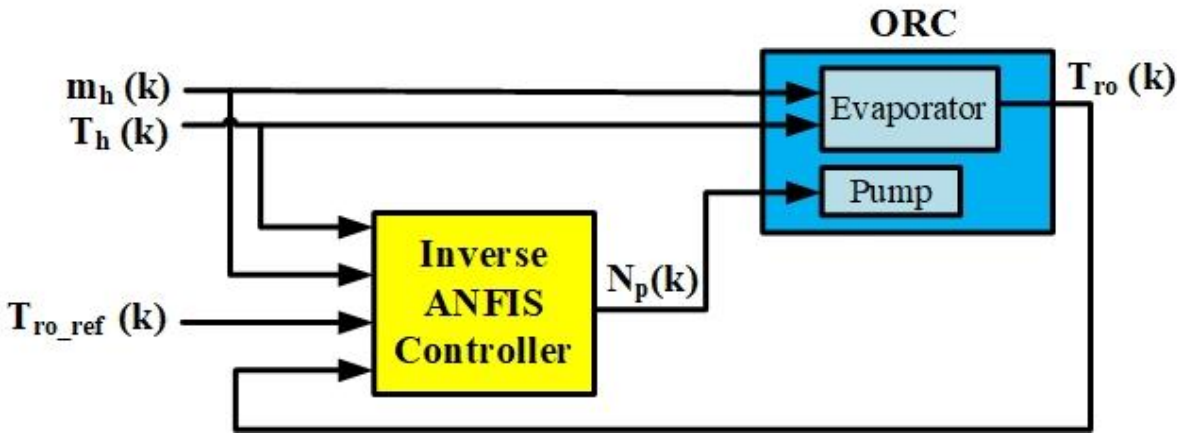

Fig. 6.7. *Structure of the ORC with inverse ANFIS controller*

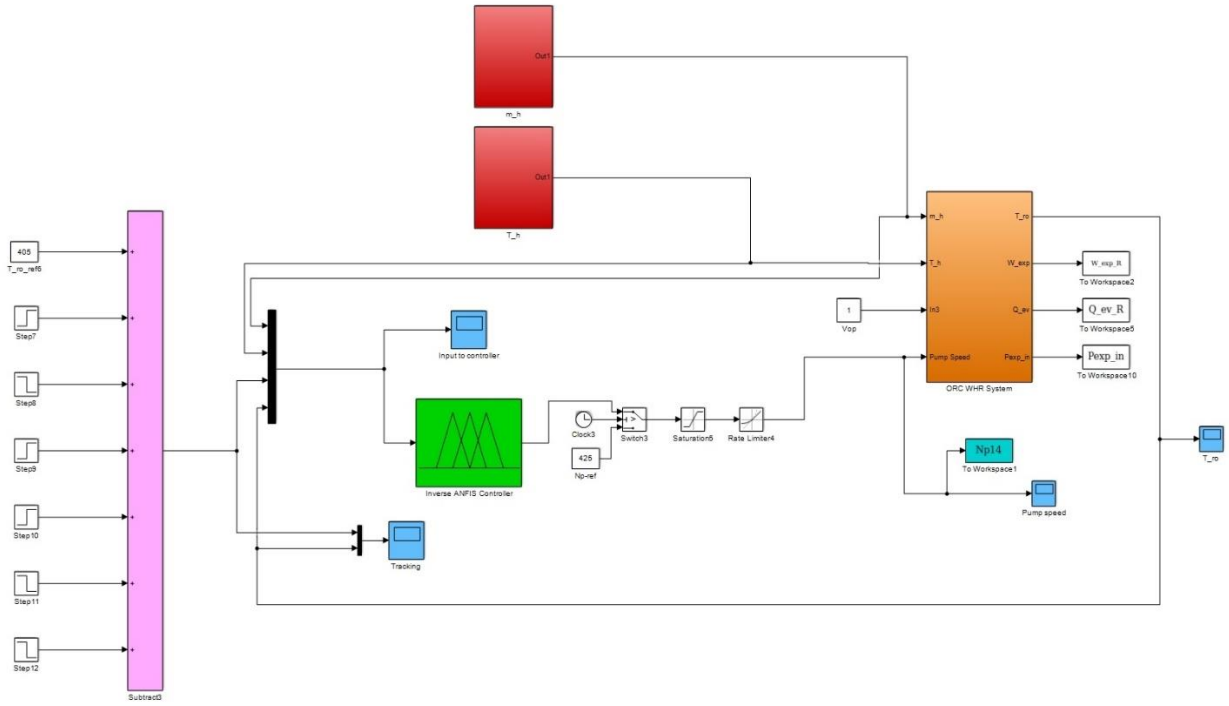

Fig. 6.8. *Simulink diagram of the ORC with inverse ANFIS controller*

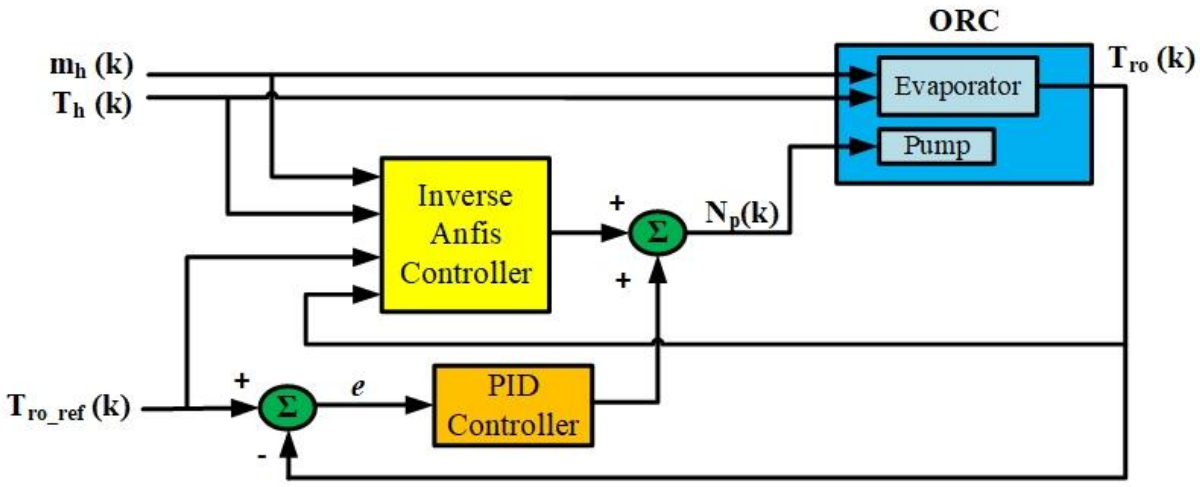

Fig. 6.9. *Structure of the ORC with combination of inverse ANFIS and PID controllers*

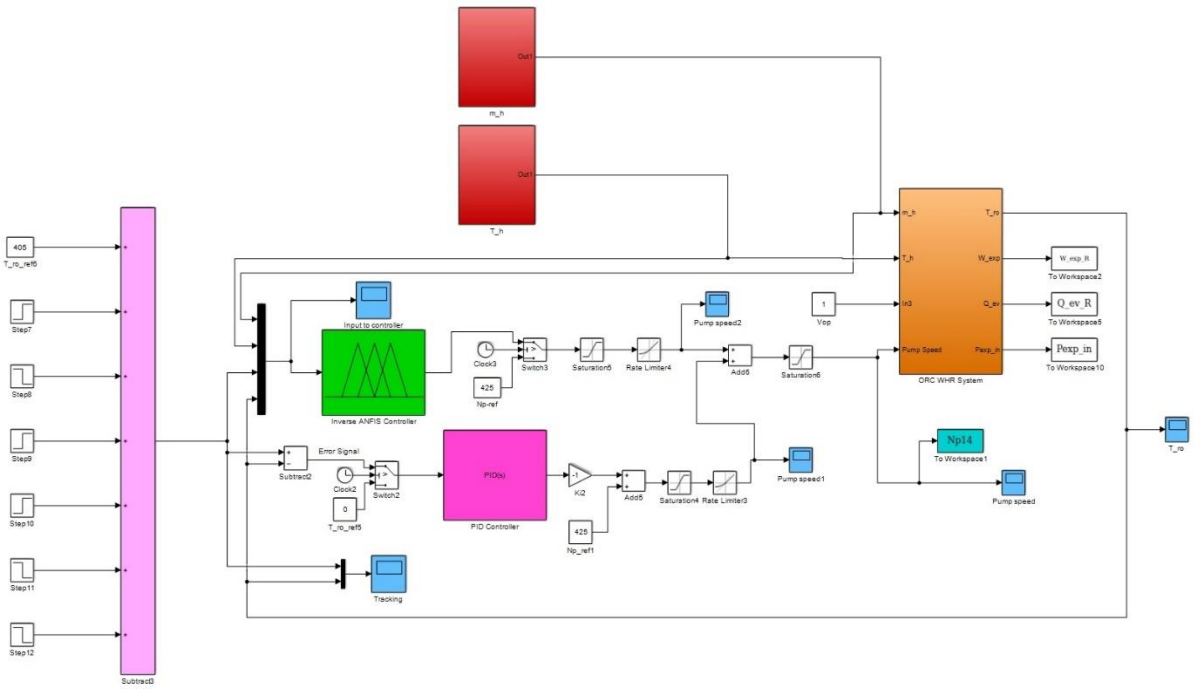

Fig. 6.10. *Simulink diagram of the ORC with combination of inverse ANFIS and PID controllers*

6.3 Control performance of combination of PID and inverse neuro-fuzzy controller

The performance of control strategies described in this chapter are now tested in terms of set-point tracking and robustness in presence of a highly transient heat source. The success of the control strategies is judged based on the ability to track the reference set-points for the working fluid temperature at the evaporator outlet and expander work output within acceptable limits. Moreover, since in practical applications environmental noise may affect the sensor readings, the robustness of controllers is also assessed in the presence of noise.

6.3.1 Set-point tracking performance of the control system

To test the set-point tracking ability of the inverse ANFIS and combination of inverse ANFIS and PID controllers, the closed loop control systems shown in the **Figs. 6.7** and **6.9** are

subjected to random signals for the heat source mass flow rate and temperature within the range of 0.18 – 0.24 Kg/s and 495 – 525 K, respectively. These ranges are selected to represent the temperature and mass flow rate variations of a typical waste heat source in heavy-duty trucks. The heat source mass flow rate and temperature variations are shown in **Fig. 6.11**.

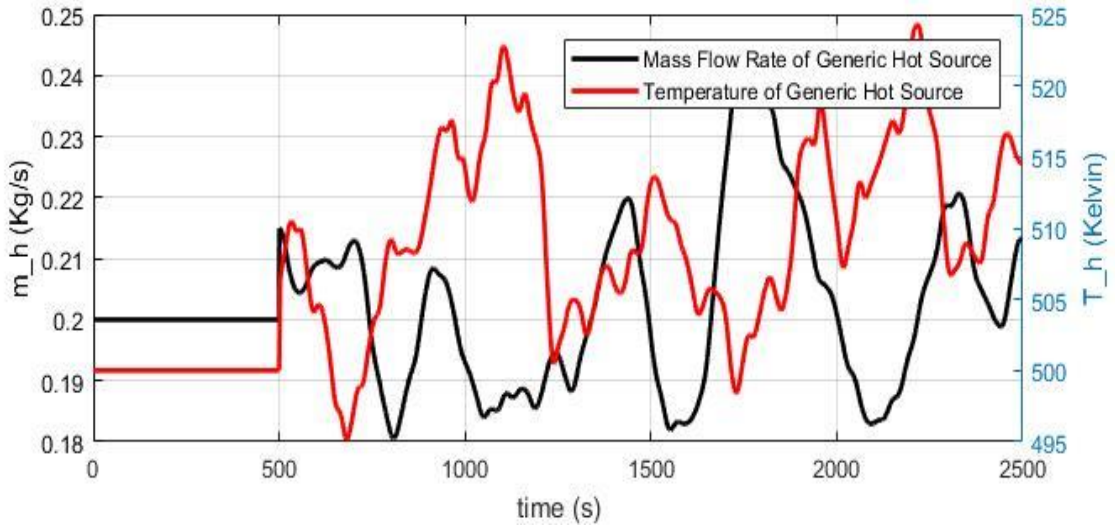

Fig. 6.11. *Heat source mass flow rate and temperature variations*

To ensure that the system reaches its steady-state condition before introducing transients to the ORC at $t = 500s$ the simulations start under steady-state heat source condition with $T_h = 500\ K$ and $m_h = 0.2\ Kg/s$. Furthermore, during this period the controller is off and a fixed pump speed of 850RPM is exerted to the system. At $t = 500s$ the controller becomes functional and simultaneously the transient heat source is applied to the ORC. As can be seen in **Fig. 6.12**, a reference signal with the temperature 405 K is set for the outlet temperature of evaporator. A series of step changes are applied to the reference signal. These step changes are happening at $t = 800s$, $t = 1000s$, $t = 1200s$, $t = 1400s$, $t = 1600s$, with the step sizes of +3, -3, +5, -5 and -1, respectively. Since the PID controller has fixed gains, which

are tuned for nominal temperature and mass flow rate of 500 K and 0.2 kg/s, its performance reduces in the presence of the transient heat source. Moreover, PID controller is unable to eliminate the steady-state error during the heat source disturbances. As it can be inferred from the results, the ANFIS controller is able to eliminate the steady-state error in the presence of heat source disturbances. This is achieved by intense modification of the pump speed during the transients to compensate for the changes in the heat source variations. However, the results are not very encouraging due to the chattering effect in the response of the controller. This chattering effect could be attributed to the fast adjustments of the pump speed in the presence of highly transient heat source that increases the settling time of the response. The results suggest that combination of a PID controller with the inverse ANFIS controller significantly reduces the chattering effect of the controller response and reduces its overshoot during the transients. Moreover, compared to the inverse ANFIS controller the second control strategy reduces the settling time of the response significantly. The pumps speed for different control scenarios are compared in **Fig. 6.13**.

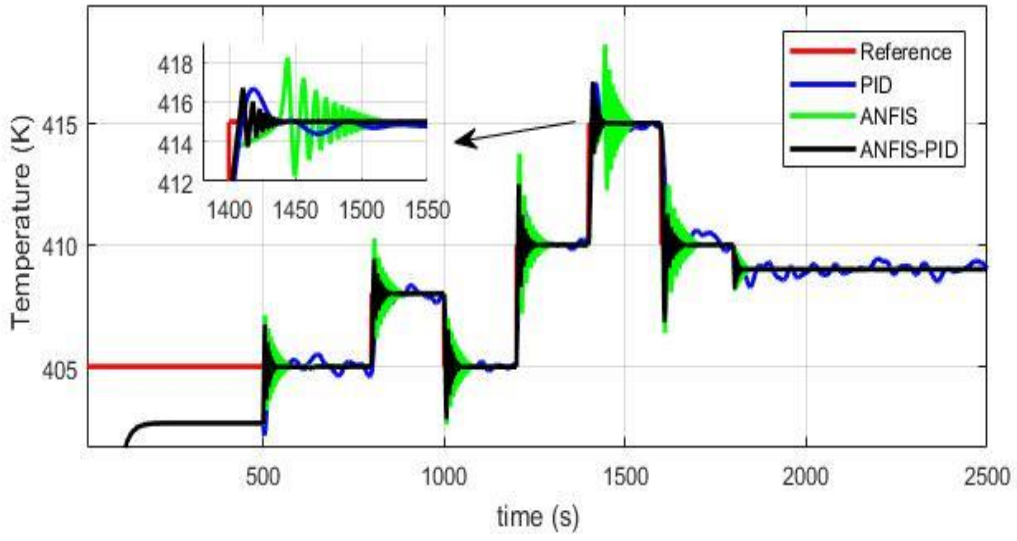

Fig. 6.12. *Comparison of set-point tracking of control strategies with transient heat source*

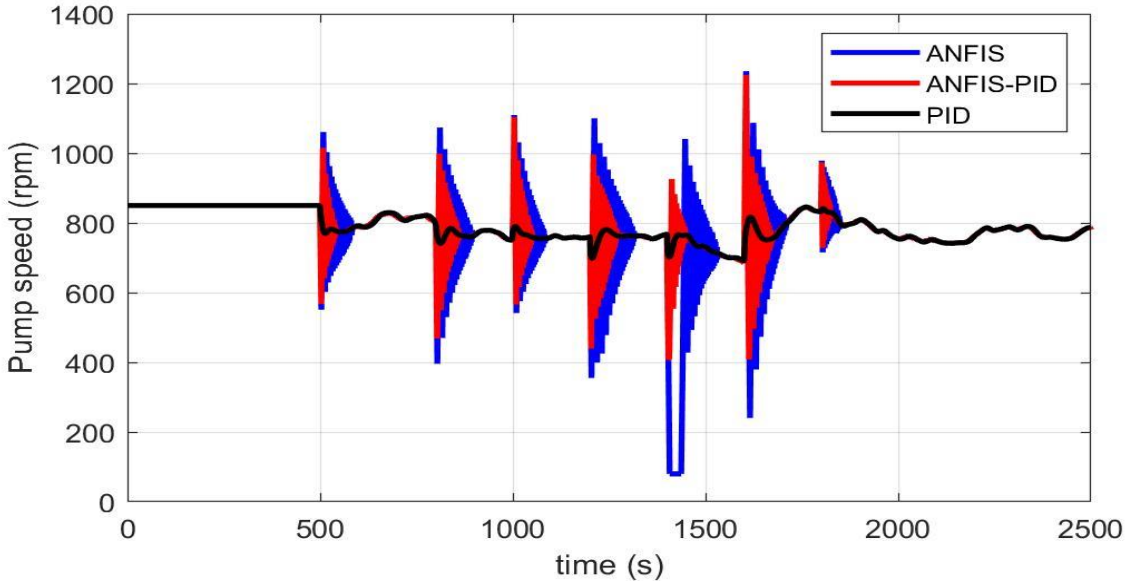

Fig. 6.13. *Comparison of response of pump for various control schemes under transient heat source*

6.3.2 Robustness of the proposed control system

Initial simulation test on evaporator outlet temperature control loops indicated the acceptable performance of combination of PID and inverse ANFIS controllers in presence of a transient heat source. However, in practical applications, the ORC works in a harsh environment and as a result, it is important to investigate the robustness of the control schemes. The robustness of the proposed controllers is assessed in terms of set-point tracking and disturbance rejection by adding a high frequency white noise to the heat source mass flow rate and temperature as represented in **Fig. 6.14**. To test the robustness of the controllers the set-point for the outlet evaporator temperature experiences several step changes with different amplitudes.

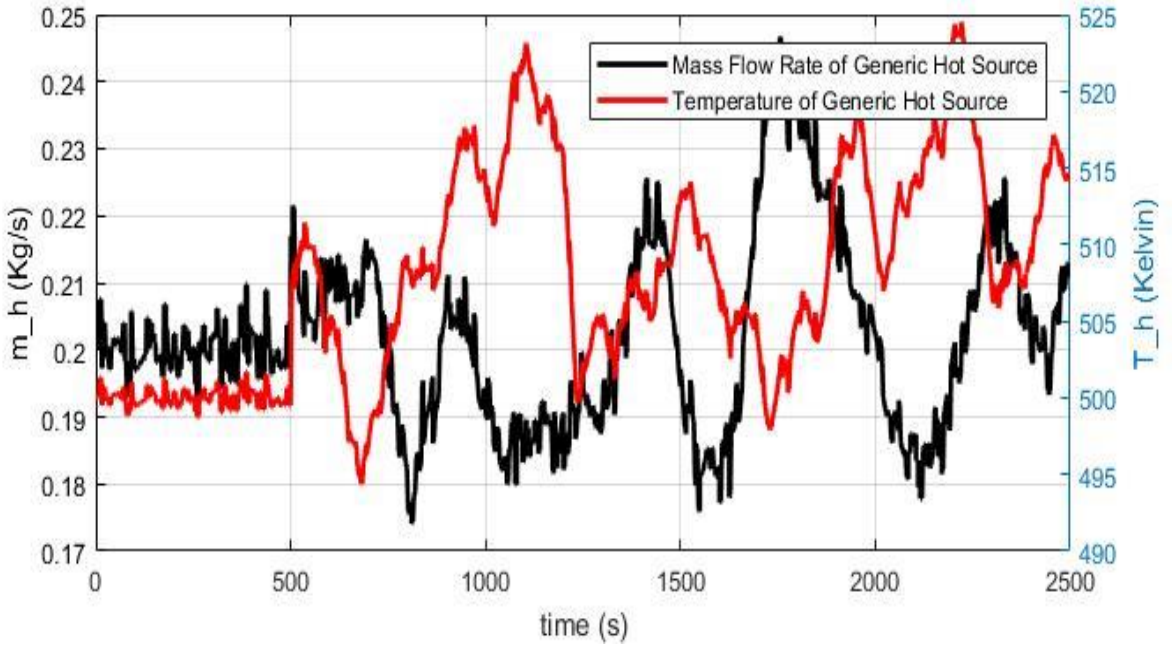

Fig. 6.14. *Heat source mass-flow rate and temperature variations in the presence of white noise*

The tracking ability of PID, inverse ANFIS and combination of PID and inverse ANFIS controllers are shown in **Fig. 6.15**. The results indicate the superior performance of combination of PID and inverse ANFIS controllers as compared to the PID controller by adjusting the pump speed in the range of 400-1250 RPM. As it can be observed from the pump speed responses in **Fig. 6.16**, the chattering effect of the pump speed is significantly reduced by combining a PID controller with the inverse ANFIS controller. Comparison of pump speed for three controllers reveals that the range of pump speed adjustment in the PID configuration is significantly less than the other two controllers. This lower adjustment range results in an undesirable increase in the working fluid temperature deviation from the set-point. The tracking ability of controllers in **Fig. 6.15** points out the ability of the controller in successfully tracking the working fluid temperature set-point at the evaporator outlet even in the presence of significant disturbances in the heat source sensors data.

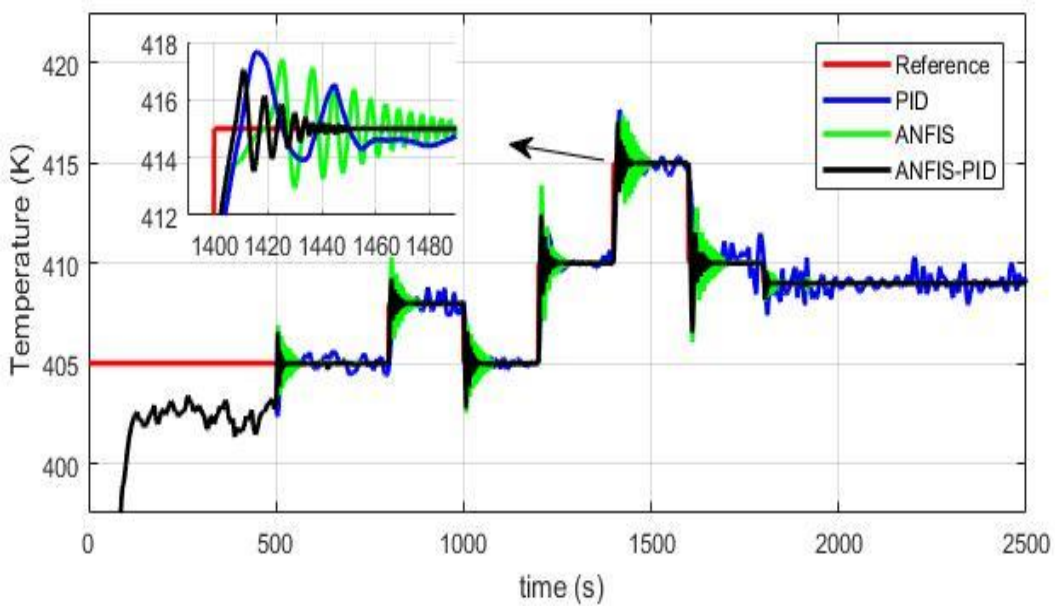

Fig. 6.15. *Comparison of set-point tracking of control strategies with transient heat source in the presence of noise*

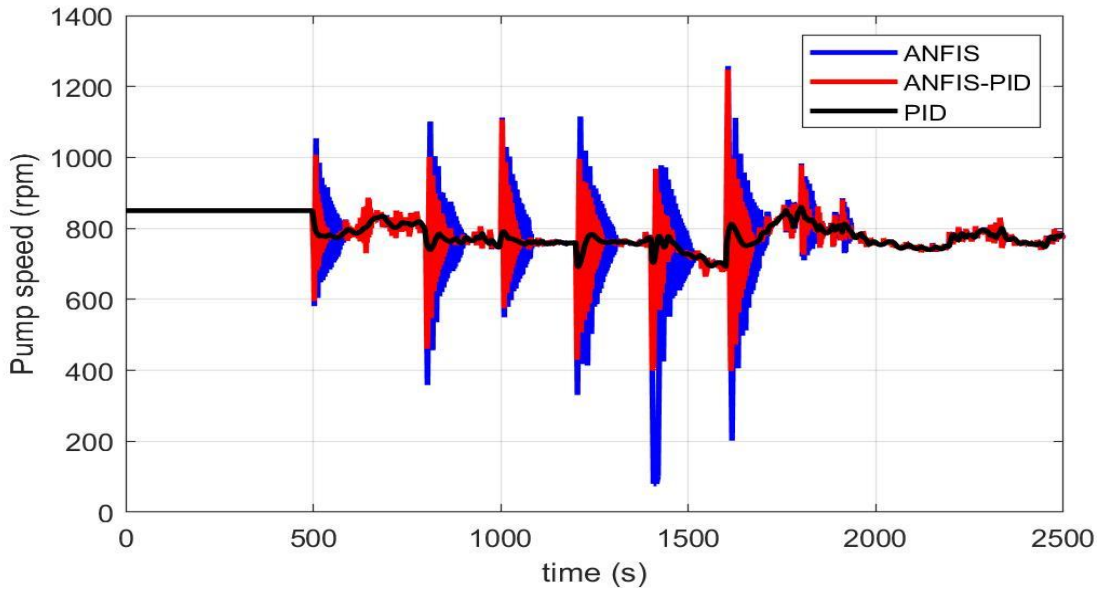

Fig. 6.16. *Comparison of response of pump for various control schemes with transient heat source in presence of noise*

6.4 Expander work output control

Control of expander speed during the transients is discussed in this section. As discussed previously, any modification in the pump speed changes the mass flow rate of working fluid

passing through expander. Since the ORC in mobile applications is imposed to a highly transient heat source, the pump speed needs to be adjusted accordingly to compensate for these transients in order to maintain the superheating at the evaporator outlet. As a result, the mass flow rate of working fluid may experience sudden changes in the ORC system that causes the expander output work $W_{ex}\ (k)$ to change abruptly. This is due to the faster dynamic of expander as compared to the evaporator. Furthermore, control of the expander work output is not effective when it is implemented independently without regulating the evaporator outlet temperature. This is due to the importance of vapour quality at the expander inlet. If a positive superheating is not maintained at the evaporator outlet, liquid droplets can form, which can harm the expander. Therefore, a simultaneous control scheme is proposed in this study to control the superheating and expander work output at the same time. The configuration of the control scheme and the Simulink diagram are illustrated in **Figs. 6.17** and **6.18**, respectively. A three-way valve is used in this configuration to bypass the excessive working fluid mass flow rate passing through the expander to maintain a steady expander work output. The percentage of valve opening ($V - O$) is determining the working fluid mass flow rate passing through the expander. A PI controller with gains $K_p = 8$, $K_i = 2.5$, and $z = 0.13$ for the proportional, integral, and filter coefficient, respectively, is tuned and implemented in the ORC control system. Since a steady-state model of the valve is used in this study, the response of the valve is filtered using a first order low-pass filter to reduce the oscillations as follows:

$$V - O_f = \frac{1}{\tau_v.s+1} \tag{6.2}$$

where $V - O_f$ is the valve filter and τ_v is the time constant for the filter which is assumed to be 1s.

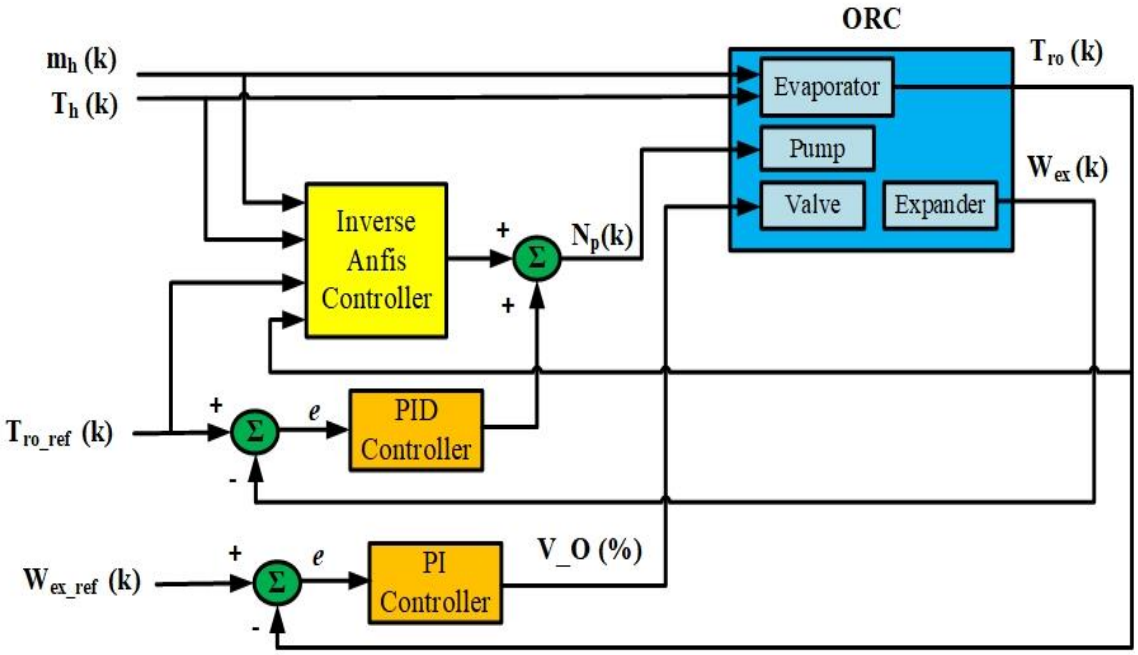

Fig. 6.17. *Structure for simultaneous control of superheating and expander work output*

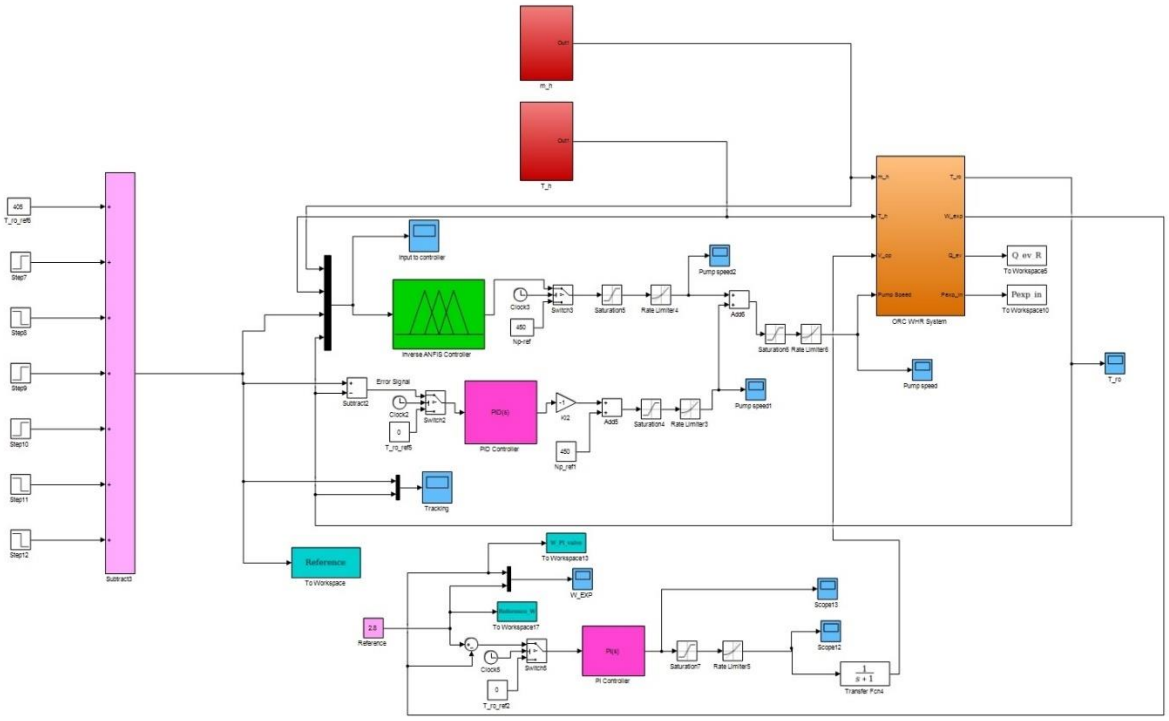

Fig. 6.18. *Simulink diagram for simultaneous control of superheating and expander work output*

6.4.1.1 Performance of expander work output controller

The ability of the expander control loop is investigated in this section. The expander control loop is added to the combination of PID and inverse ANFIS control loops to simultaneously regulate the work outlet of expander as well as the superheating at the evaporator outlet. The simulation results for expander work output and percentage of valve opening are shown in **Figs. 6.19** and **6.20**, respectively. A fixed set-point of 2.8 kW for the expander work output is considered. As can be seen in the **Fig. 6.19**, the PI controller is able to successfully maintain the desired expander work output by adjusting the valve opening for majority of the test duration. To achieve this, the controller adjusts the valve opening in the range of 87-100 percent. It can be seen in **Fig. 6.20** that the valve opening saturates at certain periods during the test, specially between $t = 1030s$ and $t = 1210s$. This is because the transient nature of the heat source. In this specific period, the heat source quantity is not enough to superheat

the working fluid therefore the ORC superheating control loop tries to reduce the pump speed to compensate for the heat source transients and maintain the evaporator outlet temperature set-point. As a result, the mass flow rate of working fluid at the valve inlet decreases. Subsequently, the expander work output control loop responds to this change in mass flow rate by completely opening the three-way valve to allow more superheated vapor to enter the expander and this causes deviation from the set-point. However, after the quantity of the transient heat source improves the controller tries to adjust the mass flow rate by suddenly reducing the percentage of valve opening. Due to this fast transition an overshoot happens in the response of the expander output work until the expander work control loop regains control and the work output returns to its defined set-point.

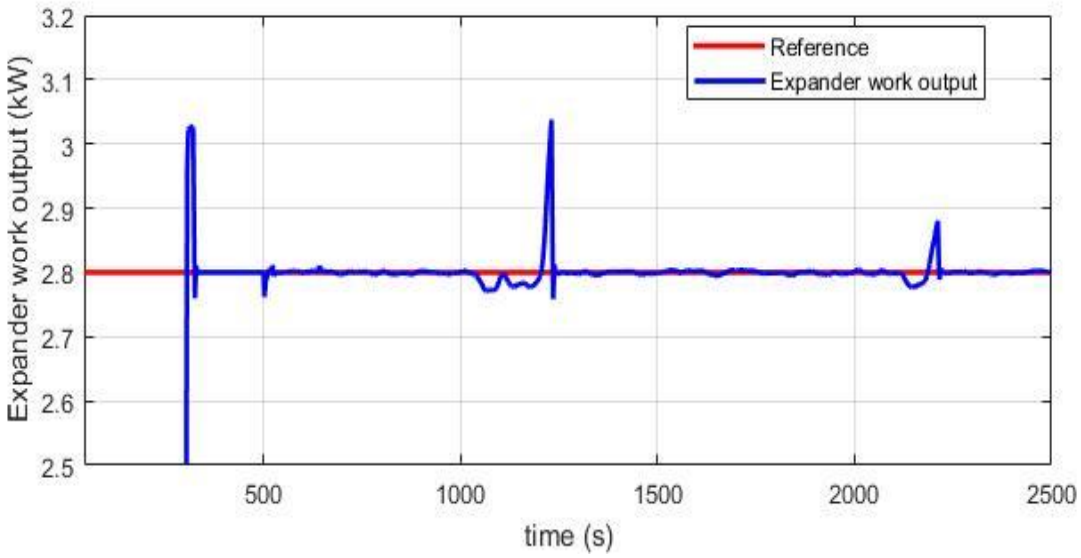

Fig. 6.19. *Set-point tracking of expander work output*

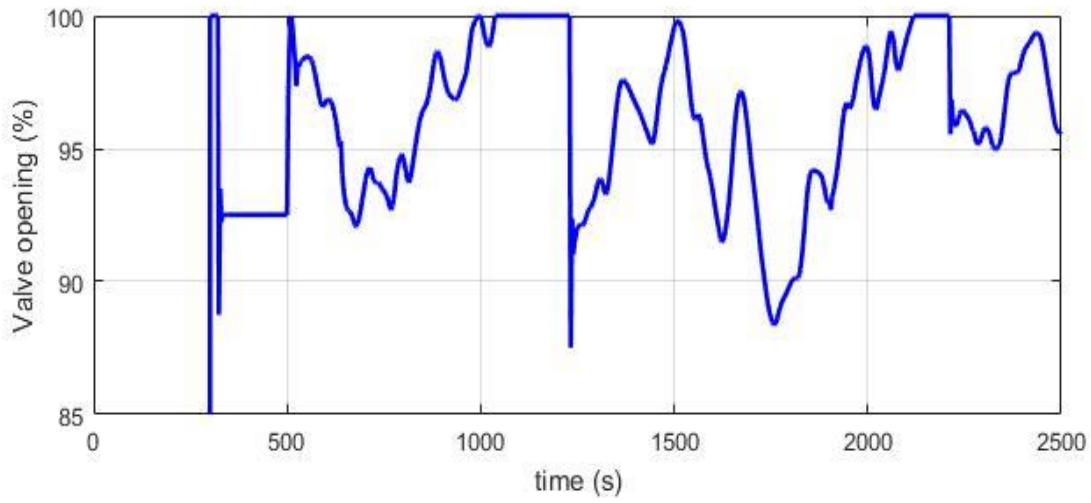

Fig. 6.20. *Percentage of valve opening using the PI controller*

6.5 Summary

In this chapter a new control structure comprised of two independent loops is proposed to control an ORC subjected to a transient heat source with heavy-duty diesel engine waste heat characteristics. The controlled parameters are chosen as superheating at the evaporator outlet and the expander work output which controlled respectively by adjusting the pump speed and bypassing the flow at the expander inlet using a three-way valve. The proposed control scheme is compared with a conventional PID controller in terms of set-point tracking and robustness in the presence of noises. Based on the simulation results, the main conclusions are as follows:

• The performance of PID controller with fixed gains is not satisfactory for control of superheating at the evaporator outlet under transient heat source conditions.

• The inverse neuro-fuzzy controller was able to reduce the steady state error for controlling the temperature at the evaporator outlet; however, due to the logic-based structure of the

controller the chattering in the pump speed increases, this fast adjustment of pump speed reduces the overall efficiency of the ORC.

- Combining a PID controller with the inverse neuro-fuzzy controller improves the settling time of the controller and reduces the chattering effect in the pump speed. Furthermore, this control strategy is shown to track the desirable temperature at the evaporator outlet with an acceptable precision.

- The performance of the proposed controller is compared with a PID controller in terms of set-point tracking and disturbance rejection, and the results suggest that the robustness of the controller is improved as compared to the PID controller.

- The performance of the PI controller is satisfactory for controlling the expander work output at its set-point. However, due to the importance of vapour quality at the expander inlet, this control strategy cannot be implemented independently without controlling the superheating at the evaporator outlet.

Chapter 7: Summary, conclusions and future work

7.1 Summary

This thesis involves modelling and control of an ORC waste heat recovery systems for applications in automotive industry where the systems are subjected to heat sources with unsteady characteristics. The ORC is a promising technology, which offers the potential to reduce the CO_2 emissions in internal combustion engines as the main technology currently used in the transportation sector. Review of the main waste heat recovery technologies presented in chapter 2 shows that, recently various methods of waste heat recovery have been explored to utilise the significant amount of energy that is released to the atmosphere from the exhaust and coolant of IC engines. These technologies include thermoelectric generators, Stirling engine, phase change material engine, Kalina cycle and organic Rankine cycle engines. Among them, ORC is the preferred method of waste heat recovery in internal combustion engines as it offers low manufacturing cost and high efficiency in recovery of waste heat from the low to medium temperature range heat sources. To adopt the ORC as a waste heat recovery method, the components of system need to be modelled and a control scheme is required to address the fluctuations of heat source during the driving conditions and ensure the safety of system.

Therefore, the specific objectives of this study are firstly to investigate the waste heat recovery technologies and their suitability for mobile applications. Secondly, developing a model of the chosen waste heat recovery method (ORC) that can be deployed to achieve the control requirements in real-time. Thirdly, developing a control scheme that can ensure the safety of system when it is subjected to the heat source variations due to the different driving

conditions. Lastly, regulating the work output of the ORC system regardless of the driving condition by adjusting the working fluid mass flow rate.

To deploy the ORC as a waste heat recovery method for mobile applications, in chapter 3, the potential architectures of the ORC are reviewed which shows that, SRORC, DRORC and RORC due to the complexity of their expanders are not generally suitable architectures. However, ORC with recuperator architecture can be deployed to preheat the working fluid before entering the evaporator. This cycle will be beneficial as it reduces the amount of heat required for vaporizing the working fluid in the evaporator. Furthermore, it was found that selection of the appropriate working fluid is of prominent importance as it affects the performance of the ORC. The substances need to have certain properties to be considered as a potential working fluid for the ORC in automotive applications. Moreover, despite the broad range of available substances, there is not a single optimal working fluid for all applications of the ORC and only a few of the available substances are deployed in commercial ORC applications. Therefore, in this study R134a and R245fa due to their suitable critical temperature, appropriate temperature profile matching with the heat source, low cost, relatively high auto-ignition temperature, zero ODP and wide availability are chosen for investigation of ORC waste heat recovery system.

To address the modelling requirements of this thesis, in chapter 4, the mathematical representation of the ORC components including pump, evaporator, expander, condenser, valve and liquid receiver are presented. The particular emphasis is given to the evaporator unit since it is the key component of the system as it is responsible for a large share of the overall exergy destruction (heat transfer over a finite temperature difference being irreversible by nature) and dominates the dynamic response of the ORC system. Furthermore, the evaporator unit is challenging to model due to the high nonlinearity of its governing

equations. In addition, the dynamic behaviour of ORC engines is governed by the large thermal inertia of the heat exchangers, in particular by that of the evaporator, which has a direct impact on the response time of an ORC engine subject to fluctuations in heat-source conditions (namely, temperature and mass flowrate). Therefore, an accurate model of the evaporator unit is required to capture the dynamics of the system. An accurate model of the evaporator is of prominent importance, not only because it is necessary for cycle optimisation and working fluid selection, but also as it allows a comprehensive optimisation of the dynamic control strategy.

The evaporator models available in the literature are reviewed in chapter 4, and it was found that they can be categorised into three main categories: finite volume (FV) models, moving boundary (MB) models and fuzzy models. The main technique which is used in the literature for modelling the evaporator unit is the FV model which is computationally expensive due to its numerical approach and high nonlinearity of the evaporator governing equations. Therefore, despite high accuracy of the FV models, it is usually appropriate for performance assessment and working fluid selection, but cannot be applied to high-frequency, real-time control purposes.

To provide an agile and control-oriented model of evaporator, in chapter 5, the potential of artificial intelligence techniques are investigated. An artificial neural network (ANN) model of evaporator is presented to predict the outlet temperature of heat source and outlet temperature of refrigerant. This model benefits from high accuracy and low response time in prediction of the desired evaporator outlet parameters, however, as oppose to the principle-based models, due to its black-box nature the mathematical relations are unknown to the designer and have no physical meaning. Another drawback of this model is that training this model involves a trial-and-error task and the model performance depends on several design

parameters such as model architecture, number of neurons in the hidden layer, activation function of the neurons, optimization algorithm and learning rate parameter.

To overcome the issues arising from the black-box nature of the neural network models, in chapter 5, neuro-fuzzy technique in introduced by combining the modelling benefits of fuzzy systems and pattern recognition power of neural networks. Neuro-fuzzy models are data-driven techniques that require training before implementation. As opposed to the principle-based methods, which are slow due to their iterative solution, neuro-fuzzy models are much faster and can be utilised for real-time control purposes. Adaptive neuro-fuzzy inference system (ANFIS) is an intelligent modelling technique acquiring the modelling benefits of Sugeno fuzzy inference system and learning ability of feedforward neural network.

To contribute to the advancement of waste heat recovery based on the ORC technology, in chapter 5, a new neuro-fuzzy model of the evaporator based on the available data from a FV model of evaporator has been developed in this thesis. This evaporator model offers reduced complexity, high accuracy and lower computational burden for prediction of the working fluid and heat source temperatures at the evaporator outlet. Moreover, the effect of training the ANFIS evaporator model using the hybrid GD-LSE and PSO algorithms is investigated. The statistical analysis of the results indicates the higher accuracy and generalization ability of the ANFIS models trained using the PSO algorithm.

To further validate the results obtained from the simulations, the application of neuro-fuzzy technique for modelling the evaporator in a 1-kWe ORC testing prototype is also investigated in chapter 5. Comparison of the results between the data obtained from the testing facility and the ANFIS evaporator models trained by GD-LSE and PSO algorithms indicates the high accuracy of the proposed evaporator models. Training the ANFIS models using the PSO algorithm improved the obtained test data RMSE values by 29% for the evaporator outlet

temperature and by 18% for the evaporator outlet pressure. The accuracy and speed of the model illustrate its potential for real-time control purposes.

Most of current investigations on ORCs are focused on theoretical and thermodynamic analysis, cycle optimisation, techno-economic optimization, and working fluid selection. In particular, combined fluid-design optimisation studies explore the potential of novel working fluids using computer aided molecular design (CAMD) techniques. Several studies also propose advanced off-design optimisation algorithms to maximise the performance of an ORC engine operating under variable heat-source conditions. However, the latter are based on quasi-steady models of the ORC engine and are thus not suitable for dynamic applications. For safe and successful implementation of ORCs in the automotive industry, a reliable and precise control scheme is required to ensure the safe operation of the engine, prevent organic fluid decomposition and reduce the risk of component damage.

To assess the performance of the neuro-fuzzy model of evaporator in an ORC-WHR system, the models for all the components of the ORC system are developed and integrated in a single loop series model. In chapter 6, a novel approach is proposed to ensure the safe operation of ORC-WHR system and stabilise its work output when subjected to transient heat sources in a range of waste heat from heavy-duty diesel engines. The control strategy comprises a neuro-fuzzy controller based on the inverse dynamics of the ORC system to control the superheating at the evaporator outlet by adjusting the pump speed and a PI controller to maintain the expander work output by regulating the mass flow rate at the expander inlet. The performance of the proposed control strategies is investigated with respect to set-point tracking and its robustness is tested in the presence of noise. The simulation results indicate an enhancement in the controller performance by combination of feedforward and feedback controllers based on neuro-fuzzy techniques.

7.2 Conclusions

The overall conclusions considering the objectives of the thesis are:

- ORC is a promising technology for waste heat recovery in IC engines with features such as low manufacturing cost and high efficiency as compared to the other waste heat recovery methods. Due to the fluctuating nature of heat source in mobile applications a control scheme is required to ensure the safety of system and stabilise its work output.
- Evaporator is the most critical component of the ORC and an accurate and agile model of evaporator is required for real-time control of the cycle. The simulation results indicate the evaporator models developed by using neuro-fuzzy technique can be deployed for real-time control of ORC in various applications. Moreover, the effort to identify the model parameters reduced substantially in the ANFIS models as opposed to the conventional non-adaptive methods of fuzzy system tuning. The neuro-fuzzy models offer reduced complexity, high accuracy and lower computational burden for prediction of the output parameters.
- Compared to the models trained using the GD-LSE algorithm, the models trained using the population-based PSO algorithm obtained better accuracy in terms of RMSEs and R coefficients for the training and test datasets. For the evaporator outlet temperature, a 29% improvement in the RMSE was achieved for both the training and test data. Furthermore, the evaporator outlet pressure RMSE improved by 15% and 18% for the training and test datasets, respectively, by using the PSO algorithm.
- The performance of PID controller with fixed gains is not satisfactory for control of superheating at the evaporator outlet under transient heat source conditions. The

inverse neuro-fuzzy controller was able to reduce the steady state error for controlling the temperature at the evaporator outlet; however, due to the logic-based structure of the controller the chattering in the pump speed increases, this fast adjustment of pump speed reduces the overall efficiency of the ORC and increases the settling time of the response.

- Combining a PID controller with inverse neuro-fuzzy controller improves the settling time of the controller and reduces the chattering effect in the pump speed. Furthermore, this control strategy is shown to track the desirable set-point temperature at the evaporator outlet with an acceptable precision. The performance of the proposed controller is compared with a PID controller in terms of set-point tracking and disturbance rejection, and the results suggest that the robustness of the controller is improved as compared to a tuned PID controller. The proposed control scheme not only can obtain satisfactory transient response under various loading conditions, but also can achieve desirable disturbance rejection performance.
- The performance of the PI controller is satisfactory for controlling the expander work output at its set-point. However, due to the importance of vapour quality at the expander inlet, this control strategy cannot be implemented independently without controlling the superheating at the evaporator outlet.

7.3 Further work

The particular areas where this thesis has made contribution to the field is on modelling the evaporator unit in the ORC waste heat recovery system using the neuro-fuzzy technique, validating the proposed technique using the experimental data and designing a control scheme that is able to control the working fluid temperature at the evaporator outlet and

regulating the expander work output. The obtained model and control scheme will be of direct benefit to the academic community since they facilitate the applications of ORC waste heat recovery system where the heat source has an unsteady nature.

Although the focus of this study is on the application of the ORC in automotive industry, the modelling and control methods developed in this study could be applied for investigating the waste heat recovery using the ORC technology in variety of applications such as waste heat recovery in industrial processes, combined heat and power (CHP) generation, transient solar ORC, etc.

The current findings of the control strategy in this thesis have been helpful in gaining experience in assessing the feasibility of the neuro-fuzzy control system. However, the proposed control system needs to be implemented on an ORC prototype with fluctuating heat source in order to further validate the results obtained from the simulations.

The model of the individual components of the ORC system presented in this thesis can be refined to achieve higher simulation accuracy under steady and dynamic situations. For example, several simplifications are considered in development of the FV evaporator model used in this study. To achieve a more realistic model of the ORC system these simplified hypotheses need to be avoided.

Although the performance of neuro-fuzzy evaporator model is satisfactory, the performance of the training method applied for training the neuro-fuzzy evaporator model developed in this study could be compared with other heuristic algorithms in search for finding the most efficient training algorithm. Furthermore, other improvements such as more accurate models for other components of the ORC system (pump, expander, etc.), cycle optimization for

higher thermal and heat recovery efficiency, and efficiency/life cycle analysis of waste heat recovery system could be considered to enhance the accuracy of results.

References

[1] United States Environmental Protection Agency. "Sources of Greenhouse Gas Emissions." https://www.epa.gov/ghgemissions/sources-greenhouse-gas-emissions (accessed 2021, Jan 2).

[2] H. Teng, G. Regner, and C. Cowland, "Waste heat recovery of heavy-duty diesel engines by organic Rankine cycle part I: hybrid energy system of diesel and Rankine engines," SAE Technical Paper, 0148-7191, 2007.

[3] G. Saliba *et al.*, "Comparison of gasoline direct-injection (GDI) and port fuel injection (PFI) vehicle emissions: emission certification standards, cold-start, secondary organic aerosol formation potential, and potential climate impacts," *Environmental science & technology*, vol. 51, no. 11, pp. 6542-6552, 2017.

[4] B. Lecointe and G. Monnier, "Downsizing a gasoline engine using turbocharging with direct injection," SAE Technical Paper, 0148-7191, 2003.

[5] S. Ciatti, M. Johnson, B. D. Adhikary, R. D. Reitz, and A. Knock, "Efficiency and emissions performance of multizone stratified compression ignition using different octane fuels," SAE Technical Paper, 0148-7191, 2013.

[6] European Commision. "Energy roadmap 2050." https://ec.europa.eu/energy/sites/ener/files/documents/2012_energy_roadmap_2050_en_0.pdf (accessed 2020, Dec 11).

[7] G. P. Panayiotou *et al.*, "Preliminary assessment of waste heat potential in major European industries," *Energy Procedia*, vol. 123, pp. 335-345, 2017.

[8] C. Haddad, C. Périlhon, A. Danlos, M.-X. François, and G. Descombes, "Some efficient solutions to recover low and medium waste heat: competitiveness of the thermoacoustic technology," *Energy Procedia*, vol. 50, pp. 1056-1069, 2014.

[9] B. Peris, J. Navarro-Esbrí, F. Molés, and A. Mota-Babiloni, "Experimental study of an ORC (organic Rankine cycle) for low grade waste heat recovery in a ceramic industry," *Energy*, vol. 85, pp. 534-542, 2015.

[10] C. Sprouse III and C. Depcik, "Review of organic Rankine cycles for internal combustion engine exhaust waste heat recovery," *Applied thermal engineering*, vol. 51, no. 1-2, pp. 711-722, 2013.

[11] J. I. Chowdhury, B. K. Nguyen, and D. Thornhill, "Investigation of waste heat recovery system at supercritical conditions with vehicle drive cycles," *Journal of Mechanical Science and Technology*, vol. 31, no. 2, pp. 923-936, 2017/02/01 2017, doi: 10.1007/s12206-017-0145-x.

[12] J. Jadhao and D. Thombare, "Review on exhaust gas heat recovery for IC engine," *International Journal of Engineering and Innovative Technology (IJEIT) Volume*, vol. 2, 2013.

[13] D. Champier, "Thermoelectric generators: A review of applications," *Energy Conversion and Management*, vol. 140, pp. 167-181, 2017.

[14] F. Frobenius, G. Gaiser, U. Rusche, and B. Weller, "Thermoelectric generators for the integration into automotive exhaust systems for passenger cars and commercial vehicles," *Journal of Electronic Materials*, vol. 45, no. 3, pp. 1433-1440, 2016.

[15] D. Crane and J. LaGrandeur, "Progress report on BSST-led US Department of Energy automotive waste heat recovery program," *Journal of electronic materials*, vol. 39, no. 9, pp. 2142-2148, 2010.

[16] J. LaGrandeur, D. Crane, S. Hung, B. Mazar, and A. Eder, "Automotive waste heat conversion to electric power using skutterudite, TAGS, PbTe and BiTe," in *2006 25th international conference on thermoelectrics*, 2006: IEEE, pp. 343-348.

[17] Q. E. Hussain, D. R. Brigham, and C. W. Maranville, "Thermoelectric exhaust heat recovery for hybrid vehicles," *SAE International Journal of Engines*, vol. 2, no. 1, pp. 1132-1142, 2009.

[18] N. Espinosa, M. Lazard, L. Aixala, and H. Scherrer, "Modeling a thermoelectric generator applied to diesel automotive heat recovery," *Journal of Electronic materials*, vol. 39, no. 9, pp. 1446-1455, 2010.

[19] M. Mori, T. Yamagami, M. Sorazawa, T. Miyabe, S. Takahashi, and T. Haraguchi, "Simulation of fuel economy effectiveness of exhaust heat recovery system using thermoelectric generator in a series hybrid," *SAE International journal of materials and manufacturing*, vol. 4, no. 1, pp. 1268-1276, 2011.

[20] S. Alfarawi, M. Webb-Martin, S. Mahmoud, and R. Al-Dadah, "Thermal analysis of Stirling engine to power automotive alternator using heat from exhaust gases," *Energy Procedia*, vol. 61, pp. 2395-2398, 2014.

[21] M. Güven, H. Bedir, and G. Anlaş, "Optimization and application of Stirling engine for waste heat recovery from a heavy-duty truck engine," *Energy Conversion and Management*, vol. 180, pp. 411-424, 2019.

[22] I. Kubo, "Technical and economic study of Stirling and Rankine cycle bottoming systems for heavy truck diesel engines," 1987.

[23] M. Bianchi and A. De Pascale, "Bottoming cycles for electric energy generation: parametric investigation of available and innovative solutions for the exploitation of

low and medium temperature heat sources," *Applied Energy,* vol. 88, no. 5, pp. 1500-1509, 2011.

[24] V. V. Rao, R. Parameshwaran, and V. V. Ram, "PCM-mortar based construction materials for energy efficient buildings: A review on research trends," *Energy and Buildings,* vol. 158, pp. 95-122, 2018.

[25] Y. Konuklu, M. Ostry, H. O. Paksoy, and P. Charvat, "Review on using microencapsulated phase change materials (PCM) in building applications," *Energy and Buildings,* vol. 106, pp. 134-155, 2015.

[26] A. Sharma, V. V. Tyagi, C. Chen, and D. Buddhi, "Review on thermal energy storage with phase change materials and applications," *Renewable and Sustainable energy reviews,* vol. 13, no. 2, pp. 318-345, 2009.

[27] B. Zalba, J. M. Marın, L. F. Cabeza, and H. Mehling, "Review on thermal energy storage with phase change: materials, heat transfer analysis and applications," *Applied thermal engineering,* vol. 23, no. 3, pp. 251-283, 2003.

[28] K. N. Gopal, R. Subbarao, V. Pandiyarajan, and R. Velraj, "Thermodynamic analysis of a diesel engine integrated with a PCM based energy storage system," *International Journal of Thermodynamics*, vol. 13, no. 1, pp. 15-21, 2010.

[29] M. T. Johansson and M. Söderström, "Electricity generation from low-temperature industrial excess heat—an opportunity for the steel industry," *Energy efficiency,* vol. 7, no. 2, pp. 203-215, 2014.

[30] J. Bugge, S. Kjaer, and R. Blum, "High-efficiency coal-fired power plants development and perspectives," *Energy*, vol. 31, no. 10-11, pp. 1437-1445, 2006.

[31] M. J. Moran, H. N. Shapiro, D. D. Boettner, and M. B. Bailey, *Fundamentals of engineering thermodynamics*. John Wiley & Sons, 2010.

[32] C. Wu, *Thermodynamic Cycles: Computer-aided design and optimization*. CRC Press, 2003.

[33] B. F. Tchanche, G. Lambrinos, A. Frangoudakis, and G. Papadakis, "Low-grade heat conversion into power using organic Rankine cycles – A review of various applications," *Renewable and Sustainable Energy Reviews*, vol. 15, no. 8, pp. 3963-3979, 2011/10/01/ 2011, doi: https://doi.org/10.1016/j.rser.2011.07.024.

[34] A. Nemati, H. Nami, F. Ranjbar, and M. Yari, "A comparative thermodynamic analysis of ORC and Kalina cycles for waste heat recovery: A case study for CGAM cogeneration system," *Case Studies in Thermal Engineering*, vol. 9, pp. 1-13, 2017/03/01/ 2017, doi: https://doi.org/10.1016/j.csite.2016.11.003.

[35] R. Saidur, M. Rezaei, W. K. Muzammil, M. H. Hassan, S. Paria, and M. Hasanuzzaman, "Technologies to recover exhaust heat from internal combustion engines," *Renewable and Sustainable Energy Reviews*, vol. 16, no. 8, pp. 5649-5659, 2012/10/01/ 2012, doi: https://doi.org/10.1016/j.rser.2012.05.018.

[36] T. Wang, Y. Zhang, Z. Peng, and G. Shu, "A review of researches on thermal exhaust heat recovery with Rankine cycle," *Renewable and sustainable energy reviews*, vol. 15, no. 6, pp. 2862-2871, 2011.

[37] T. Yamamoto, T. Furuhata, N. Arai, and K. Mori, "Design and testing of the Organic Rankine Cycle," *Energy*, vol. 26, no. 3, pp. 239-251, 2001/03/01/ 2001, doi: https://doi.org/10.1016/S0360-5442(00)00063-3.

[38] S. Karellas, A. Schuster, and A. D. Leontaritis, "Influence of supercritical ORC parameters on plate heat exchanger design," *Applied Thermal Engineering*, Article vol. 33-34, no. 1, pp. 70-76, 2012, doi: 10.1016/j.applthermaleng.2011.09.013.

[39] D. Morgan, P. Patel, E. DOYLE, R. RAYMOND, R. Sakhuja, and K. BARBER, "Laboratory test results, low emission ranking-cycle engine with organic-based working fluid and reciprocating expander for automobiles," presented at the Intersociety Energy Conversion Engineering Conference, 1973.

[40] P. S. Patel and E. F. Doyle, "Compounding the truck diesel engine with an organic Rankine-cycle system," SAE Technical Paper, 0148-7191, 1976.

[41] E. Doyle, L. DiNanno, and S. Kramer, "Installation of a diesel-organic Rankine compound engine in a class 8 truck for a single-vehicle test," SAE Technical Paper, 0148-7191, 1979.

[42] O. Delgado and N. Lutsey, "The US SuperTruck program: Expediting the development of advanced heavy-duty vehicle efficiency technologies," *The International Council on Clean Transportation,* June 2014.

[43] J. Ringler, M. Seifert, V. Guyotot, and W. Hübner, "Rankine cycle for waste heat recovery of IC engines," *SAE International Journal of Engines,* vol. 2, no. 1, pp. 67-76, 2009.

[44] T. A. Horst, H.-S. Rottengruber, M. Seifert, and J. Ringler, "Dynamic heat exchanger model for performance prediction and control system design of automotive waste heat recovery systems," *Applied Energy*, vol. 105, pp. 293-303, 2013/05/01/ 2013, doi: https://doi.org/10.1016/j.apenergy.2012.12.060.

[45] T. A. Horst, W. Tegethoff, P. Eilts, and J. Koehler, "Prediction of dynamic Rankine Cycle waste heat recovery performance and fuel saving potential in passenger car applications considering interactions with vehicles' energy management," *Energy Conversion and Management,* vol. 78, pp. 438-451, 2014.

[46] H. Teng, "Waste heat recovery concept to reduce fuel consumption and heat rejection from a diesel engine," *SAE International Journal of Commercial Vehicles*, vol. 3, no. 2010-01-1928, pp. 60-68, 2010.

[47] T. Park, H. Teng, G. L. Hunter, B. van der Velde, and J. Klaver, "A rankine cycle system for recovering waste heat from hd diesel engines-experimental results," SAE Technical Paper, 0148-7191, 2011.

[48] D. V. Singh and E. Pedersen, "A review of waste heat recovery technologies for maritime applications," *Energy conversion and management*, vol. 111, pp. 315-328, 2016.

[49] A. Gabriel-Buenaventura and B. Azzopardi, "Energy recovery systems for retrofitting in internal combustion engine vehicles: A review of techniques," *Renewable and Sustainable Energy Reviews*, vol. 41, pp. 955-964, 2015.

[50] X. Liang, X. Wang, G. Shu, H. Wei, H. Tian, and X. Wang, "A review and selection of engine waste heat recovery technologies using analytic hierarchy process and grey relational analysis," *International Journal of Energy Research*, vol. 39, no. 4, pp. 453-471, 2015.

[51] R. Saidur, M. Rezaei, W. K. Muzammil, M. Hassan, S. Paria, and M. Hasanuzzaman, "Technologies to recover exhaust heat from internal combustion engines," *Renewable and sustainable energy reviews*, vol. 16, no. 8, pp. 5649-5659, 2012.

[52] M. Karvonen, R. Kapoor, A. Uusitalo, and V. Ojanen, "Technology competition in the internal combustion engine waste heat recovery: a patent landscape analysis," *Journal of Cleaner Production*, vol. 112, pp. 3735-3743, 2016.

[53] A. Mahmoudi, M. Fazli, and M. R. Morad, "A recent review of waste heat recovery by Organic Rankine Cycle," *Applied Thermal Engineering*, vol. 143, pp. 660-675, 2018/10/01/ 2018, doi: https://doi.org/10.1016/j.applthermaleng.2018.07.136.

[54] B. Peris, J. Navarro-Esbrí, and F. Molés, "Bottoming organic Rankine cycle configurations to increase Internal Combustion Engines power output from cooling water waste heat recovery," *Applied Thermal Engineering*, vol. 61, no. 2, pp. 364-371, 2013.

[55] H. Xi, M.-J. Li, C. Xu, and Y.-L. He, "Parametric optimization of regenerative organic Rankine cycle (ORC) for low grade waste heat recovery using genetic algorithm," *Energy*, vol. 58, pp. 473-482, 2013.

[56] G. Angelino, M. Gaia, and E. Macchi, "A review of Italian activity in the field of organic Rankine cycles," *VDI-Berichte*, no. 539, pp. 465-482, 1984.

[57] A. Uusitalo, J. Honkatukia, T. Turunen-Saaresti, and J. Larjola, "A thermodynamic analysis of waste heat recovery from reciprocating engine power plants by means of Organic Rankine Cycles," *Applied thermal engineering*, vol. 70, no. 1, pp. 33-41, 2014.

[58] Y. Zhou, Y. Wu, F. Li, and L. Yu, "Performance analysis of zeotropic mixtures for the dual-loop system combined with internal combustion engine," *Energy Conversion and Management*, vol. 118, pp. 406-414, 2016.

[59] F. Yang *et al.*, "Performance analysis of waste heat recovery with a dual loop organic Rankine cycle (ORC) system for diesel engine under various operating conditions," *Energy Conversion and Management*, vol. 80, pp. 243-255, 2014.

[60] E. Wang, H. Zhang, B. Fan, and Y. Wu, "Optimized performances comparison of organic Rankine cycles for low grade waste heat recovery," *Journal of Mechanical Science and Technology*, vol. 26, no. 8, pp. 2301-2312, 2012.

[61] T. Erhart, U. Eicker, and D. Infield, "Part-load characteristics of Organic-Rankine-Cycles," presented at the 2nd Eur. Conf. Polygeneration, Spain, 2011.

[62] V. Maizza and A. Maizza, "Unconventional working fluids in organic Rankine-cycles for waste energy recovery systems," *Applied thermal engineering*, vol. 21, no. 3, pp. 381-390, 2001.

[63] O. Badr, P. O'callaghan, and S. Probert, "Rankine-cycle systems for harnessing power from low-grade energy sources," *Applied Energy*, vol. 36, no. 4, pp. 263-292, 1990.

[64] P. J. Mago, L. M. Chamra, K. Srinivasan, and C. Somayaji, "An examination of regenerative organic Rankine cycles using dry fluids," *Applied thermal engineering*, vol. 28, no. 8-9, pp. 998-1007, 2008.

[65] D. Mikielewicz and J. Mikielewicz, "A thermodynamic criterion for selection of working fluid for subcritical and supercritical domestic micro CHP," *Applied Thermal Engineering*, vol. 30, no. 16, pp. 2357-2362, 2010.

[66] E. Wang, H. Zhang, B. Fan, M. Ouyang, Y. Zhao, and Q. Mu, "Study of working fluid selection of organic Rankine cycle (ORC) for engine waste heat recovery," *Energy*, vol. 36, no. 5, pp. 3406-3418, 2011.

[67] S. Quoilin, M. Van Den Broek, S. Declaye, P. Dewallef, and V. Lemort, "Techno-economic survey of Organic Rankine Cycle (ORC) systems," *Renewable and Sustainable Energy Reviews*, vol. 22, pp. 168-186, 2013.

[68] G. Shu, G. Yu, H. Tian, H. Wei, and X. Liang, "A multi-approach evaluation system (MA-ES) of Organic Rankine Cycles (ORC) used in waste heat utilization," *Applied Energy*, vol. 132, pp. 325-338, 2014.

[69] S. Glover, R. Douglas, L. Glover, G. McCullough, and S. McKenna, "Automotive waste heat recovery: Working fluid selection and related boundary conditions," *International Journal of Automotive Technology*, vol. 16, no. 3, pp. 399-409, 2015.

[70] A. Karvountzis-Kontakiotis *et al.*, "Effect of an ORC waste heat recovery system on diesel engine fuel economy for off-highway vehicles," SAE Technical Paper, 0148-7191, 2017.

[71] M. Imran, M. Usman, B.-S. Park, and D.-H. Lee, "Volumetric expanders for low grade heat and waste heat recovery applications," *Renewable and Sustainable Energy Reviews*, vol. 57, pp. 1090-1109, 2016.

[72] M. O. Bamgbopa and E. Uzgoren, "Numerical analysis of an organic Rankine cycle under steady and variable heat input," *Applied Energy*, vol. 107, pp. 219-228, 2013/07/01/ 2013, doi: https://doi.org/10.1016/j.apenergy.2013.02.040.

[73] J. Sun and W. Li, "Operation optimization of an organic Rankine cycle (ORC) heat recovery power plant," *Applied Thermal Engineering*, vol. 31, no. 11-12, pp. 2032-2041, 2011.

[74] S. Quoilin, R. Aumann, A. Grill, A. Schuster, V. Lemort, and H. Spliethoff, "Dynamic modeling and optimal control strategy of waste heat recovery Organic Rankine Cycles," *Applied energy*, vol. 88, no. 6, pp. 2183-2190, 2011.

[75] S. Quoilin, V. Lemort, and J. Lebrun, "Experimental study and modeling of an Organic Rankine Cycle using scroll expander," *Applied energy*, vol. 87, no. 4, pp. 1260-1268, 2010.

[76] S. Declaye, S. Quoilin, L. Guillaume, and V. Lemort, "Experimental study on an open-drive scroll expander integrated into an ORC (Organic Rankine Cycle) system with R245fa as working fluid," *Energy*, vol. 55, pp. 173-183, 2013.

[77] X. Yang, J. Xu, Z. Miao, J. Zou, and C. Yu, "Operation of an organic Rankine cycle dependent on pumping flow rates and expander torques," *Energy*, vol. 90, pp. 864-878, 2015.

[78] A. Landelle, N. Tauveron, R. Revellin, P. Haberschill, S. Colasson, and V. Roussel, "Performance investigation of reciprocating pump running with organic fluid for organic Rankine cycle," *Applied Thermal Engineering*, vol. 113, pp. 962-969, 2017.

[79] A. Kheiri, M. Feidt, and S. Pelloux-Prayer, "Thermodynamic and economic optimizations of a waste heat to power plant driven by a subcritical ORC (Organic Rankine Cycle) using pure or zeotropic working fluid," *Energy*, vol. 78, pp. 622-638, 2014.

[80] S. Kakac, H. Liu, and A. Pramuanjaroenkij, *Heat exchangers: selection, rating, and thermal design*. CRC press, 2020.

[81] A. Domingues, H. Santos, and M. Costa, "Analysis of vehicle exhaust waste heat recovery potential using a Rankine cycle," *Energy*, vol. 49, pp. 71-85, 2013/01/01/ 2013, doi: https://doi.org/10.1016/j.energy.2012.11.001.

[82] D. Walraven, B. Laenen, and W. D'haeseleer, "Optimum configuration of shell-and-tube heat exchangers for the use in low-temperature organic Rankine cycles," *Energy Conversion and Management*, vol. 83, pp. 177-187, 2014/07/01/ 2014, doi: https://doi.org/10.1016/j.enconman.2014.03.066.

[83] D. Walraven, B. Laenen, and W. D'haeseleer, "Comparison of shell-and-tube with plate heat exchangers for the use in low-temperature organic Rankine cycles,"

Energy Conversion and Management, vol. 87, pp. 227-237, 2014/11/01/ 2014, doi: https://doi.org/10.1016/j.enconman.2014.07.019.

[84] http://www.can-coil.com/?q=content/finned-coils/oem-finned-tube-heat-exchangers-coils&slide=5 (accessed 12.04.2021).

[85] http://www.thermex.co.uk/product/shell-and-tube-heat-exchangers/exhaust-gas-heat-exchangers (accessed 11.04.2021).

[86] https://www.uk-exchangers.com/heat-exchange-products/brazed-plate-heat-exchangers/ (accessed 13.04.2021).

[87] G. Qiu, H. Liu, and S. Riffat, "Expanders for micro-CHP systems with organic Rankine cycle," *Applied Thermal Engineering*, vol. 31, no. 16, pp. 3301-3307, 2011.

[88] J. Bao and L. Zhao, "A review of working fluid and expander selections for organic Rankine cycle," *Renewable and sustainable energy reviews*, vol. 24, pp. 325-342, 2013.

[89] D. Fiaschi, G. Manfrida, and F. Maraschiello, "Thermo-fluid dynamics preliminary design of turbo-expanders for ORC cycles," *Applied energy*, vol. 97, pp. 601-608, 2012.

[90] V. Krishna Avadhanula and C.-S. Lin, "Empirical models for a screw expander based on experimental data from organic Rankine cycle system testing," *Journal of engineering for gas turbines and power*, vol. 136, no. 6, 2014.

[91] V. K. Avadhanula, C.-S. Lin, and T. Johnson, "Testing a 50kW ORC at different heating and cooling source conditions to map the performance characteristics," SAE Technical Paper, 0148-7191, 2013.

[92] W. Wang, Y.-t. Wu, C.-f. Ma, G.-d. Xia, and J.-f. Wang, "Experimental study on the performance of single screw expanders by gap adjustment," *Energy*, vol. 62, pp. 379-384, 2013.

[93] W. Wang, Y.-t. Wu, G.-d. Xia, C.-f. Ma, J.-f. Wang, and Y. Zhang, "Experimental study on the performance of the single screw expander prototype by optimizing configuration," in *Energy Sustainability*, 2012, vol. 44816: American Society of Mechanical Engineers, pp. 1281-1286.

[94] R. A. McKay, "International test and demonstration of a 1-MW wellhead generator: Helical screw expander power plant," 1984.

[95] I. H. Park, H. Taniguchi, K. Kudo, W. Giedt, and M. J. Cho, "Investigation of Two-Phase Flow Screw Expanders for Power Generation," in *KSME/JSME THERMAL and FLUID Engineering Conference*, 1988, pp. 138-143.

[96] Y. Zhang, "Experimental study on the performance of single screw expander with 195 mm diameter screw," in *Proceedings of the ASME ORC 2013 2nd International Seminar ORC Power System Rotterdam, Netherlands*, 2013.

[97] T. Kaneko and N. Hirayama, "Study on fundamental performance of helical screw expander," *Bulletin of JSME*, vol. 28, no. 243, pp. 1970-1977, 1985.

[98] V. Lemort, L. Guillaume, A. Legros, S. Declaye, and S. Quoilin, "A comparison of piston, screw and scroll expanders for small scale Rankine cycle systems," in *Proceedings of the 3rd international conference on microgeneration and related technologies*, 2013.

[99] https://greensecure.org/screw-expander/ (accessed 08.04.2021).

[100] Y. Jiang, Y. Ma, L. Fu, and M. Li, "Some design features of CO2 two-rolling piston expander," *Energy*, vol. 55, pp. 916-924, 2013.

[101] T. Hua, M. Yitai, L. Minxia, G. Haiqing, and L. Zhongyan, "Influence of a non-condensable gas on the performance of a piston expander for use in carbon dioxide trans-critical heat pumps," *Applied thermal engineering,* vol. 31, no. 11-12, pp. 1943-1949, 2011.

[102] G. Haiqing, M. Yitai, and L. Minxia, "Some design features of CO2 swing piston expander," *Applied Thermal Engineering,* vol. 26, no. 2-3, pp. 237-243, 2006.

[103] M. Li, Y. Ma, and H. Tian, "A rolling piston-type two-phase expander in the transcritical CO2 cycle," *HVAC&R Research,* vol. 15, no. 4, pp. 729-741, 2009.

[104] D. Seher, T. Lengenfelder, J. Gerhardt, N. Eisenmenger, M. Hackner, and I. Krinn, "Waste heat recovery for commercial vehicles with a Rankine process," in *21st Aachen colloquium automobile and engine technology*, 2012, vol. 2012.

[105] N. Zheng, L. Zhao, X. Wang, and Y. Tan, "Experimental verification of a rolling-piston expander that applied for low-temperature Organic Rankine Cycle," *Applied Energy,* vol. 112, pp. 1265-1274, 2013.

[106] H. Kim, J. Ahn, I. Park, and P. Rha, "Scroll expander for power generation from a low-grade steam source," *Proceedings of the Institution of Mechanical Engineers, Part A: Journal of Power and Energy*, vol. 221, no. 5, pp. 705-711, 2007.

[107] J.-C. Chang, C.-W. Chang, T.-C. Hung, J.-R. Lin, and K.-C. Huang, "Experimental study and CFD approach for scroll type expander used in low-temperature organic Rankine cycle," *Applied Thermal Engineering*, vol. 73, no. 2, pp. 1444-1452, 2014.

[108] J.-C. Chang, T.-C. Hung, Y.-L. He, and W. Zhang, "Experimental study on low-temperature organic Rankine cycle utilizing scroll type expander," *Applied Energy,* vol. 155, pp. 150-159, 2015.

[109] S. Quoilin, "Sustainable energy conversion through the use of organic Rankine cycles for waste heat recovery and solar applications," University of Liège, Liège, Belgium, 2011.

[110] J. Zhang, W. Zhang, G. Hou, and F. Fang, "Dynamic modeling and multivariable control of organic Rankine cycles in waste heat utilizing processes," *Computers and Mathematics with Applications*, Conference Paper vol. 64, no. 5, pp. 908-921, 2012, doi: 10.1016/j.camwa.2012.01.054.

[111] J. Zhang, Y. Zhou, R. Wang, J. Xu, and F. Fang, "Modeling and constrained multivariable predictive control for ORC (Organic Rankine Cycle) based waste heat energy conversion systems," *Energy*, vol. 66, pp. 128-138, 2014.

[112] S. Lecompte, H. Huisseune, M. Van den Broek, S. De Schampheleire, and M. De Paepe, "Part load based thermo-economic optimization of the Organic Rankine Cycle (ORC) applied to a combined heat and power (CHP) system," *Applied Energy*, vol. 111, pp. 871-881, 2013.

[113] S. Lecompte, H. Huisseune, M. Van Den Broek, B. Vanslambrouck, and M. De Paepe, "Review of organic Rankine cycle (ORC) architectures for waste heat recovery," *Renewable and sustainable energy reviews*, vol. 47, pp. 448-461, 2015.

[114] D. Ziviani, A. Beyene, and M. Venturini, "Advances and challenges in ORC systems modeling for low grade thermal energy recovery," *Applied Energy*, vol. 121, pp. 79-95, 2014.

[115] D. Wei, X. Lu, Z. Lu, and J. Gu, "Dynamic modeling and simulation of an Organic Rankine Cycle (ORC) system for waste heat recovery," *Applied Thermal Engineering*, vol. 28, no. 10, pp. 1216-1224, 2008.

[116] H. Koppauer, W. Kemmetmüller, and A. Kugi, "Model predictive control of an automotive waste heat recovery system," *Control Engineering Practice*, vol. 81, pp. 28-42, 2018/12/01/ 2018, doi: https://doi.org/10.1016/j.conengprac.2018.09.005.

[117] R. Freymann, W. Strobl, and A. Obieglo, "The turbosteamer: A system introducing the principle of cogeneration in automotive applications," *MTZ worldwide*, vol. 69, no. 5, pp. 20-27, 2008/05/01 2008, doi: 10.1007/BF03226909.

[118] M. Jiménez-Arreola, R. Pili, F. Dal Magro, C. Wieland, S. Rajoo, and A. Romagnoli, "Thermal power fluctuations in waste heat to power systems: An overview on the challenges and current solutions," *Applied Thermal Engineering*, vol. 134, pp. 576-584, 2018/04/01/ 2018, doi: https://doi.org/10.1016/j.applthermaleng.2018.02.033.

[119] D. Seitz, O. Gehring, C. Bunz, M. Brunschier, and O. Sawodny, "Model-based control of exhaust heat recovery in a heavy-duty vehicle," *Control Engineering Practice*, vol. 70, pp. 15-28, 2018/01/01/ 2018, doi: https://doi.org/10.1016/j.conengprac.2017.08.010.

[120] T. Endo *et al.*, "Study on maximizing exergy in automotive engines," SAE Technical Paper, 0148-7191, 2007.

[121] J. Peralez *et al.*, "Improving the control performance of an organic rankine cycle system for waste heat recovery from a heavy-duty diesel engine using a model-based approach," in *52nd IEEE Conference on Decision and Control*, 2013: IEEE, pp. 6830-6836.

[122] J. Peralez, P. Tona, M. Nadri, P. Dufour, and A. Sciarretta, "Optimal control for an organic rankine cycle on board a diesel-electric railcar," *Journal of Process Control*, vol. 33, pp. 1-13, 2015.

[123] G. Hou, S. Bi, M. Lin, J. Zhang, and J. Xu, "Minimum variance control of organic Rankine cycle based waste heat recovery," *Energy Conversion and Management*, Article vol. 86, pp. 576-586, 2014, doi: 10.1016/j.enconman.2014.06.004.

[124] X. Liu *et al.*, "Model Predictive Control of an Organic Rankine Cycle System," *Energy Procedia*, vol. 129, pp. 184-191, 2017/09/01/ 2017, doi: https://doi.org/10.1016/j.egypro.2017.09.109.

[125] R. Zanelli and D. Favrat, "Experimental investigation of a hermetic scroll expander-generator," 1994.

[126] S. E. Haaland, "Simple and explicit formulas for the friction factor in turbulent pipe flow," *Journal of Fluids Engineering*, vol. 105, no. 1, pp. 89-90, 1983.

[127] K. Assawamartbunlue and M. Brandemuehl, "The Effect of Void Fraction Models and Heat Flux Assumption on Predicting Refrigerant Charge Level in Receivers," 2000.

[128] R. Shi, T. He, J. Peng, Y. Zhang, and W. Zhuge, "System design and control for waste heat recovery of automotive engines based on Organic Rankine Cycle," *Energy*, vol. 102, pp. 276-286, 2016.

[129] J. Chowdhury, B. Nguyen, and D. Thornhill, "Modelling of evaporator in waste heat recovery system using finite volume method and fuzzy technique," *Energies*, vol. 8, no. 12, pp. 14078-14097, 2015.

[130] I. Vaja, "Definition of an object oriented library for the dynamic simulation of advanced energy systems: methodologies, tools and application to combined ICE-ORC power plants," 2009.

[131] M. Willatzen, N. B. O. L. Pettit, and L. Ploug-Sørensen, "A general dynamic simulation model for evaporators and condensers in refrigeration. Part I: moving-

boundary formulation of two-phase flows with heat exchange: Modèle général dynamique pour évaporateurs et condenseurs frigorifiques. Partic I: Formulation des conditions aux limites variables de flux biphasiques avec échange de chaleur," *International Journal of Refrigeration,* vol. 21, no. 5, pp. 398-403, 1998/08/01/ 1998, doi: https://doi.org/10.1016/S0140-7007(97)00091-1.

[132] T. L. McKinley and A. G. Alleyne, "An advanced nonlinear switched heat exchanger model for vapor compression cycles using the moving-boundary method," *International Journal of refrigeration,* vol. 31, no. 7, pp. 1253-1264, 2008.

[133] A. M. Abdulshahed, A. P. Longstaff, and S. Fletcher, "The application of ANFIS prediction models for thermal error compensation on CNC machine tools," *Applied Soft Computing,* vol. 27, pp. 158-168, 2015.

[134] R. Shah, A. G. Alleyne, C. W. Bullard, B. P. Rasmussen, and P. Hrnjak, "Dynamic modeling and control of single and multi-evaporator subcritical vapor compression systems," Air Conditioning and Refrigeration Center. College of Engineering …, 2003.

[135] A. Benato, M. R. Kærn, L. Pierobon, A. Stoppato, and F. Haglind, "Analysis of hot spots in boilers of organic Rankine cycle units during transient operation," *Applied energy,* vol. 151, pp. 119-131, 2015.

[136] M. Jiménez-Arreola, R. Pili, C. Wieland, and A. Romagnoli, "Analysis and comparison of dynamic behavior of heat exchangers for direct evaporation in ORC waste heat recovery applications from fluctuating sources," *Applied energy,* vol. 216, pp. 724-740, 2018.

[137] A. Desideri *et al.*, "Comparison of moving boundary and finite-volume heat exchanger models in the modelica language," *Energies*, vol. 9, no. 5, p. 339, 2016.

[138] J. Chowdhury, B. Nguyen, and D. Thornhill, "Modelling of Evaporator in Waste Heat Recovery System using Finite Volume Method and Fuzzy Technique," *Energies*, vol. 8, no. 12, p. 12413, 2015. [Online]. Available: http://www.mdpi.com/1996-1073/8/12/12413.

[139] E. Feru, F. Willems, B. De Jager, and M. Steinbuch, "Modeling and control of a parallel waste heat recovery system for Euro-VI heavy-duty diesel engines," *Energies*, vol. 7, no. 10, pp. 6571-6592, 2014.

[140] E. Rodriguez and B. Rasmussen, "A comparison of modeling paradigms for dynamic evaporator simulations with variable fluid phases," *Applied Thermal Engineering*, vol. 112, pp. 1326-1342, 2017/02/05/ 2017, doi: https://doi.org/10.1016/j.applthermaleng.2016.10.131.

[141] S. Bendapudi, J. E. Braun, and E. A. Groll, "Dynamic modeling of shell-and-tube heat-exchangers: Moving boundary vs. finite volume," 2004.

[142] S. S. Haykin, "Neural networks and learning machines/Simon Haykin," ed: New York: Prentice Hall, 2009.

[143] J. Huang, Q. Xiao, J. Liu, and H. Wang, "Modeling heat transfer properties in an ORC direct contact evaporator using RBF neural network combined with EMD," *Energy*, vol. 173, pp. 306-316, 2019.

[144] L. A. Zadeh, "Fuzzy sets," *Information and Control*, vol. 8, no. 3, pp. 338-353, 1965/06/01/ 1965, doi: https://doi.org/10.1016/S0019-9958(65)90241-X.

[145] R. Babuška and H. B. Verbruggen, "An overview of fuzzy modeling for control," *Control Engineering Practice*, vol. 4, no. 11, pp. 1593-1606, 1996.

[146] J.-S. R. Jang and C.-T. Sun, *Neuro-fuzzy and soft computing: a computational approach to learning and machine intelligence*. Prentice-Hall, Inc., 1997, p. 614.

[147] L. A. Zadeh, "The concept of a linguistic variable and its application to approximate reasoning—I," *Information Sciences*, vol. 8, no. 3, pp. 199-249, 1975/01/01/ 1975, doi: https://doi.org/10.1016/0020-0255(75)90036-5.

[148] M. Negnevitsky, *Artificial intelligence: a guide to intelligent systems*. Pearson education, 2005.

[149] J. R. Jang, "ANFIS: adaptive-network-based fuzzy inference system," *IEEE Transactions on Systems, Man, and Cybernetics*, vol. 23, no. 3, pp. 665-685, 1993, doi: 10.1109/21.256541.

[150] J. Chowdhury *et al.*, "Fuzzy nonlinear dynamic evaporator model in supercritical organic rankine cycle waste heat recovery systems," *Energies*, vol. 11, no. 4, p. 901, 2018.

[151] M. Kumar and D. P. Garg, "Intelligent learning of fuzzy logic controllers via neural network and genetic algorithm," in *Proceedings of*, 2004, pp. 1-8.

[152] N. Talpur, M. N. M. Salleh, and K. Hussain, "An investigation of membership functions on performance of ANFIS for solving classification problems," in *IOP Conference Series: Materials Science and Engineering*, 2017, vol. 226, 1 ed., doi: 10.1088/1757-899X/226/1/012103. [Online]. Available: https://www.scopus.com/inward/record.uri?eid=2-s2.0-85028665667&doi=10.1088%2f1757-899X%2f226%2f1%2f012103&partnerID=40&md5=d3aad6de029897742ffab3b57349422e

[153] J.-S. Jang, "ANFIS: adaptive-network-based fuzzy inference system," *IEEE transactions on systems, man, and cybernetics*, vol. 23, no. 3, pp. 665-685, 1993.

[154] M. A. Shoorehdeli, M. Teshnehlab, A. K. Sedigh, and M. A. Khanesar, "Identification using ANFIS with intelligent hybrid stable learning algorithm approaches and stability analysis of training methods," *Applied Soft Computing*, vol. 9, no. 2, pp. 833-850, 2009.

[155] M. A. Shoorehdeli, M. Teshnehlab, and A. K. Sedigh, "Training ANFIS as an identifier with intelligent hybrid stable learning algorithm based on particle swarm optimization and extended Kalman filter," *Fuzzy Sets and Systems*, vol. 160, no. 7, pp. 922-948, 2009.

[156] A. Sargolzaei, K. Faez, and S. Sargolzaei, "A new method for Foetal Electrocardiogram extraction using Adaptive Nero-Fuzzy Interference System trained with PSO algorithm," in *2011 IEEE INTERNATIONAL CONFERENCE ON ELECTRO/INFORMATION TECHNOLOGY*, 2011: IEEE, pp. 1-5.

[157] M. Turki, S. Bouzaida, A. Sakly, and F. M'Sahli, "Adaptive control of nonlinear system using neuro-fuzzy learning by PSO algorithm," in *2012 16th IEEE Mediterranean Electrotechnical Conference*, 2012: IEEE, pp. 519-523.

[158] D. P. Rini, S. M. Shamsuddin, and S. S. Yuhaniz, "Balanced the trade-offs problem of anfis using particle swarm optimisation," *TELKOMNIKA Telecommunication, Computing, Electronics and Control*, vol. 11, no. 3, pp. 611-616, 2013.

[159] D. Karaboga and E. Kaya, "Training ANFIS using artificial bee colony algorithm," in *2013 IEEE INISTA*, 2013: IEEE, pp. 1-5.

[160] J. Soto, P. Melin, and O. Castillo, "Optimization of interval type-2 fuzzy integrators in ensembles of ANFIS models for prediction of the Mackey-Glass time series," in

2014 IEEE Conference on Norbert Wiener in the 21st Century (21CW), 2014: IEEE, pp. 1-8.

[161] J. J. Cárdenas, A. Garcia, J. Romeral, and K. Kampouropoulos, "Evolutive ANFIS training for energy load profile forecast for an IEMS in an automated factory," in *ETFA2011*, 2011: IEEE, pp. 1-8.

[162] M. Aliyari Shoorehdeli, M. Teshnehlab, and A. K. Sedigh, "Identification using ANFIS with intelligent hybrid stable learning algorithm approaches," *Neural Computing and Applications*, journal article vol. 18, no. 2, pp. 157-174, February 01 2009, doi: 10.1007/s00521-007-0168-9.

[163] R. Eberhart and J. Kennedy, "A new optimizer using particle swarm theory," in *MHS'95. Proceedings of the Sixth International Symposium on Micro Machine and Human Science*, 1995: Ieee, pp. 39-43.

[164] A. Noghrehabadi, R. Mirzaei, M. Ghalambaz, A. Chamkha, and A. Ghanbarzadeh, "Boundary layer flow heat and mass transfer study of Sakiadis flow of viscoelastic nanofluids using hybrid neural network-particle swarm optimization (HNNPSO)," *Thermal Science and Engineering Progress*, vol. 4, pp. 150-159, 2017/12/01/ 2017, doi: https://doi.org/10.1016/j.tsep.2017.09.003.

[165] K. H. Jyothiprakash, J. Harshith, A. Sharan, K. N. Seetharamu, and Y. T. Krishnegowda, "Thermodynamic Optimization of Three-Fluid Cross-Flow Heat Exchanger Using GA and PSO Heuristics," *Thermal Science and Engineering Progress*, vol. 11, pp. 289-301, 2019/06/01/ 2019, doi: https://doi.org/10.1016/j.tsep.2019.04.009.

[166] J. Kennedy, "Swarm intelligence," in *Handbook of nature-inspired and innovative computing*: Springer, 2006, pp. 187-219.

[167] J. Kennedy, "The Behavior of Particles," presented at the Proceedings of the 7th International Conference on Evolutionary Programming VII, 1998.

[168] C. K. Unamba *et al.*, "Operational optimisation of a non-recuperative 1-kWe organic rankine cycle engine prototype," *Applied Sciences*, vol. 9, no. 15, p. 3024, 2019.

[169] S. E. Haaland, "Simple and explicit formulas for the friction factor in turbulent pipe flow," 1983.

[170] M. A. Denai, F. Palis, and A. Zeghbib, "ANFIS based modelling and control of non-linear systems : a tutorial," in *2004 IEEE International Conference on Systems, Man and Cybernetics (IEEE Cat. No.04CH37583)*, 10-13 Oct. 2004 2004, vol. 4, pp. 3433-3438 vol.4, doi: 10.1109/ICSMC.2004.1400873.